Universidad Pública de Navarra

Departamento de Ingeniería Eléctrica y Electrónica

upna
Universidad
Pública de Navarra
Nafarroako
Unibertsitate Publikoa

CONTRIBUTION TO THE DEVELOPMENT OF DISTRIBUTED FIBER OPTIC SENSORS BASED ON STIMULATED BRILLOUIN SCATTERING

Memoria de la Tesis Doctoral realizada por

Ander Zornoza Indart

Y dirigida por

Dr. Alayn Loayssa Lara

Para optar al grado de

Doctora por la Universidad Pública de Navarra

Pamplona, 2014

UNIVERSIDAD PÚBLICA DE NAVARRA
DEPARTAMENTO DE INGENIERÍA ELÉCTRICA Y ELECTRÓNICA

Tesis doctoral: Contribution to the development of distributed fiber optic sensors based on stimulated Brillouin scattering

Autor: Ander Zornoza Indart

Ingeniero de Telecomunicación

Director: Alayn Loayssa Lara

Doctor Ingeniero de Telecomunicación

Profesor titular (UPNA)

Tribunal nombrado para juzgar la Tesis Doctoral citada:

Presidente: _____

_____

Vocal: _____

_____

Secretario: _____

_____

Acuerda otorgar la calificación de

_____

Pamplona, a   de   de 2010

AGRADECIMIENTOS

Lehenik eta behin, Ainara eta Esther, tesi hau zuei dedikatzen dizuet, zuen laguntza ezinbestekoa izan da eta.

A mis amigos y compañeros. En especial a Rosana y a Leo. Vuestro consejo, punto de vista, apoyo y experiencia es algo que ha significado mucho para mí.

A Luigi ed Aldo, perché a Napoli ho imparato tantissimo. Questa tesi, e anche la mia vita sarebbe molto diversa se non ero mai andato a Napoli.

Thanks also Orlando, Porto is one of the best cities I have ever been to, and I am glad I could spend some time learning in Inesc.

Y finalmente al director de esta tesis, Alayn, gracias a quien he aprendido muchísimo.

ACKNOWLEDGEMENTS

LIST OF ACRONYMS

AM = amplitude modulation

ASE = amplified spontaneous emission

ASS = amplified spontaneous scattering

AWG = arbitrary waveform generator

BDS = Brillouind distributed sensors

BFL = Brillouin fiber laser

BGS = Brillouin gain spectra

BOCDA =Brillouin optical correlation domain analysis

BOFDA =Brillouin optical frequency domain analysis

BOTDA =Brillouin optical time domain analysis

BOTDR = Brillouin optical time domain reflectometry

CW = continuous wave

DPMZ = parallel Mach-Zehnder

DSF = dispersion-shifted fiber

EDFA = Erbium-doped fiber amplifier

EOM   = Electro optic modulator

ER   = Extinction ratio

ESA   = electrical spectrum analyzer

LO   = local oscillator

MI   = modulation instability

MZ-EOM   = Mach-Zehnder electro optic modulator

OFDR   = optical frequency domain reflectometry

OSNR   = optical signal to noise ratio

OSSB-SC   = optical single-sideband suppressed-carrier

OTDR   = optical time domain reflectometry

PM   = phase modulation

POSSB-SC   = pulsed optical single side band suppressed carrier modulation

PPP-BOTDA   = pulse pre-pump BOTDA

PS   = polarization scrambler

RF   = Radio frequency

RIN   = relative intensity noise

SBS   = stimulated Brillouin scattering

SF-BOTDA   = sweep-free BOTDA

SNR   = signal to noise ratio

SSMF   = standard single mode fiber

TDM-BOTDA = time domain multiplexing BOTDA

WDM   = wavelength division multiplexing

LIST OF VARIABLES

A = strain coefficient

A' = normalized strain coefficient

A_{eff} = effective Area of the fiber

A_{OSSB} = amplitude of the detected current while using OSSB modulation

A_{PM} = amplitude of the detected electrical current while using PM modulation

B = temperature coefficient

B' = normalized temperature coefficient

c = speed of light

d = depletion factor of the pump power

D = dispersion parameter of the fiber

E_0 = complex amplitude of the carrier

E_1 = second order nonlinearity of Young's modulus of the fiber

E_{LO} = complex amplitude of the optical local oscillator

E_{OSSB} = optical field of a OSSB modulation after Brillouin interaction

E_P = amplitude of the pump field

E_{PM} = optical field of a PM modulation after Brillouin interaction

ER = Extinction ratio of a pulse

E_S = amplitude of the Stokes field

E_{S0} = complex amplitude of the optical field of the probe wave

E_{S0} = complex amplitude of the probe wave

E_{SB} = complex amplitude of the optical sideband

E_T = optical field after Brillouin interaction

$f_{\mu w}$ = frequency of the microwave local oscillator

f_{IF} = frequency difference between the probe and the local oscillator

f_m = frequency difference between pump and probe while performing wavelength sweep

F_n = photo-detector's preamplifier noise figure

f_{step} = separation of each step in the frequency sweep

g_1 = combination of all the parameters that affect the Brillouin gain

g_B = Brillouin gain spectrum

g_{max} = maximum of Brillouin gain

g_{SBS} = amplitude of the SBS gain in logarithmic scale

G_{SBS} = gain experienced by the continuous wave due to SBS

H_{LC} = measured spectrum of the interaction between leakage and probe

H_M = measured spectrum of the combined contribution of leakage and pulse

H_{pulse} = spectrum of the pulse

H_{SBS} = transfer function given by Brillouin scattering

H_{SBS_tot} = total spectrum of the BOTDA interaction

H_{SBS_gain} = Brillouin gain transfer function

H_{SBS_loss} = Brillouin loss transfer function

I = electrical current after detection

I^{**}_{CW} = probe intensity after interacting with the leakage and the pulse

I^{*}_{CW} = probe intensity after interacting with the leakage over the whole fiber length

I_{CW} = Continuous wave intensity

I_d = photo-detector's dark current

I_L = Leakage intensity

I_p	= pump intensity
I_s	=Stokes intensity
K_A	= acoustic wave momentum
K_B	= Boltzmann constant
K_P	= Pump wave momentum
K_S	= Stokes wave momentum
L	= length of fiber
L_{eff}	= effective length of the fiber
n	= effective refractive index of the fiber
N	= number of averages performed in each acquisition
$n(t)$	= band pass filtered noise
N'	= number of averages performed in each acquisition using TDM-BOTDA
n'_I	= projection in the signal of the in phase component of the pass band noise
n'_Q	= projection in the signal of the quadrature component of the pass band noise
n_g	= effective refractive index at the operating wavelength
n_I	= in phase component of the pass band noise
n_Q	= quadrature component of the pass band noise
n_s	= number of sections for TDM-BOTDA
P'_{S0}	= maximum probe power to be used in TDM-BOTDA avoiding non-local effects
P_0	= power of the carrier
p_{12}	= longitudinal elasto-optic coefficient of the fiber
P_{LO}	= optical power of the local oscillator
P_P	= pump power with Brillouin interaction
P_{P0}	= pump power without Brillouin interaction
P_S	= power of the probe wave
P_{S0}	= power of the probe wave without Brillouin interaction
P_{SB}	= power of the sideband
Q	= amplitude of the acoustic field

q	= the electron charge
r	= amplitude of the pass band noise
R_C	= detector responsivity
R_D	= the responsivity of the detector
RIN	= relative intensity noise of the laser source
R_L	= output resistance of the detector
S_0	=is the zero dispersion slope at the zero dispersion wavelength
SNR_C	= SNR using coherent detection
SNR_D	= SNR using direct detection
T	= temperature
t	= time
T'_m	= duration of a measurement using TDM-BOTDA
T_0	= reference temperature
T_m	= duration of a measurement
T_P	= temporal length of the pump pulse
v_a	= acoustic velocity in the fiber
v_g	= group velocity in the fiber
$w(t)$	= white and Gaussian noise
z	= distance
$z(t)$	= electrical current after detection in the presence of noise
η	= spectral density of the noise
α	= fiber attenuation coefficient
γ	= polarization orientation factor
φ	= is the phase of the pass band noise
τ	= time spent by a pulse travelling in the fiber
$\Delta\lambda$	= measuring wavelength span
$\delta\varepsilon$	= strain difference
δT	= temperature change

Δv = frequency difference to the Brillouin frequency shift

Δv_i = frequency difference between pump and probe for wavelength sweep

$\Delta \tau$ = pulse delay due to chromatic dispersion

δv_B = precision of the estimated frequency in the measurement

Δv_B = Brillouin line-width

Δv_{pulse} = line-width of the pulse spectrum

Δf = span of the RF sweep

Δz = spatial resolution

ρ_0 = density of the fiber

v_0 = optical frequency of the carrier

v_B = Brillouin frequency shift

v_P = pump wave frequency

v_S = optical frequency of the probe wave

ϕ_0 = phase difference between the probe and the local oscillator

ϕ_{OSSB} = phase of the detected current while using OSSB modulation

ϕ_{PM} = phase of the detected electrical current while using PM modulation

ϕ_{SBS} = phase shift due to SBS

σ^2_C = noise in coherent detection

σ^2_D = noise in direct detection

σ^2_{RD} = relative intensity noise power

σ^2_{SD} = shot noise power

σ^2_{TD} = thermal noise power

σ_v^2 = variance of the noise floor in the BOTDA trace

τ_a = phonon lifetime for silica fibers

τ_{probe} = duration of the probe pulse in TDM-BOTDA

λ_0 = zero dispersion wavelength

λ_P = wavelength of the pump wave

λ_{max} = maximum obtained in the Lorentzian fit while performing wavelength sweep

ω_A = acoustic wave frequency

ω_P = Pump wave frequency

ω_S = Stokes wave frequency

ABSTRACT

Fiber optic sensors are becoming a disruptive technology in monitoring integrity of structures. Their low loss, electromagnetic immunity, remote sensing possibilities, multiplexing possibilities and light weight are very attractive in field measurements. Also, the possibility of performing distributed measurements is only possible with fiber optics. In distributed fiber sensors the fiber itself is the transducer, and the measurement of a given parameter i.e. temperature, strain… is given continuously along the fiber at a given spatial resolution, without blind spots. Between the different types of fiber optics distributed sensors, the ones based on stimulated Brillouin scattering are the most promising technology, since they potentially allow high resolution measurements in tenths of kilometer long fibers. However, field applications of these sensors require better performance: faster response sensors in hundreds of kilometer long fibers, at high resolutions (better than 1 meter) at the lowest possible cost. This thesis contributes to the development of fiber optics sensors based on stimulated Brillouin scattering in that direction. We first develop theoretical models so as to study the behavior of the sensor and focus in the main limitations these sensors manifest. Then, after studying different solutions in the literature, we show our contributions. A sensing setup, based on the RF-shaping of pump pulses is presented as a solution to simplify the sensor setup. Furthermore this setup helps in extending the overall sensing length by minimizing non-local effects. An alternative to the common Brillouin spectrum scan, exploiting the wavelength dependence of Brillouin frequency shift, is introduced. This adds a new degree of freedom to the existing Brillouin based sensors. The work carried out during a research stay in Aversa, Italy, is also explained. It consists in a technique, TDM-BOTDA, which enhances the SNR in detection and minimizes non-local effects, improving the sensor performance. In order to integrate point sensors in a distributed sensors network, two designs are proposed and demonstrated. They take advantage of Raman distributed amplification

so as to reduce the loss generated by long fibers and multiplexing. Finally, the application of coherent light-wave systems to BOTDA is studied by the introduction of BOTDA sensors with self-heterodyne detection. Self-heterodyne BOTDA sensors increase the SNR in detection considerably. Furthermore, they add the possibility of measuring the Brillouin phase shift generated along the fiber. This is very important, since it enables the possibility of performing dynamic measurements which are independent of loss.

TABLE OF CONTENTS

CHAPTER 2: RF-SHAPING OF PUMP PULSES FOR BOTDA

CHAPTER 3: WAVELENGTH SWEEP BASED BOTDA SENSOR

CHAPTER 4: TIME DIVISION MULTIPLEXING BOTDA

CHAPTER 5: HYBRID NETWORK WITH POINT AND DISTRIBUTED SENSORS

xx

INTRODUCTION TO THE THESIS

0.1 MOTIVATION

Optical fibers have become a very important technology in Telecommunication Engineering during the last decades. Furthermore, the broadband access in the information technology we have nowadays could not be imaginable without fiber optics, and are said to be a major factor in the advent of the information age [AGRAWAL 2002]. This is mainly due to its advantages as a very attractive propagating medium, where very long distances can be reached at very high bit-rates at a reasonable cost. Fiber optics sensors are devices based on fiber optic technology that can measure environmental parameters such as strain, temperature, gas concentration etc. due to variations of the signals traveling in the fiber. They are a very attractive technology for the monitoring of structures, because, as in communications, they offer some advantages which are not possible with any other sensing technology [CULSHAW 2010]. For example, they are very light compared with other technologies such as electrical sensors, and furthermore they can be placed in passive networks, so they do not need external power supplies, opening the field for remote sensing. Fiber optics sensors are also immune to electromagnetic fields. Moreover they offer multiplexing possibilities which are not possible with any other technologies.

There are different types of fiber optic sensors. The most widely used are point sensors, like for example fiber Bragg gratings [ERDOGAN 1997] or interferometric sensors [LAY 1970]. In this case, fiber optics are used as a part of the sensing network to propagate the signals that reach the point sensors.

The other types of sensors are the so-called fiber optics distributed sensors. With these sensors the fiber optic itself, is the transducer, and the measurement is quasi distributed, made all along the fiber. The main advantage, when compared to point

sensors, is that there are not blind spots which cannot be sensed. However, when using point sensors, we only measure in the specific locations where the sensors have been placed. The sampling interval of the distributed measurement can be made arbitrarily small and, for each sample, we usually have an average value of the measurands integrated over the spatial resolution of the sensor. Therefore, a single distributed sensor can replace many point sensors. This translates to an important reduction in costs when monitoring large structures. A further reduction in costs comes from the fact that standard telecommunication fibers without any modifications are deployed as transducers. In contrast, most point fiber optic sensors require in the first place an elaborate manufacturing process, and also the network can be very complex due to the need for multiplexing [FENG 2010].

Distributed sensors are based on different kinds of scattering phenomena happening in the fiber: Raman, Rayleigh or Brillouin scattering. Therefore there are three different families of distributed sensors depending on the scattering in which they are based. Raman distributed sensors are based on the measurement of the ratio between Stokes and anti-Stokes signals generated by spontaneous Raman scattering [DAKIN 1985]. Although the setups needed to perform such measurements are quite simple when compared to other distributed sensing schemes, the performance of Raman sensors is quite low. This is mainly since any loss in the fiber can be very destructive for the measurements. The performance of these sensors at their best is a sensing distance of NEAR 100km at 0.5 meter resolutions [TAKI 2013, ANGULO 2012] and 240km at 5m resolution [SOTO 2014]. Rayleigh scattering based distributed sensors can be based in optical time reflectometry (OTDR) [LESSELIER 1978] or optical frequency domain reflectometry (OFDR) [SOLLER 2005]. Are the later the ones that exhibit best performance, since commercial devices can measure with millimeter spatial resolutions in up to 2km long fibers.

On the other hand, sensors based on stimulated Brillouin scattering exhibit the best performance of all of them. With this technology, resolutions in the millimeter range can be achieved in short fibers (some kilometers long fibers). Nevertheless, it is in long range measurements where Brillouin sensors have no competence, since measurements over 100km long fibers have been achieved at spatial resolutions near 1m [ANGULO 2012, SOTO 2011, RAO 2012]. Therefore fiber-optic sensors based on the stimulated Brillouin scattering effect are becoming a truly disruptive technology in the field of structural health monitoring. These sensors, when embedded within materials and structures provide a fiber-optic "nerve system" that feels the "pain" that the structures are suffering in the form of strain, stress, deformation, delamination, cracks, temperature variations [HOTATE 2008], and others like nuclear radiation [ALASIA 2006]. Hence, this type of sensor can be deployed in monitoring applications such as in

2

power lines, bridges, pipelines, fire detection, process control, nuclear energy plants etc. For instance, Brillouin distributed sensors (BDS) can be used in electric power lines to measure temperature, which gives an indirect assessment of local current load and degradation of the line. Temperature change detection can also give an indication of leakage in oil or gas pipelines. In roads and railways, distributed strain measurements serve to detect ground displacements that may affect the stability of the infrastructure. Furthermore, BDS sensors can also be configured to measure displacement [WYLIE 2010], birefringence [GOGOLLA 2000] and chromatic dispersion [GONZALEZ 2003] in addition to temperature and strain.

Brillouin distributed sensors need to fit applications of great complexity and show a good response. Therefore, especial effort must be made in order to enhance the Brillouin distributed sensor's performance and increase the accessibility of applications which may take advantage of them. That means that longer distances at higher resolutions should be measured with a cost which can compete with other technologies. So there is still room for improvement in Brillouin distributed sensors, which has been the motivation of this thesis.

0.2   OBJECTIVES OF THE THESIS

The main objective of this thesis is the contribution to the development of distributed fiber optics sensors based on stimulated Brillouin scattering, so the performance of the sensors is enhanced. In order to achieve such general goal, we have centered our research in applying techniques of photonic signal processing that can improve sensors setups and measurement quality; redesigning optical networks so as to integrate point and distributed sensors; and taking advantage of physical principles in order to enhance the sensors behavior and add degrees of freedom to the design of the setup.

Therefore we defined the following working lines:

- Investigation of techniques that simplify existing setups, while reducing leakage of pump pulses.
- Investigation of novel sweeping methods to characterize Brillouin spectra.
- Investigation of techniques to reduce non-local effects.
- Investigation of network designs that allow hybrid networks of point and distributed sensors.
- Investigation of noise reducing techniques to enhance the signal quality and increase the measuring range.

3

- Investigation of distributed phase measurements to perform high quality fast dynamic measurements.

0.3   STRUCTURE OF THE THESIS

The content of this dissertation is addressed in five main chapters, driven by the objectives previously explained.

In order to introduce, comprehend and study the working principle and research trends of Brillouin distributed sensors, a detailed introduction is performed in **chapter 1**. Initially, the SBS nonlinear phenomenon in optical fibers is explained, focusing in its potential for sensing. After that, the different types of Brillouin distributed sensors are introduced. Special detail is taken while describing Brillouin optical time domain analysis (BOTDA) sensors, since they are the ones that exhibit better performance, and thus, the ones studied in this thesis. A theoretical model for BOTDA is presented, which is of great help to predict, study and compare the experimental sensors behavior. Then, basing on the model and in the bibliography, the factors that limit the performance of Brillouin sensors are discussed: non-local effects, modulation instability, spontaneous Raman scattering, self-phase modulation, signal to noise ratio, discrimination between temperature and strain and measurement time. These factors define the research trends there are nowadays in BOTDA sensing, therefore, the current state of the art of BOTDA sensors is presented at the end of this chapter.

In **chapter 2** the RF-shaping of pump pulses for BOTDA sensors is proven to be a good solution to reduce leakage of pump pulses and simplify the sensors setup. A theoretical model is developed that takes into account the leakage of the pump pulse, which is present when using telecom grade electro optic modulators to pulse the pump. This leakage interacts with the probe power along the fiber, compromising the system performance. The model shows that pump leakage can be especially detrimental in long range measurements, because it enhances non-local effects. Experimental measurements showing the performance of the setup in accordance with the model are presented.

An alternative sweeping technique for the Brillouin spectrum is proposed and applied to BOTDA sensors in **chapter 3**. This technique is based on the dependence the Brillouin frequency shift exhibits with wavelength, so the wavelength of pump and probe wave is scanned instead of the frequency difference, which is held constant. Special care must be taken with the effect of chromatic dispersion, although a solution is proposed to avoid possible localization errors. An experimental setup suited for BOTDA sensing is presented and proofed.

4

Non-local effects are one of the main limiting factors of BOTDA long range sensors. A simple technique, based on pulsing the probe wave in order to reduce the interaction length, is presented in **chapter 4**. This technique, called time division multiplexing BOTDA (TDM-BOTDA), presents a tradeoff between measuring time, signal to noise ratio of the measurements and non-local effects, as is studied in the chapter. Measurements showing the potential of the technique are shown. This work was carried out in the Second University of Naples, during a research stay in 2010.

In **chapter 5** hybrid networks with point and distributed sensors are discussed. This work, carried out in collaboration with researches of our optical communication group specialized in point sensors and point sensor networks, results in the design of two topologies that enable point and distributed measurements in the same network. Both networks take advantage of Raman distributed amplification, which is of the essence to overcome the loss in the network. The second topology reduces amplified spontaneous scattering (ASS) noise, which is detrimental for the point sensor measurements and was present in the first topology.

In **chapter 6** the application of coherent techniques is introduced in BOTDA sensors, by self-heterodyne detection. At first, the theory of this technique is described, emphasizing the signal to noise ratio (SNR) enhancement self-heterodyne detection introduces. Then, a detailed study of the SNR improvement is performed, as well as experimental measurements that proof such improvements. Another advantage of self-heterodyne detection is that the Brillouin phase shift information is not lost in the optical to electrical conversion. A detailed study of the SNR of these Brillouin phase measurements is also performed. This shows the potential of Brillouin phase measurements for fast distributed dynamic measurements, which are also shown.

The conclusions and future work lines of this thesis are presented in **chapter 7**.

Finally, a list of the contributions by the author of the thesis is listed in **appendix I**.

0.4   REFERENCES

[AGRAWAL 2002] G. P. Agrawal, Fiber optic communication systems, 3rd ed., New York: John Wiley and sons. 2002.

[ANGULO 2012] Angulo-Vinuesa, X., Martin-Lopez, S., Corredera, P. & Gonzalez-Herraez, M. 2012, "Raman-assisted Brillouin optical time-domain analysis with sub-meter resolution over 100 km", *Optics Express,* vol. 20, no. 11, pp. 12147-12154.

 [CULSHAW 2010] Culshaw, B. 2010*, "Fibre optic sensor technology - An engineering reality or a scientific opportunity?",* Proceedings of SPIE - The International Society for Optical Engineering, 765304.

[DAKIN 1985] Dakin, J.P., Pratt, D.J., Bibby, G.W. & Ross, J.N. 1985, "Distributed optical fibre raman temperature sensor using a semiconductor light source and detector.", *Electronics Letters,* vol. 21, no. 13, pp. 569-570.

[ERDOGAN 1997]   Erdogan, T. 1997, "Fiber grating spectra", *Journal of Lightwave Technology,* vol. 15, no. 8, pp. 1277-1294.

[FENG 2010] Feng, K.-., Wu, C.-., Yan, J.-., Lin, C.-. & Peng, P.-. 2012, "Fiber Bragg Grating-Based Three-Dimensional Multipoint Ring-Mesh Sensing System With Robust Self-Healing Function", *IEEE Journal on Selected Topics in Quantum Electronics.*

[GOGOLLA 2000] Gogolla, T. & Krebber, K. 2000, "Distributed beat length measurement in single-mode optical fibers using stimulated Brillouin-scattering and frequency-domain analysis", *Journal of Lightwave Technology,* vol. 18, no. 3, pp. 320-328.

[GONZALEZ 2003] González Herráez, M., Thévenaz, L. & Robert, P. 2003, "Distributed measurement of chromatic dispersion by four-wave mixing and Brillouin optical-time-domain analysis", *Optics Letters,* vol. 28, no. 22, pp. 2210-2212.

[HOTATE 2008] Hotate, K. 2008, "Fiber optic nerve systems for smart materials and smart structures", *2008 IEEE International Meeting on Microwave Photonics jointly held with the 2008 Asia-Pacific Microwave Photonics Conference, MWP2008/APMP2008*, pp. 31.

[LAY 1970] Lay, C.M. 1970, "Interferometric displacement indication", *Instrum Contr Syst,* vol. 43, no. 5, pp. 110-112.

[LESSELIER 1978] Lesselier, D. 1978, "Determination of index profiles by time domain reflectometry", *Journal of Optics,* vol. 9, no. 6, pp. 349-358.

[RAO 2012] Jia, X.-., Rao, Y.-., Wang, Z.-., Zhang, W.-., Ran, Z.-., Deng, K. & Yang, Z.-. 2012, "Theoretical investigations on the non-local effect in a long-distance Brillouin optical time-domain analyzer based on bi-directional Raman amplification", *Journal of Optics,* vol. 14, no. 4. 045202.

[SOLLER 2005] Soller, B.J., Gifford, D.K., Wolfe, M.S. & Froggatt, M.E. 2005, "High resolution optical frequency domain reflectometry for characterization of components and assemblies", *Optics Express,* vol. 13, no. 2, pp. 666-674.

[SOTO 2011] Soto, M.A., Bolognini, G. & Di Pasquale, F. 2011, "Optimization of long-range BOTDA sensors with high resolution using first-order bi-directional Raman amplification", *Optics Express,* vol. 19, no. 5, pp. 4444-4457.

[SOTO 2014] Soto, M.A., Angulo-Vinuesa, X., Martin-Lopez, S., Chin, S.-H., Ania-Castañon, J.D., Corredera, P., Rochat, E., Gonzalez-Herraez, M., Thévenaz, L., 2014, "Extending the real remoteness of long-range brillouin optical time-domain fiber analyzers", Journal of Lightwave Technology, vol. 32, no. 1, art. no. 6678536, pp. 152-162.

[TAKI 2013] Taki, M., Soto, M.A., Bolognini, G., Di Pasquale, F. 2013, "Study of Raman amplification in DPP-BOTDA sensing employing Simplex coding for sub-meter scale spatial resolution over long fiber distances", *Measurement Science and Technology*, vol. 24 no. 9, art. no. 094018.

8

CHAPTER 1

INTRODUCTION TO DISTRIBUTED OPTICAL FIBER SENSORS BASED ON STIMULATED BRILLOUIN SCATTERING

1.1   INTRODUCTION

Stimulated Brillouin scattering is the nonlinear phenomenon underneath Brillouin distributed sensors. This phenomenon occurs in optical fibers when a pump wave and a Stokes wave counter propagate in the fiber, and an energy transfer between the two waves via an acoustic wave takes place. Its dependence with strain and temperature makes it very interesting phenomenon to be exploited in sensing such measurands.

In this chapter a detailed introduction to distributed optical fiber sensors based on stimulated Brillouin scattering is presented. A detailed explanation of stimulated Brillouin scattering in optical fibers is given to begin with. Then, different types of Brillouin based distributed sensors are described, so as to center in BOTDA sensors, the most promising Brillouin distributed sensor. After that a study of such sensors is performed, by developing a theoretical model and showing the factors that limit such sensors. Finally the current state of the art is reviewed, which are defined by the limiting factors.

1.2   STIMULATED BRILLOUIN SCATTERING IN OPTICAL FIBERS

Stimulated Brillouin scattering is described as the nonlinear interaction between a pump wave, a Stokes wave and an acoustic wave [AGRAWAL 2006]. The power levels at which SBS occurs in an optical fiber can be much lower than those needed for other

nonlinear phenomena such as Stimulated Raman Scattering. The physical process underneath stimulated Brillouin scattering is depicted in figure 1.1. The pump and the Stokes wave propagate in opposite directions in the fiber, inducing an acoustic wave because of electrostriction effect. This acoustic wave generates a density variation of the material as it propagates in the fiber. Due to the dependence of refractive index with the density of the material, a moving and periodic disturbance of the refractive index in the fiber is generated. As a consequence of the interaction with periodic disturbance of the refractive index, a fraction of light is transferred through Bragg diffraction from the pump to the Stokes wave. The frequency of the transferred light is downshifted due to the Doppler effect associated with the velocity of the acoustic wave. Therefore a power transfer between pump and probe power occurs which simultaneously strengths the acoustic wave, stimulating the described process consequently. Finally, the interaction ends up in an amplification of the Stokes wave and the depletion of the pump wave as they travel through the fiber. From the quantum mechanics point of view, SBS consist in the destruction of a pump photon to create simultaneously a Stokes photon and an acoustic phonon. The three waves must fulfill the energy conservation condition relating their frequencies:

$$\omega_A = \omega_P - \omega_S \qquad (1.1)$$

and the conservation of the momentum:

$$k_A = k_P - k_S \qquad (1.2)$$

where the sub-indexes *P*, *S* and *A* are referred to the pump, the Stokes and the acoustic waves respectively. These two relationships have the following consequences: the Stokes wave only experiments gain when counter-propagating with the pump wave, and the frequency shift between pump and stokes is given by:

$$\nu_B = \frac{2n v_a}{\lambda_p} = \nu_p \cdot \frac{2n v_a}{c} \qquad (1.3)$$

where *n* is the effective refractive index of the fiber, v_a the acoustic velocity in the fiber, and λ_P the wavelength of the pump wave. In telecom grade single mode fibers, this frequency shift is around 11GHz when operating in C-Band. The Stokes wave can be injected to the fiber or can be generated from the reflection of the pump wave with thermally excited phonons [CUMMINS 1972]. In the latter case, the effect is called Spontaneous Brillouin scattering.
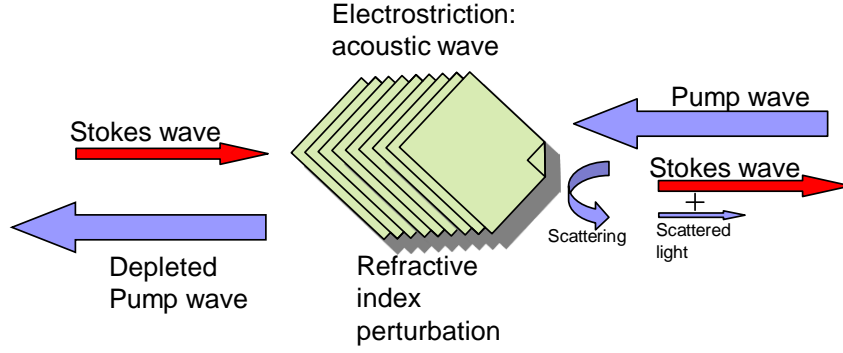
Figure 1.1: Diagram of the SBS interaction in an optical fiber.

The coupled equations that describe the interaction model are the following [Agrawal1995]:

$$\left(\frac{\partial}{\partial z}+\frac{n}{c}\frac{\partial}{\partial t}\right)E_P=-QE_S \tag{1.4a}$$

$$\left(-\frac{\partial}{\partial z}+\frac{n}{c}\frac{\partial}{\partial t}\right)E_S=Q^*E_P \tag{1.4b}$$

$$\left(\frac{\partial}{\partial t}+\Gamma\right)Q=\frac{1}{2}\Gamma_1 g_B E_P E_S^* \tag{1.4c}$$

where E_P, E_S and Q are the amplitudes of the pump, Stokes and the acoustic fields respectively, g_B the Brillouin gain spectrum, c the speed of light, n the refractive index of the fiber, and $\Gamma=\Gamma_1+j2\pi(\nu_P-\nu_B)$ with $\Gamma_1=1/(2\tau_a)$, where $\tau_a\sim$6ns is the phonon lifetime for silica fibers. The Brillouin gain spectrum, g_B, characterizes the growth of the Stokes wave, and it is related to the damping time of the acoustic waves or the phonon lifetime. It has a Lorentzian profile, and it is given by:

$$g_B(\nu)=\frac{g_{max}}{1+\dfrac{2j(\nu-\nu_P+\nu_B(z))}{\Delta\nu_B}} \tag{1.5}$$

where g_{max} is the maximum Brillouin gain, ν_B is the Brillouin frequency shift, $\Delta\nu_B$ is the Brillouin bandwidth and ν_P is the pump frequency. The maximum gain is given by:

$$g_{max}=\frac{2\pi n^7 p_{12}^2\gamma}{c\lambda_p^2\rho_0 v_a\Delta\nu_B} \tag{1.6}$$

where p_{12} is the longitudinal elasto-optic coefficient of the fiber, ρ_0 the density of the fiber, λ_P the pump wavelength and γ a factor that depends on the relative polarization orientation between pump and probe waves. This last factor reaches its maximum

11

value equal to one when the two waves have the same polarization during SBS interaction.

The nature of SBS is very appropriate to be exploited as a sensing mechanism. This is because there is a linear dependence between the Brillouin frequency shift and the temperature, *T*, or the strain difference in the medium, $\delta\varepsilon$, an optical fiber in this case. This relationship can be described with the following expression:

$$\nu_B(T,\delta\varepsilon) = \nu_B(T_0,0)[1 + A\delta\varepsilon + B(T-T_0)] \tag{1.7}$$

where T_0 is the reference temperature and the constants that relate temperature and strain variations are *A* and *B* respectively, and are given by [ZOU 2008]:

$$A' = \frac{A}{\nu_B(T_0,0)} = \frac{\partial n_{eff}}{n_{eff}\partial\varepsilon} - \frac{\partial\rho_0}{2\rho_0\partial\varepsilon} + \frac{\partial E_1}{2E_1\partial\varepsilon} \tag{1.8a}$$

$$B' = \frac{B}{\nu_B(T_0,0)} = \frac{\partial n_{eff}}{n_{eff}\partial T} - \frac{\partial\rho_0}{2\rho_0\partial T} + \frac{\partial E_1}{2E_1\partial T} \tag{1.8b}$$

where E_1 is the second order nonlinearity of Young's modulus of the fiber. Apart from this dependence, Brillouin gain and line-width have slight dependences with strain and temperature too. The Brillouin line-width decreases with temperature, due to a lower absorption of the acoustic phonon while temperature increases [NIKLES 1997]. The Brillouin gain also varies, while the product of both, $g_B \cdot \Delta\nu_B$ is kept constant. The increase of strain causes a smaller Brillouin gain. This has been related to the variations in density suffered by the material, which is proportional to Brillouin gain as expressed in (1.6) [NIKLES 1997].

Brillouin distributed sensors take advantage of these relationships in order to monitor the temperature at which the optical fiber is or the strain that has been applied to the fiber. The measurements are usually based on the characterization of the Brillouin spectrum along the fiber, and specifically, is the Brillouin frequency shift the one parameter taken as a reference. This is because it is the parameter measured with the highest resolution. Brillouin gain or line-width measurements are usually neglected since they are more sensible to noise.

1.3   TYPES OF BRILLOUIN DISTRIBUTED SENSORS

There are different types of Brillouin distributed sensors, and they are classified depending on the principle they use to scan the Brillouin spectrum along the fiber. The techniques that measure in the correlation domain, are named Brillouin Optical Correlation Domain Analysis (BOCDA) sensors. The so-called Brillouin optical

Frequency domain analysis (BOFDA) sensors measure in the frequency domain. And finally, the techniques that measure in the time domain, depending if they are based on spontaneous or stimulated Brillouin scattering, are named Brillouin optical time domain reflectometry (BOTDR) sensors or Brillouin optical time domain analysis (BOTDA) sensors respectively. We are going to introduce all this techniques, and then focus in the most interesting among them, the BOTDA, since the scope of this thesis is contributing to the development of this particular type of Brillouin distributed sensor.

1.3.1 BOCDA SENSORS

These sensors, based on the correlation domain, are very attractive to perform high spatial resolution measurements in the mm range, in short optical fibers [HOTATE 2000]. In figure 1.2 the principle behind BOCDA measurement is depicted. Two frequency modulated signals with a frequency difference near the Brillouin frequency shift of the fiber, a pump and probe wave, are counter-propagating in the fiber. The frequency modulation of both signals is the same, so that in a given section of the fiber, called the correlation peak, their frequency difference is kept constant. Meanwhile, in the rest of the fiber, the frequency shift between both signals is continuously varying. Therefore, in the correlation peak the gain experienced by the Stokes wave is given by the frequency difference with the probe, while the gain along the rest of the fiber is negligible. By sweeping the frequency difference between pump and probe, the whole Brillouin spectrum is scanned in the correlation peak. The spatial resolution is defined by the modulating parameters such as frequency and depth. In order to measure different sections of the fiber, the correlation peak must appear in different positions of the fiber. This can be easily performed just varying the modulating frequency applied to the signals. Therefore, at each correlation peak, the Brillouin spectra must be measured by performing a sweep in the frequency difference between pump and probe waves.

There are three main drawbacks of this technique. The first one is that the measuring time increases with the resolution, since a whole scan of the Brillouin spectrum must be performed at each correlation peak. The second is that the maximum length of the fiber is limited by the spatial resolution, since from a given limit more than one correlation peak can appear simultaneously in the fiber. The third one is the complexity of the setup, which leads to an expensive sensor. Even though, recent research in BOCDA sensors have led to measurements with spatial resolutions of up to 1.6mm in 1km long fibers [SONG 2006].
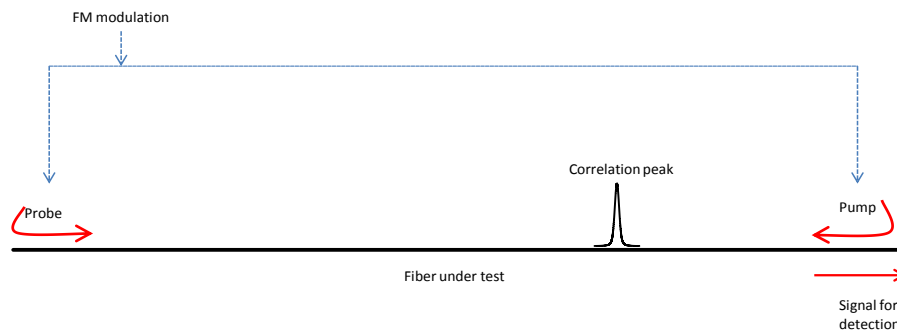
Figure 1.2: Operating principle of BOCDA.

1.3.2 BOFDA SENSORS

BOFDA sensors rest on the measurement of the distributed transfer function of the fiber [GARUS 1996]. As depicted in figure 1.3 the probe signal is modulated with a frequency varying signal. After SBS interaction with the counter-propagating pump signal, the probe is detected and demodulated using the same frequency varying signal. This way, by sweeping the frequency difference of pump and probe signals, the distributed transfer function of the SBS along the fiber is obtained. After that, by performing the Inverse Fourier Transform of the data, the Brillouin for each section of the fiber is calculated. The modulating frequency variation range gives the spatial resolution of the measurements. The cost of these sensors is higher than other type of sensors. This is mainly because in the modulation and demodulation process, an electrical network analyzer is usually deployed. Although their performance has been worse than other Brillouin distributed sensors in the literature, lately they have demonstrated their ability to perform high performance measurements, proving them as a valid solution for distributed sensing [BERNINI 2012]
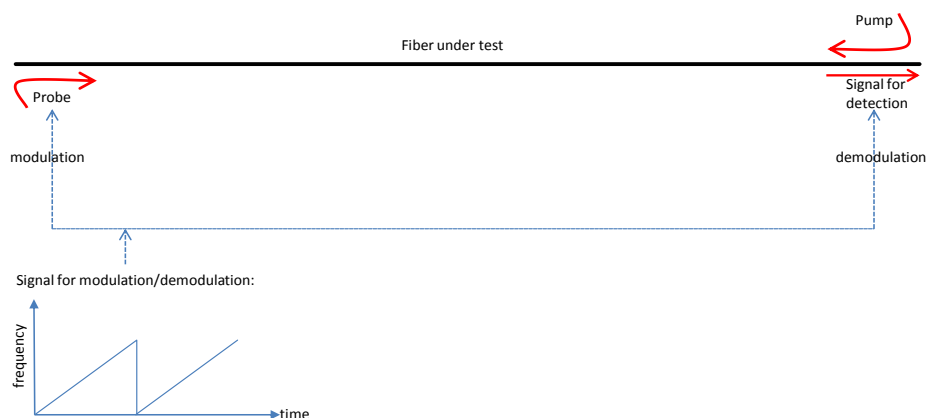

Figure 1.3: Operating principle of BOFDA.

14

1.3.3 BOTDR

BOTDR sensors are based in spontaneous Brillouin scattering in the fiber. Therefore, there is not an externally injected Stokes wave: just a Pump wave is launched into the fiber [HORIGUCHI 1995]. The Stokes wave is generated by the interaction of the pump with thermally excited phonons. This technique is named after OTDR techniques, because the measuring technique and setup, although more complicated, really resembles an OTDR. In figure 1.4 the operating principle of BOTDR is depicted. A pulsed pump wave is launched to the fiber, so a Stokes wave is generated in the opposite direction as this pulse propagates through the fiber and interacts with thermally excited phonons. The Stokes wave is monitored at the start of the fiber. The signal arriving at each moment has been generated at a given point by the pump pulse, so its frequency difference with the pump wave gives the Brillouin frequency shift, and consequently, the characteristics of the fiber at that point. Note that the only difference with OTDR systems is that the monitored signal is the Stokes wave instead of the Rayleigh backscattered signal. Therefore, filtering is required to avoid any crosstalk between the two signals. The spatial resolution is given by the length of the pump pulse, as in OTDR. Nevertheless, there is a limit in spatial resolution due to the phonon lifetime, which is near 1m.

BOTDR sensors have some advantages compared to other Brillouin distributed sensors. In first place, the setup needed to perform such measurements is quite simpler compared to the other Brillouin distributed sensing setups. Note also, that access at one end of the fiber is needed, a characteristic that is well suited for some applications.

However, since the Stokes wave is generated from the interaction with noise, the Stokes signal is very weak and noisy. Therefore, its performance is much worse than other types of Brillouin sensors. Recent improvements of the setups, mainly due to the deployment of Raman distributed amplification, have led to measurements of 150km at 50m resolutions with an accuracy of 5.2Cº [ALAHBABI 2005].
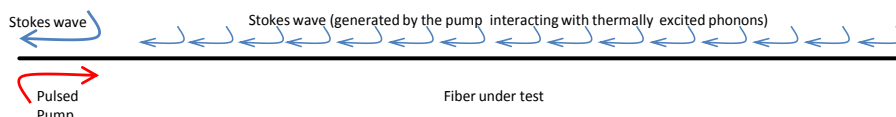

Figure 1.4: Operating principle of BOTDR.

1.3.4 BOTDA

The most widely used Brillouin distributed sensor are BOTDA sensors. Their operating principle is very similar to BOTDR sensors, but in this case the measurements are based

on Stimulated Brillouin scattering [HORIGUCHI 1985]. Therefore, apart from introducing a pulsed Pump wave in one end of the fiber, a continuous Stokes wave in the opposite end is introduced, as depicted in figure 1.5. Consequently, the pulsed Pump generates gain in the continuous Stokes wave along the fiber. So, by monitoring the Stokes wave at the output of the fiber, the gain generated for a certain frequency shift between pump and probe is measured. The Stokes signal arriving at each moment to the end of the fiber has been amplified at a given localization in the fiber by the pump pulse. The relationship is given by:

$$z = \frac{v_g \cdot t}{2}$$ (1.9)

where v_g is the group velocity in the fiber and t, the time since the pump pulse entered the fiber. So the amplitude of the signal at each moment depends on the frequency shift between pump and stokes and the Brillouin frequency shift of the given section. Therefore, by performing a frequency sweep of the difference between pump and probe and taking the time dependent Stokes output signal for each frequency difference, we can reconstruct the Brillouin spectrum for each point in the fiber. The spatial resolution is given by:

$$\Delta z = \frac{v_g \cdot T_P}{2}$$ (1.10)

where T_P is the temporal length of the pump pulse. If the frequency difference between pump and probe is near $-v_B$, we generate loss in the signals. Therefore, g_{max} in (1.6) can be taken as negative. However there is not any advantage between both systems [THEVENAZ 2011]. In figure 1.6 an example of the generated signal is depicted. The gain decays exponentially, as the pump pulse propagates along the fiber.
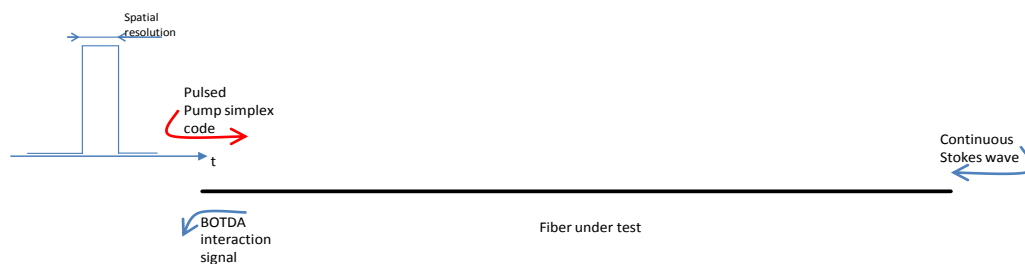

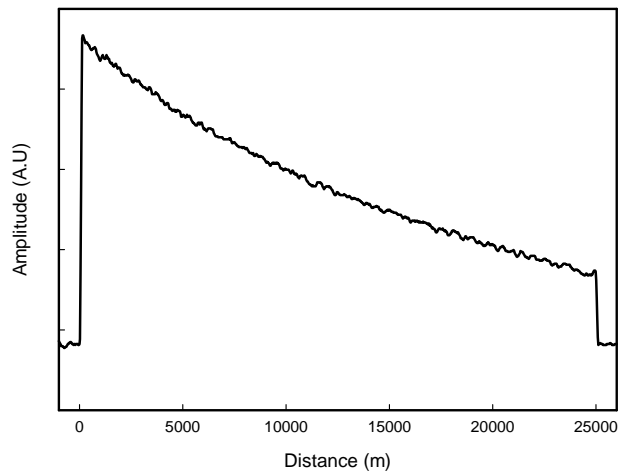*Figure 1.5: Operating principle of BOTDA.*

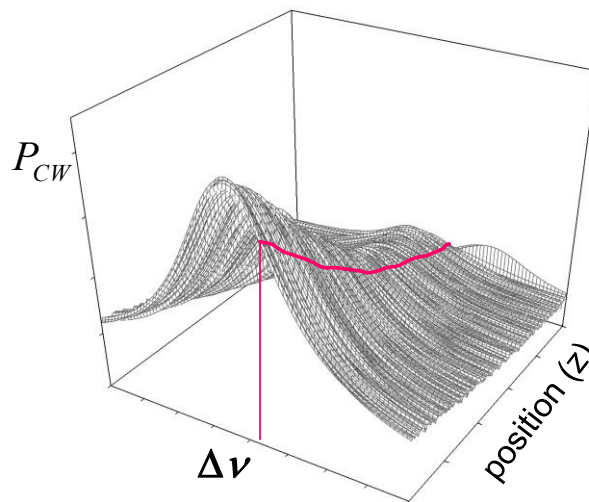*Figure 1.6: Measured BOTDA interaction signal in gain.*

Figure 1.7: Reconstruction of the measured spectra. The pink line corresponds to an interaction at a given frequency shift between pump and probe, as the signal of figure 1.6.

BOTDA sensors are the most widely used type of Brillouin distributed sensors. They show better behavior than the other distributed Brillouin sensing technologies. Measuring distances of more than 100Km with resolutions better than 2m have been reached with these sensors. Since the scope of this thesis is to contribute to the development of these sensors, we will focus in BOTDA from now on.

1.4   BOTDA MODELLING

Theoretical models are a very important tool to understand physical phenomena and predict results in practical research. Moreover, they can help us save an important amount of time since they let us anticipate some practical behaviors we can find in the laboratory or field measurements. With such strong arguments, we consider of the

essence to build a complete BOTDA interaction model as one of the first steps in a doctoral thesis that contributes to develop this kind of sensors. The theoretical model is described in the following paragraphs.

The general interaction that takes place in a BOTDA sensor involves two optical waves that are travelling in a fiber in opposite directions: a pulsed pump wave, I_p and a continuous probe wave (CW), I_s. There are two main methods to solve this interaction. In one hand we have models developed to study the behavior of high spatial resolution BOTDA systems. These models solve the time-domain differential equations (1.4) that describe the interaction between optical and acoustic waves [MINARDO 2011]. Such models are required when the interaction length is near the lifetime of acoustic phonons, i.e. when the pump pulse duration is less than ~6ns long.

On the other hand, since in long-range BOTDA we generally have longer length pulses, we have the family of models that solve the interaction between waves defined by the steady-state coupled intensity SBS equations [BAO 1995]:

$$\frac{dI_P}{dz} = -g_B(v,z) \cdot I_P \cdot I_S - \alpha \cdot I_P$$

(1.11a)

$$\frac{dI_S}{dz} = -g_B(v,z) \cdot I_P \cdot I_S + \alpha \cdot I_S$$

(1.11b)

Where α is the fiber attenuation coefficient and $g_B(v,z)$ represents the Brillouin gain spectrum, which depends on the frequency difference between pump and probe waves and the temperature and strain characteristics of the fiber, as described in (1.5) and (1.6). I_s is a continuous signal of value I_{CW} launched in $z=L$, and I_p is a pump pulse introduced in $z=0$. Equations (1.11) are usually solved by using a perturbation method in which CW is initially affected only by the fiber loss [BAO 1995].
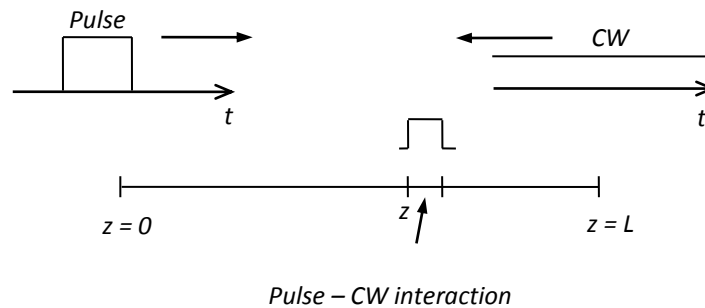

Pulse – CW interaction

Figure 1.8: Scheme of the SBS interaction between pump pulse and stokes CW considered by the theoretical model.

A numeric solution for the evolution of the pulsed wave power (I_P) can be calculated as follows:

$$I_P(v,z) = I_P(0) \cdot Exp\left[\int_0^z - g_B(v,z) \cdot I_{CW}(v,z)dz - \alpha \cdot z\right]$$

(1.12)

Substituting (1.12) in (1.13) and integrating over the interaction region between the pulsed and the amplified CW waves, *u*, we can obtain the expression for the gain experienced by the CW due to SBS interaction with the pump pulse at position z. The result is:

$$G_{SBS}(v,z) = \frac{I_{CW}(v,z)}{I_{CW}(v,z+u)}$$

$$= Exp\left\{\int_{\exp(-\alpha z)}^{\exp(-\alpha(z+u))} \frac{g_B(v,z)I_P(0)}{\alpha x^2}\exp\left(\frac{-g_B I_{CW}(L)\exp(-\alpha L)(x-1)}{\alpha}\right)dx - \alpha \cdot u\right\}$$

(1.13)

So the CW intensity value can be expressed as:

$$I_{CW}(v,z) = I_{CW}(v,z+u) \cdot G_{SBS}(v,z)$$

(1.14)

In Figure 1.9 we compare the output of the model described and an experimental BOTDA trace under the same circumstances. In this particular case we used a 24.2-km long fiber with attenuation $\alpha=0.198dB/Km$, an effective core area $A_{eff}=2.665 \cdot 10^{-10}m^2$ while measuring with 25m resolution and operating at a wavelength of 1544nm. The Stokes CW and pulsed pump powers were *-7.14dBm* and *18dBm* respectively. The Brillouin gain of the fiber, a parameter that was not given by the fiber vendor, was approximated to be $g_{max}=6.8185 \cdot 10^{-11}m/W$.
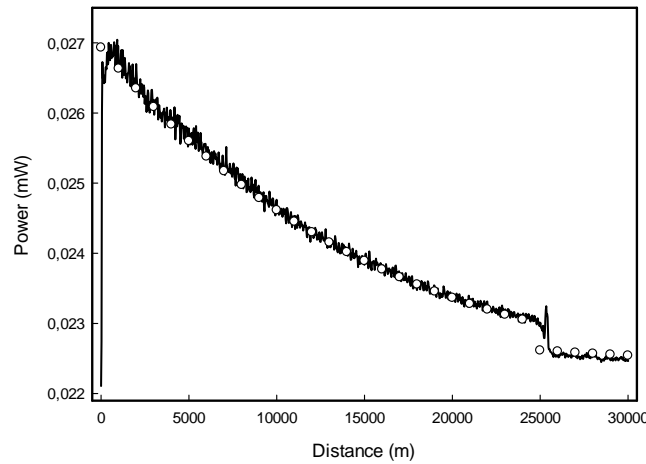

Figure 1.9: Theoretical BOTDA trace calculated with the model (dotted line) and experimental BOTDA trace measured in the laboratory (solid line).

19

For a given position in the fiber, we can define the transfer function given by Brillouin scattering, H_{SBS}, as:

$$H_{SBS}(\nu, z) = \exp\left(\frac{g_1}{1 + \frac{2j(\nu - \nu_P + \nu_B(z))}{\Delta\nu_B}}\right) = \exp(g_{SBS}(\nu, z))\exp(j\phi_{SBS}(\nu, z)) \qquad (1.15)$$

where g_1 includes the combination of all the parameters that affect the gain experienced by the probe wave respectively, g_{SBS} is the amplitude of the gain in logarithmic scale and ϕ_{SBS} is the phase. Expression for the Brillouin spectrum (1.15) is a general expression that is accurate when the pump pulse is significantly longer than the phonon lifetime in the fiber. However, with pulses of the order of the phonon lifetime, (1.5) does not describe the measured spectrum. A possible approximation in these cases is the convolution between the Brillouin spectrum, H_{SBS} and the spectrum of the pulse H_{pulse}:

$$H_{SBS\_tot}(\nu, z) = H_{SBS}(\nu, z) \otimes H_{pulse}(\nu) \qquad (1.16)$$

Since the Brillouin spectrum is Lorentzian, and the pulse spectrum can be approximated to a Gaussian profile, the convolution of both is given by the Voigt function [THOMPSON 1993], and when the variables are complex, by faddeeva function [WELLS 1999] we can express (1.16) as:

$$H_{SBS\_total}(\nu, z) = g_1 faddeeva\left(\frac{\nu}{\Delta\nu_{pulse}} + i\frac{\Delta\nu_B}{2\Delta\nu_{pulse}}\right) \qquad (1.17)$$

where $\Delta\nu_{pulse}$ is the line-width of the pulse spectrum. In figure 1.10 we depict a measured spectrum using 10ns long pulses and the correspondent fit. While the fit using (1.5) does not match up correctly the measured profile, the fit using expression (1.12) matches perfectly the measured spectrum. Note that the three spectra are not symmetric, while the model defined it is. This is because a special BOTDA setup using coherent techniques was used, which has this effect in the reconstruction of the spectra. This effect was taken into account while performing the fit. The setup and technique will be explained in detail in chapter 6 of this thesis.
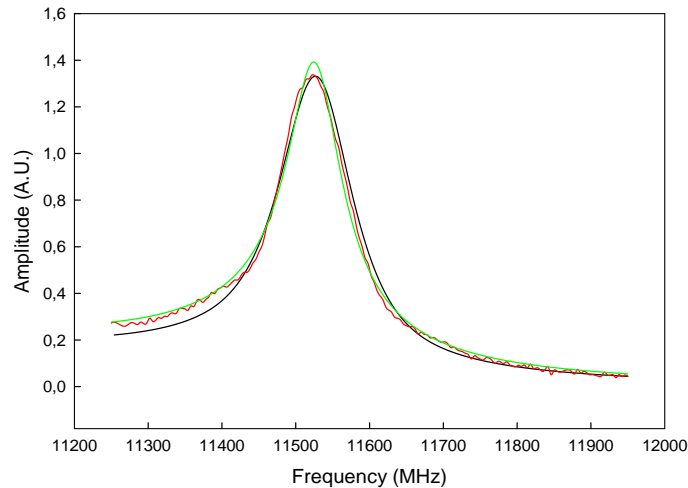
figure 1.10: Measured spectrum with 10ns pulses (red) and fits using expression (1.15) (green) and expression (1.17) (black).

Now that we have a valid model that can be used to predict the behavior of a BOTDA system, we are going to present the limitations of performance that they exhibit.

1.5 FACTORS THAT LIMIT THE PERFORMANCE OF BRILLOUIN SENSORS

1.5.1 NON-LOCAL EFFECTS

Non-local effects refer to a situation in which the measurement of a given position along the fiber is dependent on the interaction at every preceding location of the fiber. Although ideally, as the pump pulse travels to a given measurement location, it is just affected by the attenuation of the fiber, in reality when the probe wave is present there is Brillouin interaction at all the previous sections with energy been transferred from pump to probe. This can be seen in the theoretical model previously explained. This depletion is clear in equation (1.12) of the theoretical model, repeated here for clarity:

$$I_P(v,z) = I_P(0) \cdot Exp\left[\int_0^z - g_B(v,z) \cdot I_{CW}(v,z)dz - \alpha \cdot z \right] \tag{1.18}$$

where there are two terms, the first one due to Brillouin interaction and the second one due to propagation loss in the fiber. Note that the depletion caused by the Brillouin interaction depends on the Brillouin gain profile of the previous sections of the fiber. Let's suppose a fiber with a uniform Brillouin frequency shift. In this case, the depletion of the pulse would be maximum when the frequency shift between pump and probe is equal to the Brillouin frequency shift of the fiber. The further we travel along the fiber, the greater the depletion is. However it is negligible when the

21

frequency difference between pump and probe is far away from the Brillouin frequency shift of the fiber. Therefore, the gain the pulse causes along the fiber depends on the previous interactions apart from the frequency detuning between pump and Stokes waves. This phenomenon is the so-called non-local effect, because of the dependence of the Brillouin gain at a given point with the previous sections of the fiber. The main consequence for the measurements is a distortion of the measured Brillouin spectra, since g_1 is not constant with the frequency shift in (1.15).

In figure 1.11 some simulated spectra are depicted in order to demonstrate the effect of the error in long range measurements. We used the model previously described, simulating a worst case scenario, where a 25km fiber has the same Brillouin frequency shift along the fiber, 10.815GHz, while the last section of 1km exhibited a frequency shift of 10.830GHz. The characteristics of the fiber are the same as the previously obtained: an attenuation of α=0.198dB/Km, an effective core area A_{eff}=2.665·$10^{-10}m^2$ a spatial resolution 25m and a Brillouin gain of the fiber of g_{max}=6.8185·$10^{-11}m/W$. The pump pulse power was set to 18dBm. The distortion leads to a mistaken estimation of the Brillouin frequency shift, and an error in the measurement, which is greater for greater values of probe power.
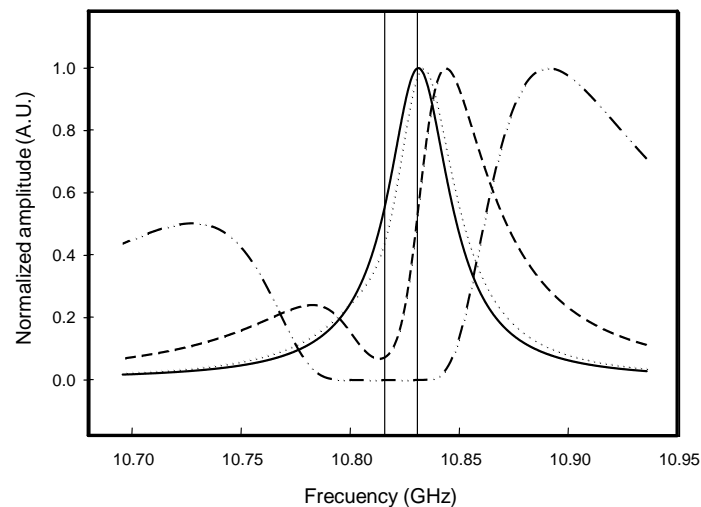
Figure 1.11: Simulated spectra for probe powers -16dBm (continuous line), -8dBm (dotted line), 0dBm (discontinuous line) and 8dBm (dotted and discontinuous line).

Consequently BOTDA sensors must be designed taking into account that this error must be avoided, even if the worst case scenario is not likely to happen in field measurements. There are three main factors that affect non-local effects: Brillouin gain, fiber length and probe power. The fiber length of a BOTDA sensor is defined by the sensing application and the Brillouin gain is defined by the fiber. Therefore it is the probe power, the one parameter we must define in order to avoid non-local effects. As

22

in the simulations previously depicted in figure 1.11, it is clear that the greater the probe power, the greater the non-local effect induced error.

In figure 1.12 we depict the maximum launchable probe power in a BOTDA system for a less than 1MHz error caused by non-local effects depending on the overall sensor length. These results were calculated with simulations using the model described previously, and supposing the sensing fiber is a smf-28 fiber operating in the worst case scenario: 500m of fiber with a BFS with a difference of $\Delta\nu_B/3$ placed at the end of a fiber with a uniform BFS. These results show good agreement with the expression for the maximum probe power to avoid non-local effects developed by Luc Thevenaz et al. [THEVENAZ 2011]:

$$P_{S0} < \ln(1-d)\frac{A_{eff}}{g_B L_{eff}}$$
(1.19)

Where L_{eff} is the effective length of the fiber and d is the depletion factor of the pump power given by:

$$d = \frac{P_{P0} - P_P}{P_{P0}}$$
(1.20)

With P_{P0} the pump power without Brillouin interaction and P_P is the pump power with Brillouin interaction. The maximum depletion factor for an error of less than 1MHz is 0.13. Note that the pump pulse power or spatial resolution does not affect non-local effects so a fixed value of 21dBm and 2m was taken for the simulations. We can clearly see that the longer the fiber length, the lower the probe power threshold that avoids non-local effects. For very long fibers, the maximum launchable probe power is near -14dBm, a very low value indeed. The main consequence of non-local effects is that in order to avoid the non-local effect induced error, the probe power launched to the fiber must be significantly low compromising the SNR of the system.

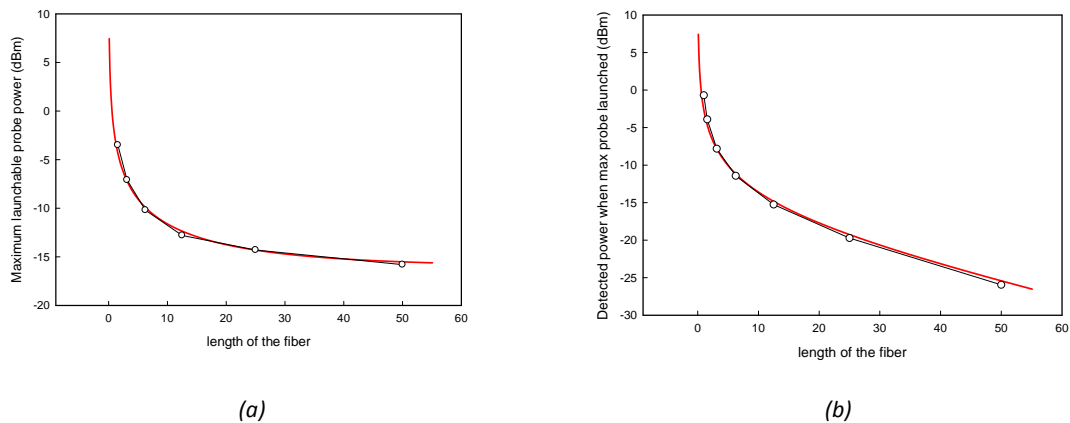(a)   (b)

Figure 1.12: Maximum probe power we can handle to have a maximum of 1MHz non-local effect induced error depending on the length of a SMF fiber (a) and power of the probe wave at detection in the same cases (b) with equation (1.19) (red line) and the theoretical model (circles with dark line).

1.5.2   MODULATION INSTABILITY

Modulation instability (MI) appears in long optical fibers when the pump pulses are very powerful. This effect is the consequence of the interplay between anomalous dispersion and the Kerr effect in the fiber [ALASIA 2005]. It causes a periodical spectral broadening of the pump pulse spectrum, the so-called Fermi-Pasta-Ulam recurrence, and hence a broadening of the measured Brillouin spectrum, increasing the measurement uncertainty [FOALENG 2011a]. Moreover, in some sections of the fiber, the pump pulse suffers such a broadening that can completely suppress the Brillouin gain. In figure 1.13 some experimental BOTDA interactions traces are shown. The measurements were performed in a 25km fiber with pump pulses of different powers, from 16dBm to 22dBm with 2dB increases. The greater the pump pulse power, the greater the distortion of the measurement and the depletion of the Brillouin gain in some sections. Modulation instability can be mitigated using normal dispersion fiber instead of standard single mode fiber (SSMF) [DONG 2010].
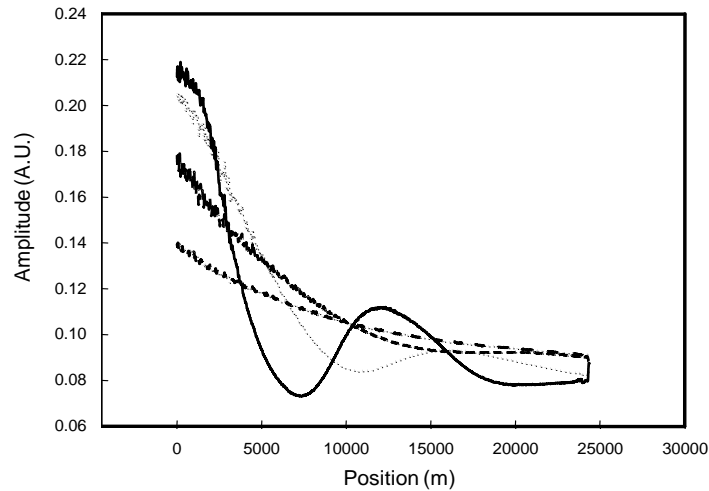
Figure 1.13: BOTDA traces influenced by MI for pump powers of 22 dBm (continuous), 20 dBm (doted), 18 dBm (discontinuous), and 16 dBm (doted-discontinuous).

1.5.3   SPONTANEOUS RAMAN SCATTERING

We have seen that MI limits the maximum pump power we can launch to the fiber. However, using normal dispersion fiber, MI is easily avoided. Therefore, while using these fibers, the pump power can be increased above the threshold of MI generation. Nevertheless we cannot increase pump power indiscriminately neither, since Spontaneous Raman scattering of the pump pulse occurs [FOALENG 2011a, DONG 2010]. For very long fibers, the threshold value of the pump pulse that avoids spontaneous Raman scattering is near 30dBm.

1.5.4   SELF PHASE MODULATION

In long fibers, when the shape of the pulse is not completely rectangular, that is, the rising and falling times of the pulse are not negligible, self-phase modulation can appear [FOALENG 2011b]. As a consequence, pump pulses suffer a spectral broadening that can have a significant effect on the measured Brillouin spectrum line width causing a reduction of the measurement resolution. However, self-phase modulation can be easily avoided by using perfectly shaped rectangular pump pulses with sharp rising and falling edges.

1.5.5   SIGNAL TO NOISE RATIO OF BOTDA SENSORS

Since the pump and probe power signals are limited below the threshold given by MI, Raman Scattering, non-local effects and self-phase modulation, BOTDA interaction is usually very weak, what is more, the amplification of the stokes wave is usually of the order of 1% in long range measurements. Therefore the presence of noise must be

25

taken into account. In this subsection a complete model for the signal to noise ratio of BOTDA signals is obtained.

In fig. 1.13 a conventional BOTDA's detection operation principle is shown. The probe wave, after propagating through the fiber while interacting via SBS with the counter-propagating pump pulse, is directed to the detector by a circulator. The detection is done in base-band converting the signal directly from the optical to the electrical domain. Therefore, the received probe wave optical field can be written as follows:

$$E_S\left(t=\frac{2z}{v_g}, v=v_s\right) = E_{S0}\exp\left(j2\pi v_s t\right)H_{SBS}(v_S,z) \tag{1.21}$$

where v_g is the group velocity in the fiber, E_{S0} is the complex amplitude of the optical field of the probe in the absence of Brillouin interaction, v_S is its optical frequency of the probe and H_{SBS} is the Brillouin gain spectrum. In this expression, it has been assumed that the Brillouin interaction of the probe and the pump pulse takes place at a distance z in the fiber and that the pulse was launched at t=0. Since the optical power is given by the square of the optical field, the detected optical power is:

$$P_S(t,v) = P_{S0}H_{SBS}^2(v,z) \tag{1.22}$$

where P_{S0} is the power of the probe without Brillouin interaction. Then, after the optical to electrical conversion in a baseband photo-receiver, the detected current is:

$$I(t,z) = R_D P_S(t,v) = R_D P_{S0}H_{SBS}^2(v,z) \tag{1.23}$$

with R_D the responsivity of the detector. We can see that the amplitude of the detected Brillouin interaction signal current is directly proportional to the received probe power.
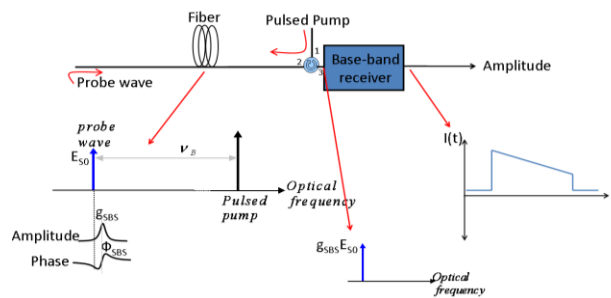

Fig. 1.13: Step by step Schematic diagram of the BOTDA interaction and detection using common direct detection.

In figure 1.15 the detection model for the system taking noise into account, is presented. We assume the presence of white and Gaussian noise, *w(t)*, with a power

spectral density of $\eta/2$. So, for the commonly used base band detection technique, following the diagram of figure 1.15, the received current in presence of noise is then:

$$z(t) = I(t) + n(t) = R_D P_{S0} H_{SBS}^2(\nu, z) + n(t) \tag{1.24}$$

Where *n(t)* is the filtered noise from *w(t)*, in the bandwidth of $I_S(t)$, Δf. The Brillouin gain and phase shift generated by a short pulse, are rather small, so considering that g_{SBS}<<1 we can approximate (1.15):

$$H_{SBS}(\nu, z) \approx \left(1 + g_{SBS}(\nu_S, z)\right) \exp(j\phi_{SBS}(\nu_S, z)) \tag{1.25}$$

Consequently, we can approximate the received current in presence of noise to:

$$z(t) \approx R_D P_{S0}\left(1 + 2g_{SBS}(\nu_S, z)\right) + n(t) = R_D P_{S0} + 2R_D P_{S0} g_{SBS}(\nu_S, z) + n(t) \tag{1.26}$$

Note that the pedestal of the BOTDA signal, given by $R_D P_{S0}$, does not affect the signal to noise ratio of the system. So we can conclude that the signal to noise ratio of a conventional BOTDA setup, when the Brillouin gain is maximum, is given by:

$$SNR_D = \frac{4R_D^2 P_{S0}^2 g_{SBS}^2}{2\eta \Delta f} = \frac{4R_D^2 P_{S0}^2 g_{SBS}^2}{\sigma_D^2} \tag{1.27}$$

where σ_D^2 is the total noise of the system in the given bandwidth, and can be expressed as:

$$\sigma_D^2 = \sigma_{TD}^2 + \sigma_{RD}^2 + \sigma_{SD}^2 =$$
$$= \frac{4 \cdot K_B \cdot T}{R_L} \cdot F_n \cdot \Delta f + RIN \cdot (P_S \cdot R_D)^2 \cdot \Delta f + 2 \cdot q \cdot (R_D \cdot P_S + I_d) \cdot \Delta f \tag{1.28}$$

where σ_{TD}^2 is the thermal noise contribution, σ_{RD}^2 the relative intensity noise (RIN) contribution, σ_{SD}^2 the shot noise contribution, K_B the Boltzmann constant, *T* the photo-detector operating temperature, R_L the output resistance, F_n the photo-detector's preamplifier noise figure, *RIN* the relative intensity noise of the laser source, *q* the electron charge and I_d the photo-detector dark current. The probe power is usually low (<-14dBm). Hence, RIN and shot contributions are negligible. Thus, in conventional BOTDA systems where direct detection is employed the noise is predominantly thermal.
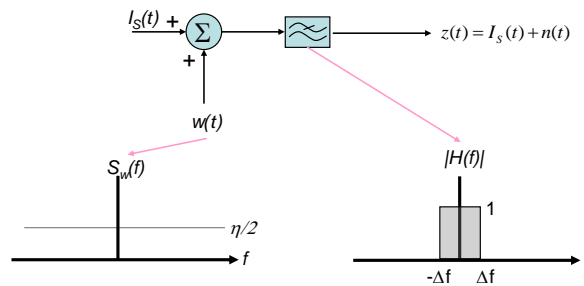
Figure 1.15: Schematic noisy demodulation model for the base band detection.

As a consequence of the previous theoretical analysis we can conclude that in conventional BOTDAs with direct detection, the SNR is directly proportional to the detected probe power. Accordingly, with a stronger P_{S0} the SNR is increased. Nevertheless, if the probe power is increased, non-local effects appear to be noticeable, which must be taken into account with powers as low as -14dBm in long range measurements [THEVENAZ 2011]. Therefore, the maximum probe power launched to the fiber in long range BOTDA measurements cannot exceed a certain level, limiting significantly the systems SNR. We can see that the SNR is also related to g_{SBS}: greater values of g_{SBS} give greater SNR. So the parameters that govern g_{SBS} affect SNR too: there is dependence with Brillouin gain, spatial resolution, and pump pulse power. Therefore, since pump pulse power is limited by MI, self-phase modulation and Raman scattering, the SNR is consequently affected by these phenomena too. Also, the higher the resolution, the smaller the result of the integral, so the lower the SNR.

1.5.6   SPATIAL RESOLUTION

The spatial resolution in BOTDA sensors is determined by the pulse width, and can be improved by using shorter pulses. However, shorter pulses provide a broadened Brillouin gain spectrum, given by the convolution of the pulse spectrum with Brillouin spectra, as expressed in (1.17) and depicted in figure 1.16. Also, since the interaction length is shortened, a weaker Brillouin gain is generated. For example, when 1ns pulses are used, the equivalent pulse spectrum width is near 1GHz. Therefore the measured spectra energy spreads over 1GHz with very low amplitude, in that case. As a result, the measurements are very noisy and not accurate. Hence, the narrower the final spectra, the better the precision in the determination of the Brillouin frequency shift. Therefore, for a given precision and measurement time, the pulse has to be longer than around 10 ns in most setups (≈ 1-m spatial resolution).
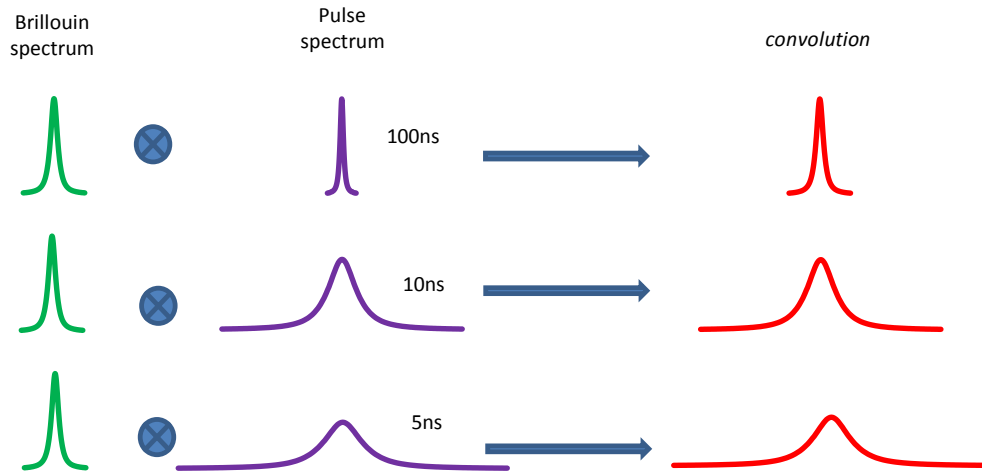
Figure 1.16: Examples of convolution of the Brillouin spectrum with short pulses, the shorter the pulse, the wider the pulse spectrum, and consequently the wider the measured spectrum.

1.5.7 DISCRIMINATION BETWEEN TEMPERATURE AND STRAIN

In Brillouin based fiber optic sensors, it is the Brillouin frequency shift the parameter that has most dependence with strain and temperature. The effect that strain and temperature have in stimulated Brillouin scattering is almost the same, as it has been previously explained [ZOU 2008].Therefore, decoupling between the two parameters is hard to achieve: when a perturbation is observed in the measurements it can be due to either temperature or strain variations. This can be a potential problem in field measurements, but it is inherent in fiber optic sensors, either distributed sensors [SOLLER 2005] or point sensors [ERDOGAN 1997].

1.5.8 MEASUREMENT TIME

BOTDA sensing in its common scheme and design only allows performing a measurement every several seconds and even minutes. The main reason under this limitation is that a frequency sweep must be performed for every measurement. The length of this sweep depends in the range of temperature or strain to be measured and the detail that is needed. It can easily consist of near 400 steps. Since for every frequency step a significant number of averages must be performed to have a good enough SNR, the measurement time is long. For example, in a 25-km fiber, the generation and detection of a single BOTDA trace takes ~0.12ms. Then, for a complete sweep of 400 frequency steps at 1024 averaging, it is physically impossible to perform a measurement under ~49.9s. Furthermore, if we take into account the response of devices such as microwave synthesizers and the data processing, this measuring time is further increased. Such high measuring times limit the application of conventional

29

BOTDAs to measuring slow changes, since the detection of real time or dynamic events is not possible.

1.6   STATE OF THE ART OF BOTDA SENSORS

We have described the factors that limit BOTDA sensors. The research in BOTDA sensors is focused in minimizing or avoiding the negative effects they produce, so the performance of the sensor is enhanced. Current research trends in Brillouin distributed sensors are defined by the needs of the potential application fields of this sensing technology. These applications demand an ideal BDS sensor that enables measurements in ranges larger than 100 km and with spatial resolutions under a meter, providing strain and temperature simultaneously, obtaining accurate results in fast quasi-"real-time" and all at a reasonable cost.

Therefore we can classify the research in BOTDA into 5 main research lines. The first one is the simplification of the setup and decrease cost, in order to make feasible their widespread application. The second is the development of temperature and strain discrimination techniques. The third is decreasing the measuring time so as to achieve real-time monitoring. The other two main research lines are related to the enhancement of the performance of BDS in terms of range and resolution. These are complementary efforts. On the one hand, there is the need to monitor large structures that can extend over hundreds of kilometers such as railways, pipelines, power lines, etc. On the other hand, increasingly detailed information of the measurands distribution is required in applications such as structural health monitoring. For instance, enhanced resolution can enable detection of small cracks in reinforced concrete structures. The main achievements in these research trends are described in this section.

1.6.1   TECHNIQUES TO IMPROVE THE SPATIAL RESOLUTION OF BOTDA SENSORS

Spatial resolution improvement is an area of research that has concentrated great efforts recently. Many potential applications of Brillouin distributed sensors require the highest possible spatial resolution to obtain an accurate assessment of the distribution of a given measurand. However, as it has previously explained, in the standard configuration of a BOTDA sensor, the spatial resolution is limited to around 1 m. In order to improve the resolution, techniques to pre-excite the acoustic wave are used.

The basic idea when pre-exciting the acoustic wave, is to have Brillouin interaction before the arrival of the pump pulse, what can overcome the BGS broadening effect. The first of the techniques taking advantage of the pre-excitation of the acoustic wave,

uses pulses with a significant level of leakage, as depicted in figure 1.17 [BAO 1999]. When the pulse enters the fiber, the presence of pre-existing CW pump and Stokes signals has already generated an acoustic wave. Consequently, the scattering the pulse generates reflects on the pre-existing grating without the need to generate its own interaction. Therefore, the interaction spectrum experienced by the pump wave is defined by the natural Brillouin linewidth and not by the convolution of the pump spectrum and Lorentzian profile, while the spatial resolution is given by the length of the pulse. Resolutions of up to 10cm [KALOSHA 2006] have been achieved with this technique.
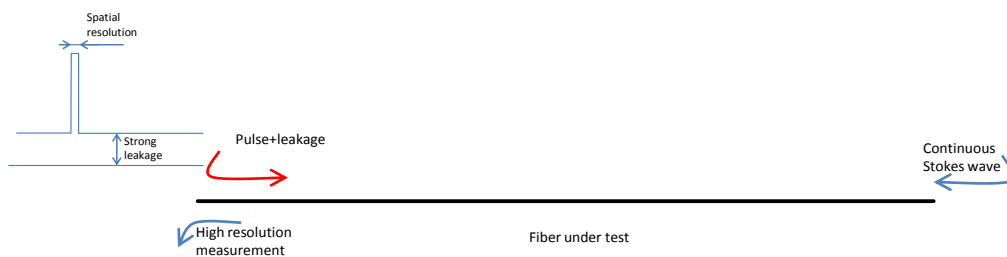

Figure 1.17: High resolution BOTDA taking advantage of pre-excitation of the acoustic wave with pulses with strong leakage level.

The so called Pulse Pre-pumping of BOTDA (PPP-BOTDA) is based on the previous technique. The only difference is that it achieves the pre pump with a stepped pulse, instead of a pulse with leakage, as depicted in figure 1.18 [KISHIDA 2005]. The first step of the pulse, which is less powerful and longer than the second, pre excites the acoustic wave. The second pulse, whose length gives the spatial resolution, scatters with the existing acoustic wave, generating a high resolution interaction. Resolutions of up to 2cm have been achieved with this technology [KISHIDA 2008]
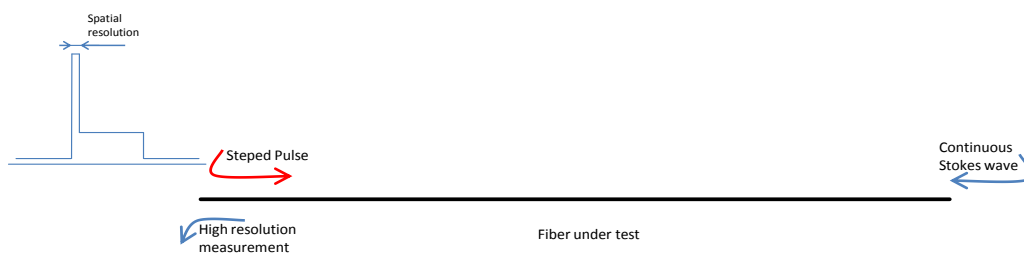

Figure 1.18: Principle of operation of PPP-BOTDA.

Another way to pre-excite the acoustic wave, is by taking advantage of the so-called dark-pulse BOTDA technique [BROWN 2007]. As depicted in figure 1.18, instead of launching a regular pulse, a temporal suppression of an otherwise continuous pump wave is introduced. The temporal suppression, or the length of the dark pulse, gives

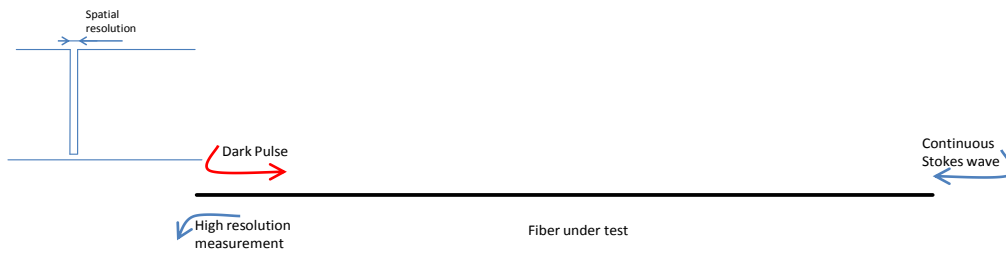the spatial resolution of the system. Resolutions of up to 2cm have been achieved with this technique.

Figure 1.18: Principle of operation of Dark pulse BOTDA.

However, the application of high resolution measurements to long range BOTDA has come from differential pulse measurements [LI 2008a]. In order to perform measurements with this technique, two independent BOTDA interactions are needed, each one with pump pulses of different length, as depicted in figure 1.20. Then, a post processing of the two traces is performed, since the actual high resolution measurement comes from the subtraction between the two measurements. The spatial resolution is given by the difference between the lengths of the two pulses. Resolutions of 2 cm in 2km long fibers have been achieved with this technique [DONG 2012].
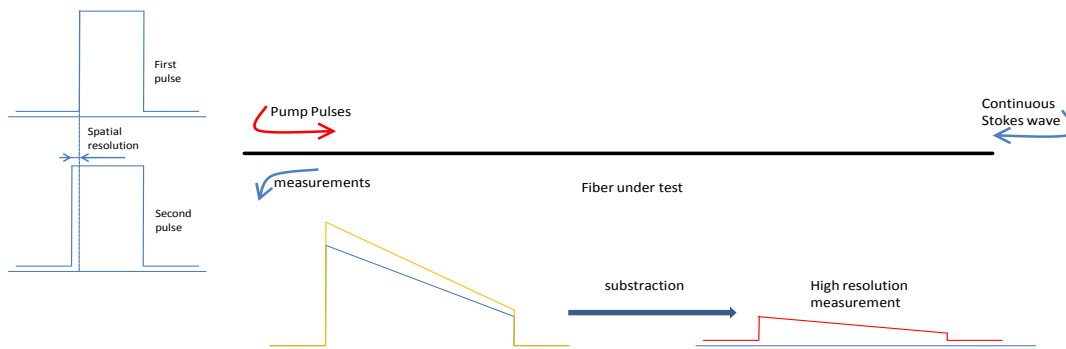
Figure 1.20: Operation principle of double pulse BOTDA.

More recently, an improved physical explanation for the acoustic wave pre-excitation has been developed that has led to an optimized setup based on using optical phase-shift instead of optical intensity pulses [FOALENG 2010]. The operating principle is the same as with dark-pulses, as depicted in figure 1.21. However, the main advantage is that the response is twice larger for an identical pump power. Therefore is the most efficient high resolution BOTDA technique. The impressive performance of

5cm resolutions over 5km sensing fibers have been achieved with such technique [BEUGNOT 2011].

Figure 1.21: Operation principle of phase shift BOTDA.

1.6.2 TECHNIQUES TO DISCRIMINATE STRAIN AND TEMPERATURE MEASUREMENTS IN BOTDA SENSORS

Structural health monitoring and other applications require measurement of either temperature or strain or both simultaneously. However, expression (1.7) highlights that basic Brillouin distributed sensors, as other optical fiber sensor technologies, display a cross sensitivity to temperature and strain that makes it impossible to isolate either of these measurands unless additional actions are taken.

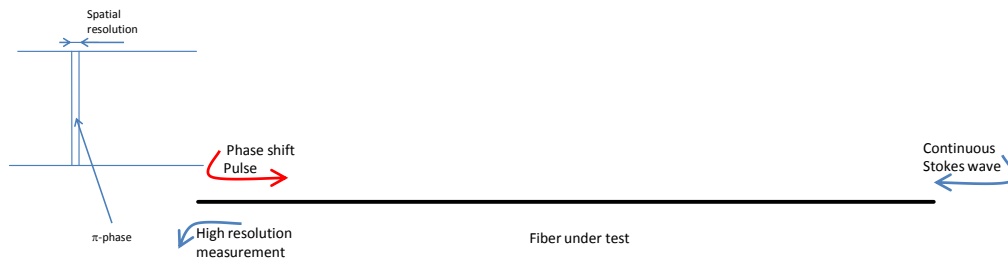The simplest solution is to use two fibers in the measurements, with one of them in a loose state dedicated just to measure temperature. However, this is only possible in short fibers, where doubling the measuring range does not lead to a significant penalty in the sensor performance.

Another solution relies on estimating the line-width and Brillouin gain apart from the Brillouin frequency shift of the measured spectrum in the fiber. As we have commented before, the Brillouin line-width decreases with temperature [NIKLES 1997] and the Brillouin gain also varies, while the product of both, $g_B \cdot \Delta v_B$ is kept constant. Meanwhile, the increase of strain causes a smaller Brillouin gain. Therefore, taking into account these parameters, we can discriminate temperature and strain variations. However, amplitude estimations are subject to variations due to mechanically induced loss, which can happen in field measurements. Moreover, Brillouin line-width is hard to estimate accurately, since very clean measurements are needed for such applications. Minimum errors of 4ºC and 82με have been measured with this technique [BAO 2004]. Therefore, this is not a very good solution.

Other approaches rely on using fibers with multiple acoustic modes [LEE 2001], since each acoustic mode exhibits a different dependence of the Brillouin frequency shift with strain and temperature. Hence, initially a calibration of each Brillouin peak dependences with strain and temperature must be performed. Afterwards, by

measuring the frequency shift of each Brillouin peak, temperature and strain can be discriminated. However, the obtained accuracy is better than the one achieved achieved with the previous technique, 1.8ºC and 37με [LIU 2012].

Another solution comes from measuring Brillouin frequency shift and the spectrum of the dynamic acoustic grating in a polarization maintaining fiber. Both parameters have the same sign of dependence with strain, but opposite signs for temperature-dependence. Therefore, using birefringence measurements combined with Brillouin frequency shift measurements with the goal of having two independent responses to strain and temperature is a solution that has led to accuracies of 0.08Cº and 3με [ZOU 2009].

1.6.3   TECHNIQUES TO SIMPLIFY BOTDA SENSOR SETUPS

In Brillouin distributed sensors, the transducer itself, i.e. SSMF, is very cheap. However, the interrogation setup is complex and expensive, using a number of broadband and microwave frequency components as well as sophisticated photonic devices. Therefore, when compared to other sensing technologies, BOTDA implementations are usually complex and use expensive components such as synthesized microwave generators, multiple electro-optic modulators, wideband detectors or semiconductor optical amplifiers. For that reason, much effort has been recently devoted to simplify the experimental setups in order to achieve cost-effective commercial systems that can compete, for instance, with the simpler and less costly distributed Raman sensors for temperature measurements. Recent examples of simplified BOTDA schemes include the use of pulsing probe with SOA, using Brillouin generators or Brillouin fiber lasers to obtain the probe wave from the pump [LECOEUCHE 1998] the deployment of injection locking to generate the pump and probe waves using DFB lasers [THEVENAZ 2004] or the use of offset-locking [LI 2008b], which are explained in detail in the following paragraphs.

One of the first steps in order to simplify BOTDA setups while improving the performance of the sensor, was using a single laser source for pump and probe generation [NIKLES 1997]. Using two lasers has the main drawback that the stability between the frequency differences between the two lasers is very hard to achieve. Also, one of the lasers must be a high resolution tunable laser. So by modulating the laser, stable probe and pump powers could be easily achieved, reducing stability issues and reducing the cost. The setup developed by Diaz et al [DIAZ 2008] takes advantage of this, while enhancing further the performance of the setup by using a SOA to generate pump pulses. The experimental setup is depicted in figure 1.22. The output of a laser is divided in two branches. In the upper branch the probe power is generated,

by modulating the output of the laser with a frequency near the Brillouin frequency shift of the fiber, which is swept in order to reconstruct the spectra. This can be easily performed with a Mach-Zehnder electro-optic modulator (MZ-EOM) driven by a microwave synthesizer. The output, a double sideband suppressed carrier modulation if the MZ-EOM is polarized in minimum transmission, is then filtered so as to suppress one of the sidebands. This way a single probe wave in the fiber is introduced. The polarization of the probe wave is introduced in a passive polarization scrambler, so as to minimize the polarization dependence of the Brillouin gain. In the lower branch, pump pulses are generated with a SOA driven with electrical pulses. The main advantage of pulsing the signal with a SOA instead of a MZ-EOM is the low leakage we can obtain at the output, which is of the order of 40dB compared to the 30dB achievable with standard telecom grade MZ-EOMs. Afterwards the pulses are amplified in an EDFA, so as to obtain the desired level of pump power. After the interaction of the pump and the probe in the fiber, the latter is detected and measured in an oscilloscope. A computer is used for the control of the devices in order to perform the whole frequency sweep.
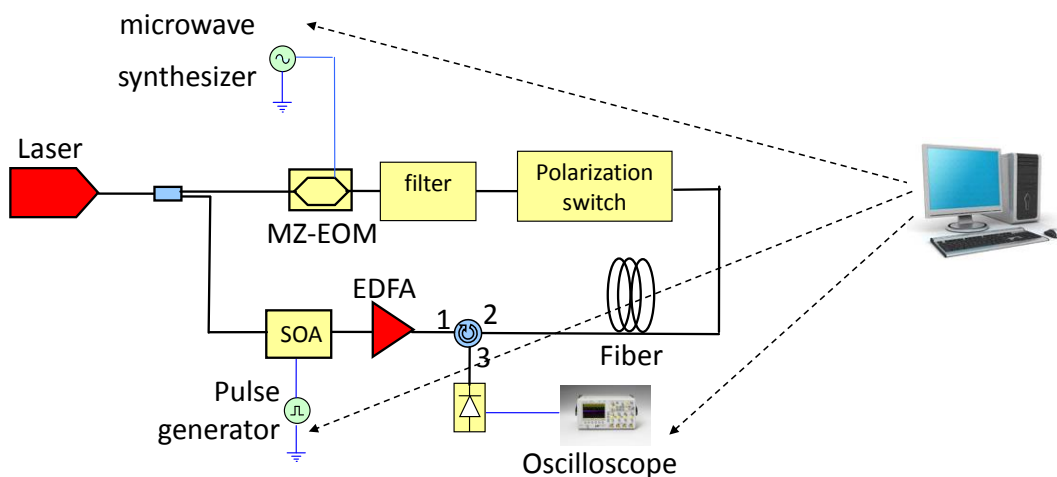
Figure 1.22: Experimental setup presented in [DIAZ 2008].

In BOTDA setups taking advantage of the injection locking effect, there is no need to use electrical to optical modulators, which are one of the costly elements of the previous setup. As depicted in figure 1.23, two DFB lasers are needed, the master and the slave [THEVENAZ 2004]. The operating principle is that while introducing a fraction of the master laser's beam in the slave, the later operates at the exact same wavelength as the master. Note that in this setup, the power that is minimized by the isolation of the circulator is enough for the injection locking.

The slave laser is modulated at a frequency near the Brillouin frequency shift of the fiber, and swept, using a microwave synthesizer. Moreover, the injection locking is

35

performed with one of the sidebands of the modulations, so the output of the slave laser can act as pump wave. The pulsing is performed by pulsing the current supply of the slave laser. Consequently, we have the continuous probe wave, the output of the master laser, and the pulsed pump, the output of the slave laser. The signals are directed to the sensing fiber by circulators, after the pump pulses are amplified with an EDFA to reach the desired level. The output for each frequency shift is detected and measured in the oscilloscope. However, injection locking is not a very stable phenomenon, and unlocking can occur quite easily, compromising the performance of the setup.
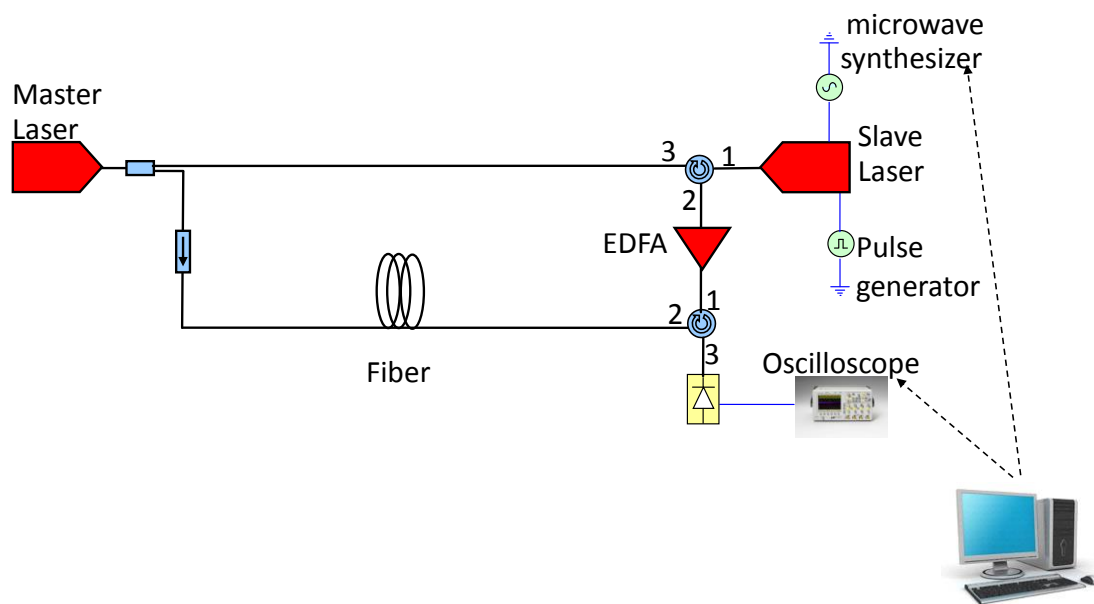
Figure 1.23: BOTDA setup based on injection locking.

In setups based on offset locking, two DFB lasers are used too, one for pump generation and the other for probe Stokes generation [LI 2008b]. However, in contrast to injection locking, the locking between the two lasers is performed in the electrical domain instead of the optical domain. The main advantage of setups based on offset locking is that there is no need for a microwave synthesizer, and the modulation of the optical waves is limited to the pulsing. As depicted in figure 1.24 a fraction of the lasers output is mixed and detected with high bandwidth detectors so as to know the frequency difference between pump and probe. The PID controls and stabilizes this frequency difference, and by varying the temperature of the DFB lasers, performs the sweep between pump and probe. The output of the pump laser is pulsed using a specialty MZ-EOM with 45dB extinction ratio (ER), so as to minimize the leakage of the pulses. The same as in the other cases, at the output of the fiber, the probe wave that has interacted with the pump pulses is detected and measured in the oscilloscope.

36

Figure 1.24: BOTDA setup based on offset locking.

1.6.4 TECHNIQUES TO EXTEND THE RANGE OF BOTDA SENSORS

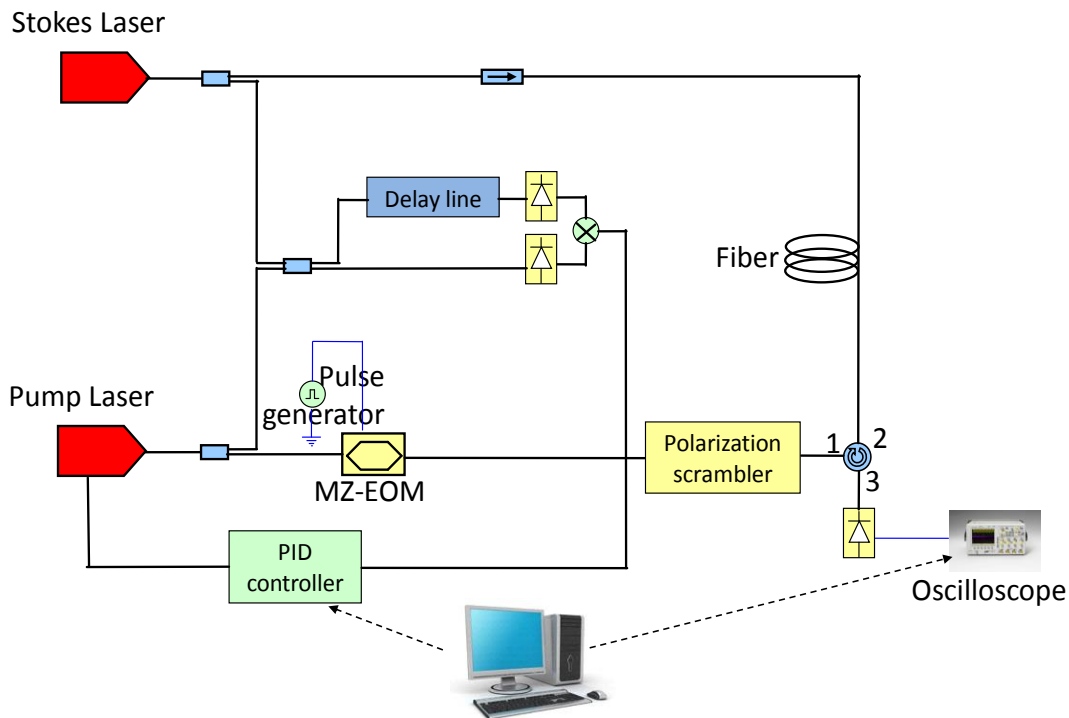The effort to enlarge the measurement range of Brillouin distributed sensors is mainly driven by applications where there is the need to monitor large structures such as pipelines, railways, power lines, etc. As in fiber optic communications, the longer the sensing fiber, the lower the performance we can achieve. The main practical problems in BOTDA setups when the length of the sensing fiber increases are the SNR reduction, the nonlinear effects and non-local effects. The measuring range is limited because of the attenuation of the pump pulse and the probe wave while they propagate along the fiber. When these signals are small, the gain of the probe wave is buried in detection noise and more averaging is demanded to obtain significant measurements; thus, the measurement time is greatly increased. A simple solution to this problem could be to increase the injected pump power, and consequently increase the Brillouin gain of the CW probe signal. However, the maximum pump power launched into the fiber is limited by the appearance of several nonlinear effects such as self-phase modulation, modulation instability or spontaneous Raman scattering, as it has been explained before.

In principle, apart from increasing the pump power, another possibility to mitigate the SNR reduction while enlarging the range of the sensor could be to increase the injected probe power. However, we have seen that the limit in this case is set by the onset of

37

non-local effects. Furthermore, we have seen that the longer the fiber, the lower the probe power we can use. The limit is near -14dBm, which is a very low value indeed. Complex computational solutions to process data and minimize the error have been developed [GEINITZ 1999, MINARDO 2005], although they are hard to apply.

Therefore it is of the essence to develop techniques to further increase the performance of the sensor in long range measurements, without affecting MI, self-phase modulation, Raman scattering or non-local effects. There are two main contributions in this area. The first one, simplex coding of BOTDA, consist in coding the BOTDA interaction so as to reduce the effect of noise [SOTO 2009]. The second, using a double spectral line, rests in a double interaction, loss and gain, over the same pump pulse, compensating non-local effects [BERNINI 2011].

In simplex coded BOTDA, instead of a single square pulse, a series of pump pulses forming a simplex code are launched to the fiber, as depicted in figure 1.25. The length of each of the pulses that compose the code gives the spatial resolution. In order to avoid pre-pump effect of the acoustic fields when high resolution (<1m) measurements are performed, RZ-coding is recommended. This way, the interaction of the fiber, is coded by the simplex code formed by the pump wave. Then, this signal is detected and a decoding process, gives the original BOTDA interaction signal. The SNR ratio improvement compared to conventional BOTDA is related to the length of the simplex code. Simplex coding of BOTDA can be applied to any setup of the previously presented. The only difference relies in the shapes of the pump pulses and the computational processing of the measurements, which can be complex.
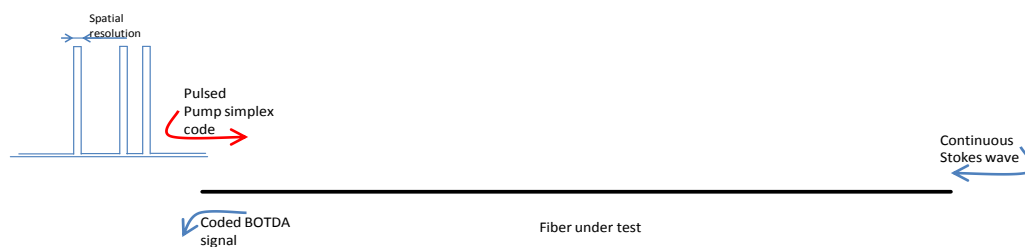
Figure 1.25: Operation principle of simplex coded BOTDA.

In figure 1.26 we depict the typical experimental setup to take advantage of the technique of double spectral lines as probe wave. The same laser source is divided in two branches, for CW and pulse generation respectively. In the lower branch the pump pulse is generated by pulsing directly the laser source with a modulating device.

In the upper branch the two spectral lines to be used as CW are generated via a DSB-SC modulation. The modulation frequency is near v_B of the fiber, so the difference of the upper and lower sidebands are v_B and $-v_B$ with the pulse. Consequently, in one

of the spectral lines, the interaction with the pump is in gain, while in the other is in loss, as depicted in figure 1.27. Therefore, if non-local effects are strong, one of the interactions generates a depletion of the pulse, while the other generates an equivalent amplification. Since non-local effects are avoided, way more powerful probe powers can be used than in a regular BOTDA scheme. However, this principle is hard to apply in setups which are not based in obtaining pump and probe waves via modulation from the same laser source. Also, care must be taken, since when the leakage of pump pulses affects the signals, different powers in the spectral lines ensure the minimizing of non-local effects [BERNINI 2011]. Measurements over 50km of fiber at 5m resolution have been achieved taking advantage of this principle.
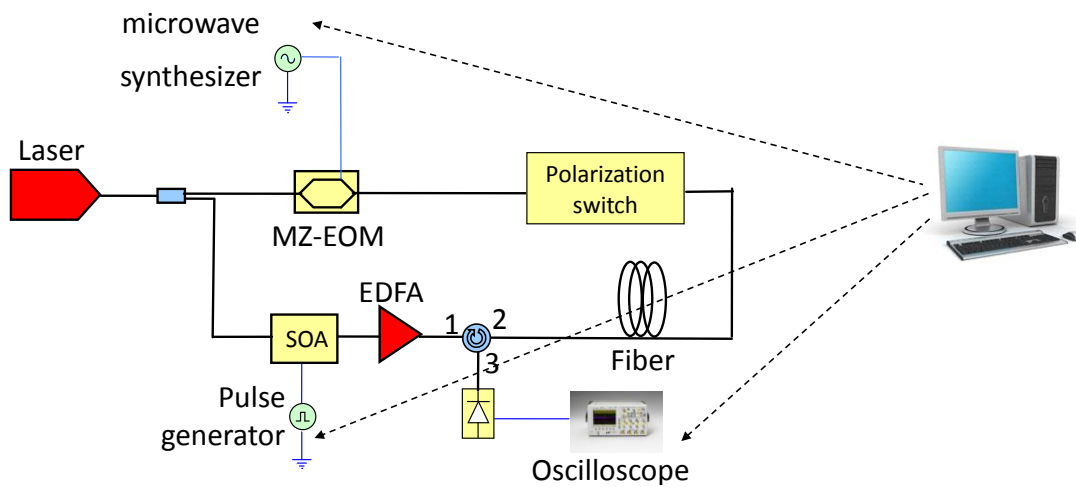

Figure 1.26: Experimental setup to take advantage of double spectral lines in probe wave to avoid non-local effects.
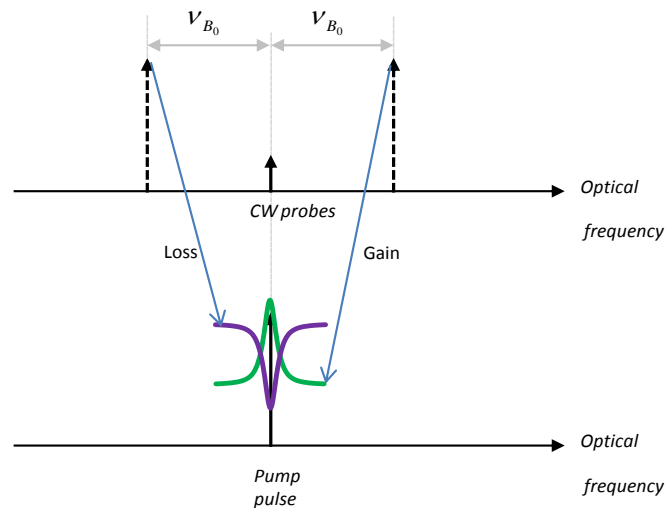

Figure 1.27: Non-local effect compensation using two spectral lines as probe powers.

1.6.5 TECHNIQUES TO REDUCE MEASURING TIME OR PERFORM DYNAMIC MEASUREMENTS

Some applications such as earthquake monitoring, wind caused strain monitoring, vibrations monitoring etc. find that BOTDA sensors are not able to fulfill their expectations because of the long time needed to perform BOTDA measurements. So, a very important potential market has forced a new research trend consisting in reducing BOTDA measuring time enough to perform distributed dynamic measurements.

This research trend is divided in two different approaches. The first, using multiple comb waves, consists in performing the complete frequency sweep in a single step, taking advantage of WDM and complex post-processing techniques. The second, the slope techniques, based on the continuous measurement of a BOTDA interaction at a fixed frequency shift between pump and probe, traduces the amplitude variations directly to Brillouin frequency shift variations.

The first approach was developed by Chaube et al. [CHAUBE 2008] and it is based on using a comb of peaks instead of a single probe. The system works in Brillouin loss. The pump wave is a single peak, at a fixed frequency shift from the carrier of the comb. The main concept is that the pulsed wave interacts with each of the probe peaks, and the loss generated is given by the frequency shift of each peak with the pump wave. This way the Brillouin profile is directly translated to the comb, as shown in figure 1.28. The peaks of the comb are equally spaced and their spacing must be as small as possible so that the entire Brillouin spectrum is mapped with a good enough frequency resolution. However, there is a limit for this spacing, and it is given by aliasing. The pump pulse broadens each probe peak, making it interact with its neighboring peaks. Pulse width, thus spatial resolution, is directly responsible for this broadening, because of the increase of bandwidth of the pulse spectrum. The shorter the pulse width, the bigger the space between peaks is needed. For example, for a 200ns long pulse (~20m resolution) a 3.5MHz spacing is enough, but for a 10ns pulse width (~1m resolution) a 70MHz spacing is needed. The overall bandwidth of the comb gives the measuring range.
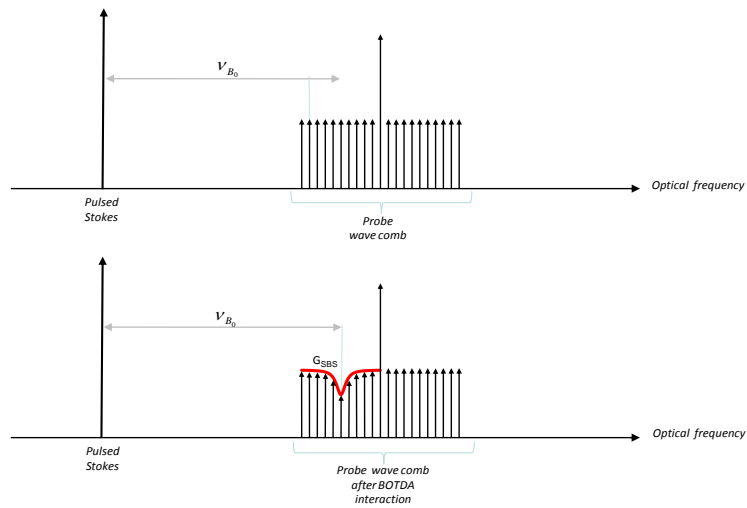
Figure. 1.28: Operation principle of the system developed by Chaube et al. [CHAUBE 2008].

The experimental setup that carries out these measurements is depicted in figure 1.29. Two lasers at a fixed frequency shift are stabilized by the so-called offset locking technique [LI 2008b]. One of the lasers, Laser 1, is used as Stokes wave, and is pulsed by modulating directly with base-band electrical pulses in a Mach-Zehnder electro-optic modulator (MZ-EOM1). Laser 2 is used to create the pump comb by electro-optic modulation in MZ-EOM2, with multiple RF tones generated in an arbitrary waveform generator (AWG). After the probe comb interacts with the counter-propagating Stokes pulse in the fiber, it is filtered and detected in a broadband photo-receiver through coherent detection. After the optical comb is translated to the electrical domain, it is mixed and processed, which basically consists separating each comb peak and envelope demodulating. The last step is to reconstruct the Brillouin spectra of each position with the data obtained from each peak of the comb.

The performance of this system is not very good, measuring with 12m resolution 500m of fiber with 20MHz spacing between peaks, it reaches an 813ue range at a 3.9-KHz frequency. Note that although the frequency of the measurement is very high, the overall data process of each measurement takes several seconds. Data about the accuracy of the sensor is not given.
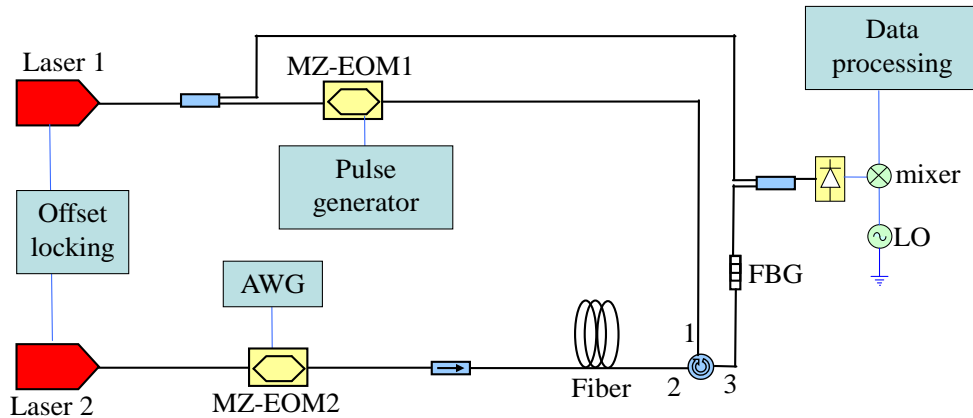
Figure 1.29: Experimental setup diagram of the system developed by Chaube et al. [2008 Chaube].

Another system that could be taken as an evolution of the previous, is the so-called Sweep-free BOTDA (SF-BOTDA), developed by Voskoboinik *et. al* [VOSKOBOINIK 2011]. In this case not only multiple probes but multiple pump pulses are used: two combs, one for probe wave and another for the pump wave. The main idea is to make each of the peaks of the probe interact with a single peak of the pulsed pump. Consequently the frequency spacing in the comb must be greater than in the previous case. Also the frequency spacing in the pump is different in pump, f_1, and probe waves, f_2, as shown in figure 1.30, so each pump and probe pair is at different frequency differences. This means that each interaction has a different frequency offset between pump and probe, and with enough peaks, the whole Brillouin spectrum is mapped. After the interaction, this results in the comb of probe waves being a comb of BOTDA traces, each one for a different frequency shift between pump and probe. So once detected, by filtering and demodulating each peak we have the BOTDA trace for each frequency difference. From now on the data processing is performed as with regular BOTDAs. In this case, the increment of spatial resolution, and thus greater Brillouin bandwidth, limits the spacing of the peaks, so the interaction does not affect the adjacent peaks. This last consideration, together with the fact that the comb cannot exceed ~11GHz (the Brillouin frequency shift), sets a trade-off between spatial resolution, measuring range and frequency resolution.
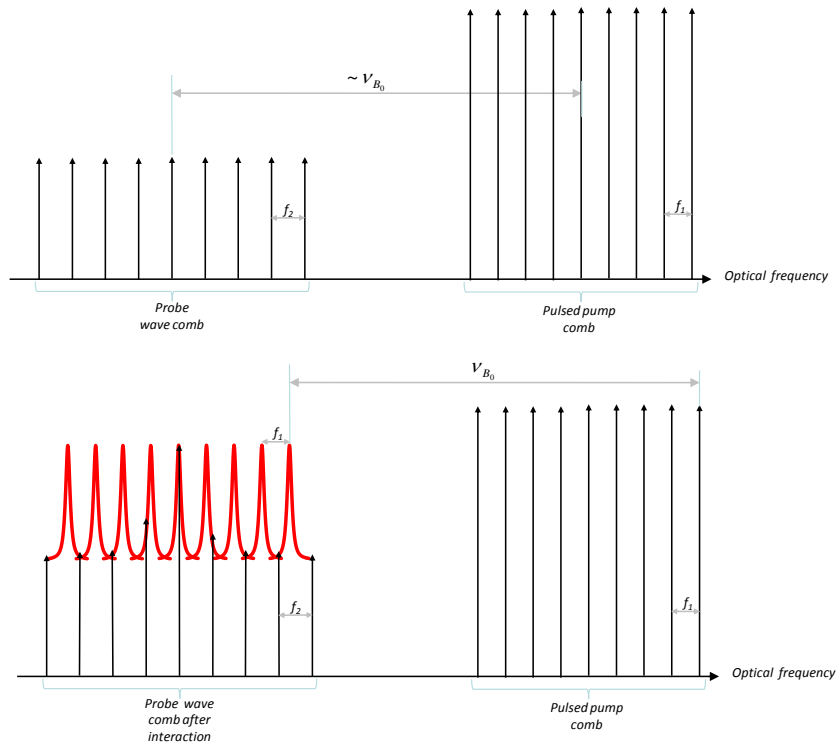
Figure 1.30: Operation principle for the SF-BOTDA.

In figure 1.31 the experimental setup for SF-BOTDA is depicted. The output of a laser is divided in two branches, in the upper the pump pulse comb is generated, while in the lower the probe comb is generated. The pump pulse comb in generated by the so-called RF-shaping of pump pulses technique, but for a comb of microwave peaks, which are directly translated to the optical domain in MZ-EOM1. EDFA1 and 2 amplify the optical signal to a desired level. Note that for a maximum amplification, each pulse of the comb has a different delay, which also prevents from pump inter-tone modulation [VOSKOBOINIK 2011]. The probe comb is generated with a comb of sinusoids mixed with a frequency near the Brillouin frequency shift of the fiber modulating the optical beam with MZ-EOM2. EDFA 3 and 4 are needed in order to amplify the wave to a given value. After the interaction the probe comb is detected with a broadband photo-receiver through self-heterodyne detection. The electrical signal resulting from optical to electrical conversion is processed so as to separate each BOTDA signal and properly reconstruct the Brillouin spectra along the fiber. With 50ns pump pulses (~5m resolution) in a 20-m long fiber, the total measuring time was calculated to be ~30usec and 280ue strain variations were clearly measured.

43

Figure. 1.31: Experimental setup diagram of the SF-BOTDA.

Regarding the other family of dynamic BOTDA sensors, they exploit similar principle as BOCDA dynamic sensors [SONG 2007], but taking advantage of simpler setups based on regular BOTDA. In the first approach, developed by Bernini et al [BERNINI 2009], just one pump pulse and one pulsed probe wave at a fixed frequency shift are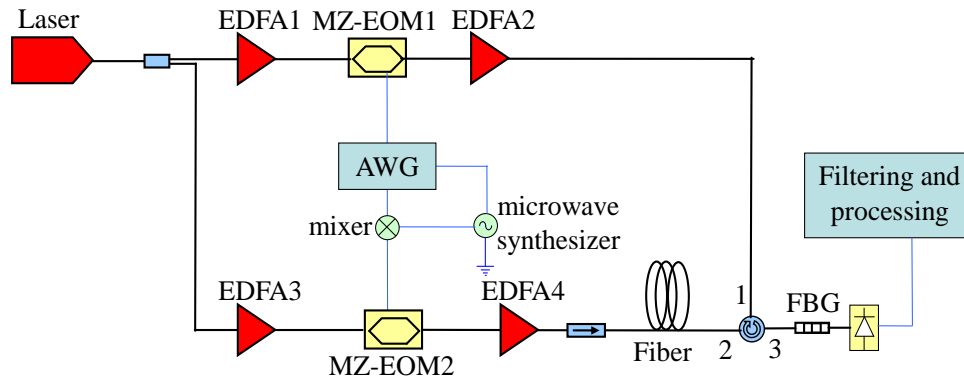 launched to the fiber. Since any strain/temperature change causes a variation in the frequency shift, it results in the alteration of the amplitude of the BOTDA interaction at the given position. So, by monitoring the BOTDA signal amplitude, we can have a real time measurement of the BFS in the fiber in a range given by the Brillouin FWHM as shown in figure 1.32. To be sure that we set the frequency shift between pump and probe in the exact value, a conventional BOTDA sweep is performed. After that, we choose the region in which we want to perform distributed measurements, take the corresponding frequency shift, and interrogate only this section of the fiber. The part interrogation of a single section of the fiber is performed using the time division multiplexing BOTDA (TDM-BOTDA) technique, which is explained in detail in chapter 4 of this thesis. Since the range of the measurement is not very large, using TDM-BOTDA helps us concentrate in a single region of the fiber. We can maximize the measuring range, because the frequency shift between the signals must coincide with half the BGS bandwidth at the location where the Brillouin interaction between both pulses occurs. The setup to perform this kind of measurement is the same as the BOTDA setup presented for TDM-BOTDA. Using 30ns pulses (~3m resolution) the dynamic range was limited to 35MHz, which corresponds to 700$\mu\varepsilon$, and measuring 30m of fiber at 98Hz, the accuracy is 95$\mu\varepsilon$.

The second approach, instead of using TDM-BOTDA, uses short enough pump pulses so as to increase the Brillouin FWHM and consequently the range of the measurement [CUI 2011]. Note that the range is supposed to be wide enough to be able to measure the whole fiber at once with a given frequency shift between pump and probe. However, shorter pump pulses involve smaller Brillouin gain, what directly translates in

a significant loss of SNR. The setup design would be any regular BOTDA setup. With 6.25ns pump pulses (~0.6m resolution) in a 168-m long fiber, a 160-MHz dynamic range is achieved, although the measurement quality is arguably poor, 8MHz of resolution. Another disadvantage of this family of dynamic BOTDA is that since the measurement is amplitude dependent, any mechanical stress that would vary the fiber loss, and hence the BOTDA amplitude, would cause more uncertainty in the measurements.

Hence we have seen that current dynamic BOTDA systems have some lack of performance quality compared with regular BOTDA. In other words, by decreasing the measuring time of BOTDA the measurement performance is jeopardized. Depending on the technique used, it can be the measurement accuracy, the spatial resolution or the measuring range what is greatly compromised.
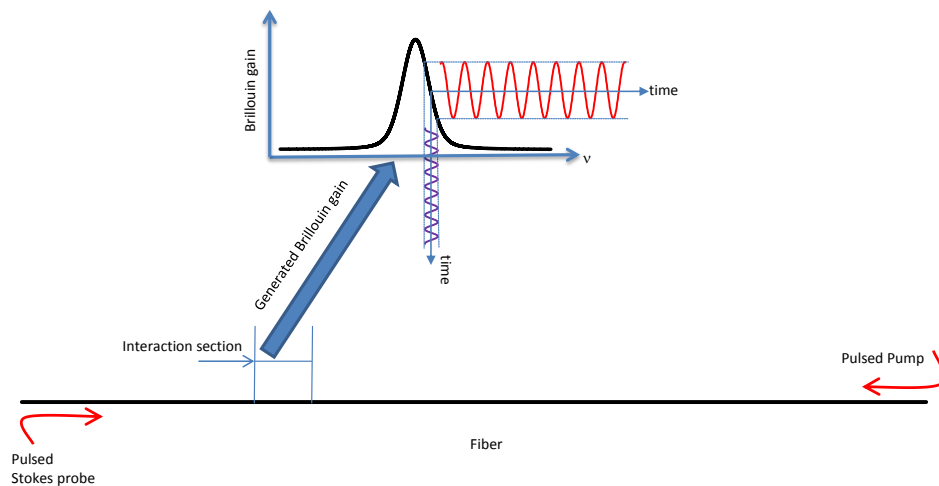
Figure. 1.32: Operation principle of the system developed by Bernini et al [2009 Bernini].

1.7 CONCLUSION

In this chapter we have presented a detailed overview of the fundamentals, limiting factors and current research lines in Brillouin distributed sensor, specially focusing in BOTDA sensors. We have seen that fiber optics sensors based on stimulated Brillouin scattering are a promising technology since they offer the possibility to perform distributed measurements in long fibers at high spatial resolutions. Hence, they can be deployed in numerous applications with the aim of monitoring the integrity of different structures.

We have first introduced SBS phenomenon in optical fibers and shown its potential to measure strain and temperature variations. This potential relies in the dependence that strain and temperature exhibit with the Brillouin frequency shift. Therefore by

measuring variation of these parameters, the strain and temperature of the fiber can be estimated.

Since in regular SMF, a cheap transducer with low loss, the Brillouin interaction is strong enough, this opens the field to distributed measurements. So, we have described the different techniques that can be deployed to perform distributed measurements based on SBS. Among them, we have specially focused in a detailed explanation of BOTDA. This is because the simplicity and good performance of this technique has focused much of the research in sensors based on SBS the last years, achieving better performance than with other techniques. Furthermore, is the contribution to the development of this technique that has centered the research of this thesis.

Therefore, a theoretical model describing BOTDA interaction has been presented in order to predict the systems behavior in laboratory and field measurements. As a consequence of the model, some of the limiting factors of BOTDA sensors have been introduced: non-local effects and SNR. The other limiting factors, such as discrimination of strain and temperature, MI, SPM, spontaneous Raman scattering, the maximum spatial resolution, the cost of the setup or the measuring time, have also been described in order to define the current research trends in BOTDA sensors. We have presented five main research trends in BOTDA sensors:

- Simplification of the setup and decrease cost is required in order to make feasible their widespread application.

- Development of temperature and strain discrimination techniques for a correct estimation of the environmental variations measured.

- Development of techniques to reduce measuring time.

- Developments of techniques to increase measuring range to monitor larger structures.

- Development of techniques for spatial resolution improvement so as to be able to measure cracks or small deformations.

Consequently, BOTDA sensors are an exciting new technology that is bound to have a very significant impact in a number of application fields. As it has been shown, its fundamentals are now clearly understood and research is currently focused on improving the sensor performance and reducing its cost so as to make its application feasible and effective. This is an ongoing effort by several research groups around the world that has lately led to a number of significant breakthroughs. Among the research

trends just described, we have centered this thesis in the research of the simplification of BOTDA sensors, the enlargement of their measuring range, combining the distributed sensing network with point sensor network, reducing non-local effects, and showing the ability to perform fast good quality dynamic measurements.

1.8   REFERENCES

[AGRAWAL 2006] G. Agrawal, Nonlinear Fiber Optics, Academic Press, 2006.

[ALAHBABI 2005] Alahbabi, M.N., Cho, Y.T. & Newson, T.P. 2005, "150-km-range distributed temperature sensor based on coherent detection of spontaneous Brillouin backscatter and in-line Raman amplification", *Journal of the Optical Society of America B: Optical Physics,* vol. 22, no. 6, pp. 1321-1324.

[ALASIA 2005] Alasia, D., Herráez, M.G., Abrardi, L., López, S.M. & Thévenaz, L. 2005, "Detrimental effect of modulation instability on distributed optical fibre sensors using stimulated Brillouin scattering", , pp. 587.

[ALASIA 2006]   Alasia, D., Fernandez Fernandez, A., Abrardi, L., Brichard, B. & Thévenaz, L. 2006, "The effects of gamma-radiation on the properties of Brillouin scattering in standard Ge-doped optical fibres", *Measurement Science and Technology,* vol. 17, no. 5, pp. 1091-1094.

[ANGULO 2012] Angulo-Vinuesa, X., Martin-Lopez, S., Corredera, P. & Gonzalez-Herraez, M. 2012, "Raman-assisted Brillouin optical time-domain analysis with sub-meter resolution over 100 km", *Optics Express,* vol. 20, no. 11, pp. 12147-12154.

[BAO 1995] Bao, X., Dhliwayo, J., Heron, N., Webb, D.J. & Jackson, D.A. 1995, "Experimental and theoretical studies on a distributed temperature sensor based on Brillouin scattering", *Journal of Lightwave Technology,* vol. 13, no. 7, pp. 1340-1348.

[BAO 1999] Bao, X., Brown, A., DeMerchant, M. & Smith, J. 1999, "Characterization of the Brillouin-loss spectrum of single-mode fibers by use of very short (<10-ns) pulses", *Optics Letters,* vol. 24, no. 8, pp. 510-512.

[BAO 2004] Bao, X., Yu, Q. & Chen, L. 2004, "Simultaneous strain and temperature measurements with polarization- maintaining fibers and their error analysis by use of a distributed Brillouin loss system", *Optics Letters,* vol. 29, no. 12, pp. 1342-1344.

[BERNINI 2009] Bernini, R., Minardo, A. & Zeni, L. 2009, "Dynamic strain measurement in optical fibers by stimulated brillouin scattering", *Optics Letters,* vol. 34, no. 17, pp. 2613-2615.

[BERNINI 2011] Bernini, R., Minardo, A. & Zeni, L. 2011, "Long-range distributed Brillouin fiber sensors by use of an unbalanced double sideband probe", *Optics Express,* vol. 19, no. 24, pp. 23845-23856.

[BERNINI 2012] Bernini, R., Minardo, A. & Zeni, L. 2012, "Distributed sensing at centimeter-scale spatial resolution by BOFDA: Measurements and signal processing", *IEEE Photonics Journal,* vol. 4, no. 1, pp. 48-56.d

[BEUGNOT 2011] Beugnot, J., Tur, M., Mafang, S.F. & Thévenaz, L. 2011, "Distributed Brillouin sensing with sub-meter spatial resolution: Modeling and processing", *Optics Express,* vol. 19, no. 8, pp. 7381-7397.

[BROWN 2007] Brown, A.W., Colpitts, B.G. & Brown, K. 2007, "Dark-pulse Brillouin optical time-domain sensor with 20-mm spatial resolution", *Journal of Lightwave Technology,* vol. 25, no. 1, pp. 381-386.

[CHAUBE 2011] Chaube, P., Colpitts, B.G., Jagannathan, D. & Brown, A.W. 2008, "Distributed fiber-optic sensor for dynamic strain measurement", *IEEE Sensors Journal,* vol. 8, no. 7, pp. 1067-1072.

[CUI 2011] Cui, Q., Pamukcu, S., Xiao, W. & Pervizpour, M. 2011, "Truly distributed fiber vibration sensor using pulse base BOTDA with wide dynamic range", *IEEE Photonics Technology Letters,* vol. 23, no. 24, pp. 1887-1889.

 [CUMMINS 1972]   H. Z. Cummins, P. E. Schoen, "Linear Scattering from Thermal Fluctuations," in *Laser Handbook, Vol 2*, cap. E1, Amsterdam: North-Holland, 1972.

 [DIAZ 2008] Diaz, S., Mafang, S.F., Lopez-Amo, M. & Thévenaz, L. 2008, "A high-performance optical time-domain brillouin distributed fiber sensor", *IEEE Sensors Journal,* vol. 8, no. 7, pp. 1268-1272.

[DONG 2010] Dong, Y., Chen, L. & Bao, X. 2010, "System optimization of a long-range Brillouin-loss-based distributed fiber sensor", *Applied Optics,* vol. 49, no. 27, pp. 5020-5025.

[DONG 2012] Dong, Y., Zhang, H., Chen, L. & Bao, X. 2012, "2 cm spatial-resolution and 2 km range Brillouin optical fiber sensor using a transient differential pulse pair", *Applied Optics,* vol. 51, no. 9, pp. 1229-1235.

 [FENG 2012] Feng, K.-., Wu, C.-., Yan, J.-., Lin, C.-. & Peng, P.-. 2012, "Fiber Bragg Grating-Based Three-Dimensional Multipoint Ring-Mesh Sensing System With Robust Self-Healing Function", *IEEE Journal on Selected Topics in Quantum Electronics* .

[FOALENG 2010] Foaleng, S.M., Tur, M., Beugnot, J.-. & Thévenaz, L. 2010, "High spatial and spectral resolution long-range sensing using Brillouin echoes", *Journal of Lightwave Technology,* vol. 28, no. 20, pp. 2993-3003.

[FOALENG 2011a] S. M. Foaleng and L. Thévenaz, "Impact of Raman scattering and modulation instability on the performances of Brillouin sensors," Proceedings of SPIE 7753, paper 77539V, 2011.

[FOALENG 2011b] Foaleng, S.M., Rodríguez-Barrios, F., Martin-Lopez, S., González-Herráez, M. & Thévenaz, L. 2011, "Detrimental effect of self-phase modulation on the performance of Brillouin distributed fiber sensors", *Optics Letters,* vol. 36, no. 2, pp. 97-99.

[GARUS 1996] Garus, D., Krebber, K., Schliep, F. & Gogolla, T. 1996, "Distributed sensing technique based on Brillouin optical-fiber frequency-domain analysis", *Optics Letters,* vol. 21, no. 17, pp. 1402-1404.

[GEINITZ 1999] Geinitz, E., Jetschke, S., Röpke, U., Schröter, S., Willsch, R. & Bartelt, H. 1999, "The influence of pulse amplification on distributed fibre-optic Brillouin sensing and a method to compensate for systematic errors", *Measurement Science and Technology,* vol. 10, no. 2, pp. 112-116.

 [HORIGUCHI 1989] Horiguchi, T. & Tateda, M. 1989, "BOTDA - Nondestructive measurement of single-mode optical fiber attenuation characteristics using Brillouin interaction: Theory", *Journal of Lightwave Technology,* vol. 7, no. 8, pp. 1170-1176.

[HORIGUCHI 1995] Horiguchi, T., Shimizu, K., Kurashima, T., Tateda, M. & Koyamada, Y. 1995, "Development of a distributed sensing technique using Brillouin scattering", *Journal of Lightwave Technology,* vol. 13, no. 7, pp. 1296-1302.

[HOTATE 2000] Hotate, K. 2000, "Measurement of brillouin gain spectrum distribution along an optical fiber using a correlation-based technique-proposal, experiment and simulation-", *IEICE Transactions on Electronics,* vol. E83-C, no. 3, pp. 405-411.

 [KALOSHA 2006] Kalosha, V.P., Ponomarev, E.A., Chen, L. & Bao, X. 2006, "How to obtain high spectral resolution of SBS-based distributed sensing by using nanosecond pulses", *Optics Express,* vol. 14, no. 6, pp. 2071-2078.

[KISHIDA 2005] Kishida, K., Che-Hien, L. & Nishiguchi, K. 2005, "Pulse pre-pump method for cm-order spatial resolution of BOTDA", *Proceedings of SPIE - The International Society for Optical Engineering*, pp. 559.

[KISHIDA 2008] Kishida, K., Li, C.H., Mizutani, T. & Takeda, N. 2008, "2 cm spatial resolution brillouin distributed sensing system using PPP-BOTDA method", *Materials Forum,* vol. 33, pp. 23-26.

[LECŒUCHE 1998] Lecœuche, V., Webb, D.J., Pannell, C.N. & Jackson, D.A. 1998, "Brillouin based distributed fibre sensor incorporating a mode-locked brillouin fibre ring laser", *Optics Communications,* vol. 152, no. 4-6, pp. 263-268.

[LEE 2001] Lee, C.C., Chiang, P.W. & Chi, S. 2001, "Utilization of a dispersion-shifted fiber for simultaneous measurement of distributed strain and temperature through Brillouin frequency shift", *IEEE Photonics Technology Letters,* vol. 13, no. 10, pp. 1094-1096.

[LI 2008a] Li, W., Bao, X., Li, Y. & Chen, L. 2008, "Differential pulse-width pair BOTDA for high spatial resolution sensing", *Optics Express,* vol. 16, no. 26, pp. 21616-21625.

[LI 2008b] Li, Y., Bao, X., Ravet, F. & Ponomarev, E. 2008, "Distributed Brillouin sensor system based on offset locking of two distributed feedback lasers", *Applied Optics,* vol. 47, no. 2, pp. 99-102.

[LIU 2012] Liu, X. & Bao, X. 2012, "Brillouin spectrum in LEAF and simultaneous temperature and strain measurement", *Journal of Lightwave Technology,* vol. 30, no. 8, pp. 1053-1059.

[MINARDO 2005] Minardo, A., Bernini, R., Zeni, L., Thevenaz, L. & Briffod, F. 2005, "A reconstruction technique for long-range stimulated Brillouin scattering distributed fibre-optic sensors: Experimental results", *Measurement Science and Technology,* vol. 16, no. 4, pp. 900-908.

[MINARDO 2011] Minardo, A., Bernini, R. & Zeni, L. 2011, "Numerical analysis of single pulse and differential pulse-width pair BOTDA systems in the high spatial resolution regime", *Optics Express,* vol. 19, no. 20, pp. 19233-19244.

[NIKLES 1997] Niklès, M., Thévenaz, L. & Robert, P.A. 1997, "Brillouin gain spectrum characterization in single-mode optical fibers", *Journal of Lightwave Technology,* vol. 15, no. 10, pp. 1842-1851.

[SONG 2006] Song, K.Y., He, Z. & Hotate, K. 2006, "Distributed strain measurement with millimeter-order spatial resolution based on Brillouin optical correlation domain analysis", *Optics Letters,* vol. 31, no. 17, pp. 2526-2528.

[SONG 2007] Song, K.-. & Hotate, K. 2007, "Distributed fiber strain sensor with 1 kHz sampling rate based on Brillouin optical correlation domain analysis", *Proceedings of SPIE - The International Society for Optical Engineering*, 67700J.

[SOTO 2009] Soto, M.A., Bolognini, G., Di Pasquale, F. & Thévenaz, L. 2010, "Simplex-coded BOTDA fiber sensor with 1 m spatial resolution over a 50 km range", *Optics Letters,* vol. 35, no. 2, pp. 259-261.

[SOTO 2010] Soto, M.A., Bolognini, G. & Pasquale, F.D. 2010, "Analysis of pulse modulation format in coded BOTDA sensors", *Optics Express,* vol. 18, no. 14, pp. 14395-14400.

[SOTO 2011] Soto, M.A., Bolognini, G. & Di Pasquale, F. 2011, "Optimization of long-range BOTDA sensors with high resolution using first-order bi-directional Raman amplification", *Optics Express,* vol. 19, no. 5, pp. 4444-4457.

[SOTO 2012] Soto, M.A., Nannipieri, T., Signorini, A., Lazzeri, A., Baronti, F., Roncella, R., Bolognini, G. & Pasquale, F.D. 2011, "Raman-based distributed temperature sensor with 1m spatial resolution over 26km SMF using low-repetition-rate cyclic pulse coding", *Optics Letters,* vol. 36, no. 13, pp. 2557-2559.

[THEVENAZ 2004] Thévenaz, L., Le Floch, S., Alasia, D. & Troger, J. 2004, "Novel schemes for optical signal generation using laser injection locking with application to Brillouin sensing", *Measurement Science and Technology,* vol. 15, no. 8, pp. 1519-1524.

[THEVENAZ 2011] Thévenaz, L., Foaleng Mafang, S. & Lin, J. 2011, "Impact of pump depletion on the determination of the Brillouin gain frequency in distributed fiber sensors", *Proceedings of SPIE - The International Society for Optical Engineering*, 775322.

[THOMPSON 1993] Thompson, W.J. 1993. "Numerous Neat Algorithms for the Voigt Profile Function", *Computational Physics*, vol. 7, pp. 627.

 [VOSKOBOINIK 2011] Voskoboinik, A., Yilmaz, O.F., Willner, A.W. & Tur, M. 2011, "Sweep-free distributed Brillouin time-domain analyzer (SF-BOTDA)", *Optics Express,* vol. 19, no. 26, pp. B842-B847.

[WELLS 1999] Wells, R.J., 1999 "Rapid approximation to the Voigt/Faddeeva function and its derivatives", *Journal of Quantitative Spectroscopy and Radiative Transfer*, vol. 62, no.11, pp. 29-48.

[WYLIE 2011] Wylie, M.T.V., Colpitts, B.G. & Brown, A.W. 2011, "Fiber optic distributed differential displacement sensor", *Journal of Lightwave Technology,* vol. 29, no. 18, pp. 2847-2852.

[ZOU 2008] Zou, W., He, Z. & Hotate, K. 2008, "Investigation of strain- and temperature-dependences of Brillouin frequency shifts in GeO2-doped optical fibers", *Journal of Lightwave Technology,* vol. 26, no. 13, pp. 1854-1861.

[ZOU 2009] Zou, W.W., He, Z. & Hotate, K. 2009, "Complete discrimination of strain and temperature using Brillouin frequency shift and birefringence in a polarization-maintaining fiber", *Optics Express,* vol. 17, no. 3, pp. 1248-1255.

CHAPTER 2

RF-SHAPING OF PUMP PULSES FOR BOTDA

2.1   INTRODUCTION

The main challenges in long-range sensing are to simplify the setups, to increase the sensing range and to compensate measurement errors caused by non-local effects. Most BOTDA implementations are complex and use expensive components such as multiple electro-optic modulators, semiconductor optical amplifiers, synthesized microwave generators or wideband detectors. Therefore, a major line of research in these sensors is to simplify the experimental setups so as to achieve a cost-effective commercial system. Some examples of contributions in this area include the deployment of injection locking to generate the pump and probe waves using inexpensive DFB lasers [THEVENAZ 2004], the use of Brillouin generators or Brillouin fiber lasers to obtain the probe wave from the pump [LECŒUCHE 1998] or the use of offset-locking [LI 2008] as presented in chapter 1 of this thesis.

When optical devices such as optical modulators are used to shape the pump pulse there is always a residual DC base or leakage. When this level is great enough, there are two different interactions happening in the fiber: the interaction between pump pulse and probe that we seek in BOTDA systems and the residual interaction between pump leakage and probe. Depending on the length of the fiber and the leakage and probe power levels the residual interaction can be stronger than the pulse-probe interaction. This can be useful in short-range high-resolution measurements, because it pre-excites the acoustic wave and makes the interaction between pump pulses and

53

probe stronger [KALOSHA 2006]. However, in long range measurements, it can be very destructive. While the leakage interacts with the probe, the latter is amplified.

The extra power in the probe wave makes the interaction with the pump pulse greater, obtaining a higher depletion of the pump pulse. Consequently, the errors given by non-local effects are increased in the measurements. There are also some other negative side effects such as a larger computational complexity during the processing of the data and a potentially greater quantification noise. Therefore, in long range BOTDA measurements, it is of the essence to minimize the leakage of pump pulses.

In this chapter we investigate the enhancement of non-local effect induced error due to leakage interaction and present an alternative high ER pump pulse shaping technique that leads to a simplified BOTDA sensing setup. It is based on shaping pump pulses in the RF domain, where it is easier and cheaper to obtain high ER pulses, and then translating them directly to the optical domain [ZORNOZA 2009, ZORNOZA 2010].

2.2   THEORETICAL STUDY OF THE BEHAVIOR OF LONG RANGE BOTDA WITH PUMP PULSE LEAKAGE

When pulsing the pump wave with devices such as electro optic modulators (EOMs), a residual DC base or leakage is present in the wave, which is travelling together with the pulse. In this case, as it has been introduced, there is SBS interaction between the leakage and probe in addition to that between the pulse and the probe. The gain of this interaction varies with the frequency shift between pump and probe and sets a different base line for every frequency shift difference of the BOTDA sweep, f_i, as depicted in figure 2.1. The baseline maximum level is reached when the frequency shift between pump and probe equals the average Brillouin frequency shift of the fiber, ν_B.
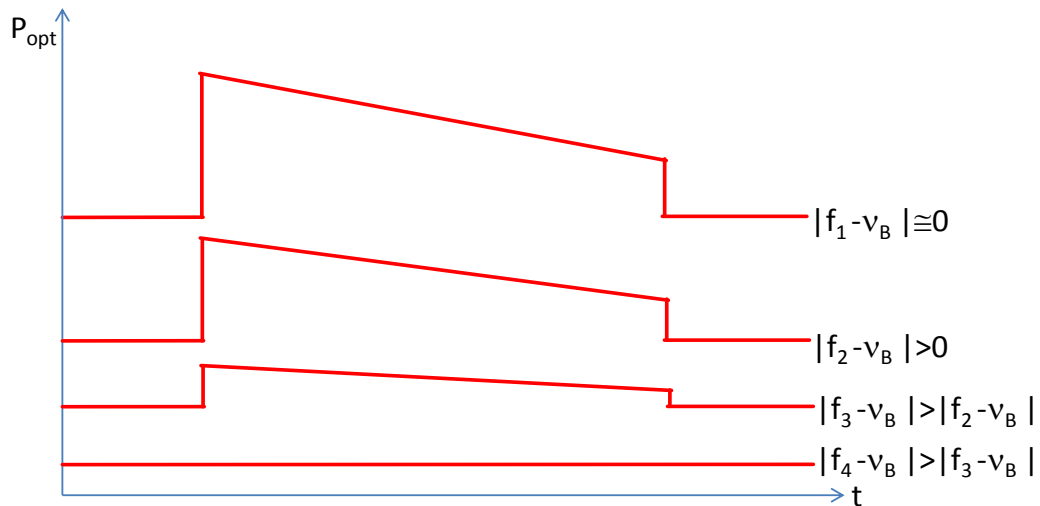
Figure 2.1: representation of the variation of the baseline of the BOTDA interaction signal depending on the frequency shift between pump and probe, when leakage of the pump signal is present.

The theoretical model introduced in chapter 1 is a valid approximation if the pulsed wave has a very high ER or if the fiber is very short, hence the SBS interaction between the leakage and the CW gain is negligible. However, if this is not the case, the interaction between pump leakage and CW must be taken into account and be included in the model.

Some authors consider the effect of the leakage decoupled from the SBS interaction between pulsed and CW beams [RAVET 2007]. Hence, the total Brillouin spectrum is the product of two different contributions: pulsed-CW and leakage-CW beams SBS interactions. Nevertheless, this approximation is just valid for short fiber sensors. In long fibers, because of the interaction with the leakage, the CW level in every section is not given just by the loss of the fiber. So the interaction between pump pulse and CW is affected too, because of the different value of the later due to the residual interaction.

In order to include the effect of leakage in long range BOTDA sensors we propose a modified theoretical model that does not require the approximation of decoupled SBS effects. We do so by taking into account three consecutive SBS interactions. As schematically depicted in Figure 2.2, the SBS interactions are divided in three steps. Assuming that the pulse is in the position z of the fiber, the first step is to solve the leakage-CW SBS interaction all along the fiber until this position. Equations (1.1) and (1.2) can be solved for two counter propagating continuous waves ($I_P=I_L$ and $I_S=I_{CW}$). Boundary conditions are the input CW intensity ($I_{CW}(L)=I_{CW}$) and the input leakage intensity ($I_L(0)=I_{P0}/ER$, where I_{P0} is the input peak intensity of the pulsed pump beam and ER is the extinction ratio of the device used to pulse the optical beam).

55

This method will provide a numeric solution for the CW after interacting with the leakage over the whole fiber length, *I*CW(z)*. Note that the effect of this interaction is to increase the CW power at each fiber position when working in gain BOTDA configuration.
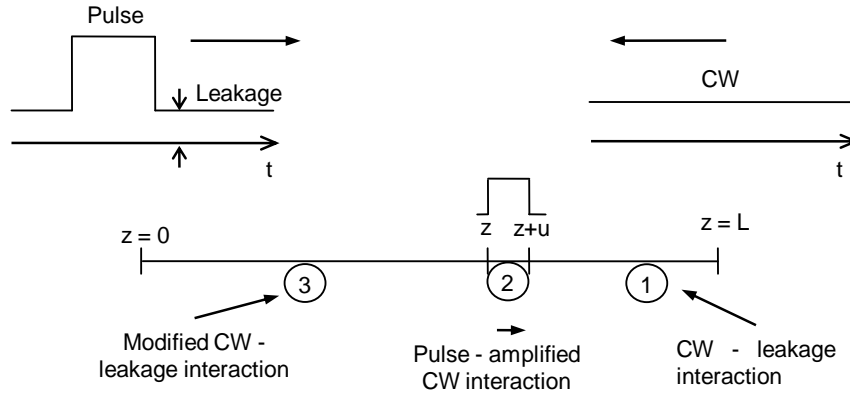

Figure 2.2: Scheme of the three different SBS interactions considered by the theoretical model.

The second step is to solve the interaction between pump pulse and modified CW, which will be made following the same steps as in the previous model. Substituting the probe wave, *IS*, by the new value of the amplified CW, *I*CW(z)*, in (1.1), we can get a numeric solution for the evolution of the pulsed wave power (*IP*) as follows:

$$I_P(v,z) = I_P(0) \cdot Exp\left[\int_0^z - g_B(v,z) \cdot I_{CW}^*(v,z)dz - \alpha \cdot z\right]$$

(2.1)

The same as in the previous model, by substituting (2.1) in the differential equations of chapter 1 (1.11), and integrating over the interaction region between the pulse and the amplified CW wave at position z, an expression for the gain experienced by the CW is obtained. The result is:

$$G_{SBS}(v,z) = \frac{I_{CW}^{**}(v,z)}{I_{CW}^*(v,z+u)} = Exp\left\{-\int_z^{z+u} g_B(v,z)I_P(0)Exp\left[\int_0^z\left(-g_B(v,z)I_{CW}^*(v,z)-\alpha z\right)dz\right]dz + \alpha \cdot u\right\}$$ (2.2)

Then, the CW intensity value after interacting with the leakage and the pulsed beam, *I**CW(v,z)*, can be obtained as follows:

$$I_{CW}^{**}(v,z) = I_{CW}^*(v,z+u) \cdot G_{SBS}(v,z)$$

(2.3)

Note that equations (2.1)-(2.3) are the same as the equation in chapter 1 (1.12)-(1.14) but with a different value of CW power. In view of the fact that we are looking for a

received intensity expression, another SBS interaction between the new modified CW, $I^{**}_{CW}(v,z)$, and the leakage must be considered. This final step takes place in the region after the interaction with the pulsed beam. We can solve this interaction with the very same method previously used to solve the first interaction between CW and leakage. Nevertheless, the boundary conditions are for the BOTDA signal $I_S=I^{**}_{CW}(v,z)$ and for the input leakage intensity $I_L(0)=I_P/ER$ in this case. So, by repeating this three steps for every section of fiber from z=0 to L, we can study the theoretical evolution of the BOTDA interaction with non-ideal ER pump pulses.

In figure 2.3 we show a simulation of a measurement of 25Km of fiber with 20m resolution using pump pulses of 20dBm with 29dB ER. The last 300m of the fiber have a different Brillouin frequency shift. However we can see that the spectra in this section are distorted, they do not follow a Lorentzian profile any more. Consequently, when low ER pulses are used a correction must be performed taking as reference the interaction between the leakage and the Stokes wave. This way we minimize the contribution of the leakage and concentrate in the interaction between pump pulses and stokes. However, since the baseline difference affects the average power of the electrical signal after detection, a greater scale in detection oscilloscopes is needed, what can increase significantly quantification noise.
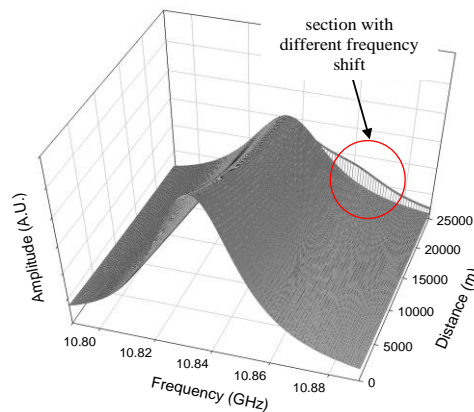
Figure 2.3: Evolution of the Brillouin spectrum along the fiber. The section with different Brillouin frequency shift (300m-long) is distorted because of the leakage presence. The parameters are: L = 25km, Δz = 20m, P_P = 20dBm, P_{CW} = -3dBm, ER = 29dB.

The spectrum of the interaction when no pulse is present in the fiber can be reconstructed with the base level value of the trace of each interaction. This spectrum, $H_{LC}(v)$, only depends on the frequency shift between leakage and CW, so its contribution is not time-dependent and can be threatened as independent from the

gain caused by the pulse. Then, so as to isolate the gain produced by the pulse we define the correction:

$$H_{SBS}(v) = \frac{H_M(v,z)}{H_{LC}(v)} \qquad (2.4)$$

Where $H_M(v)$ is the measured spectrum at each location. Note that to perform correction (2.4) properly, require that signals are detected using a photodiode operating with DC coupling. This is similar to the so-called AC detection used in the literature [KALOSHA 2006], but instead of subtracting the interaction between leakage and CW, we divide by it. This way we concentrate in the percentage of gain generated by BOTDA interaction. Note that when the leakage level is very low and the interaction between leakage and CW is negligible, correction (2.4) is unnecessary.

In figure 2.4, we depict the spectrum for the last section of a 50Km fiber with a Brillouin frequency shift of 10.830GHz, measured with 10ns long 30dBm pump pulses. The CW power is -5.5dBm and the Brillouin frequency shift of the last section is 10.850GHz. In the first spectrum, in figure 2.3(a), the ER was set to 80dB and no correction has been performed. We can clearly see that the measurement is perfectly performed. On the contrary, in figure 2.3(b), where the ER was set to 25dB, the Brillouin frequency shift difference cannot be measured. So correction (2.4) has been performed for figure 2.3(c). This spectrum shows how this correction reduces leakage contribution. However, the correction does not suppress the error generated by depletion of the pulse through non-local effects. Furthermore we can see how the compensated spectrum of figure 2.3(c) has an error in the frequency of the maximum because of this effect.

In order to study with deeper detail the enhancement of the error given by non-local effects a set of simulations was performed. We varied the pump powers, the probe powers, and ER values so as to see the dependence of the error with leakage power and with probe power. In figure 2.4(a) we depict what happens while increasing the pump powers, with the probe power fixed to a value of -5.5dBm. Note that increasing the pump power for a fixed value of ER is equivalent to amplify both, pump pulse power and the leakage power the same amount. The error is greater for the greatest pump powers with lowest ER, which correspond to greater leakage levels. So the lower the leakage level, the lower the error induced by it.

In figure 2.4(b) we confirm that the greater the CW power, the greater the non-local effect induced error, as has been seen in chapter 1. But in addition, we can see that it is strongly affected by the ER value. As the ER decreases, the error grows significantly, and it is even doubled for ERs near 20dB. We can see that for ER levels greater than

40dB, the effect of the leakage is negligible. Therefore, in this system, a leakage level greater than -10dBm, would be a negligible value for non-local effect induced error.

Consequently the ER must be maximized for enhancing the measuring accuracy of the setup. Solutions to improve ER of pump pulses have been proposed using some of the setups presented in chapter 1: the injection locking method [THÉVENAZ 2004], using semiconductor optical amplifiers as optical switches [DIAZ 2008] or using specialty ultra-high extinction ratio electro-optic modulators [LI 2008]. Nonetheless, these solutions have a negative impact in the complexity and the cost of the setup.

(a) *(b)* *(c)*
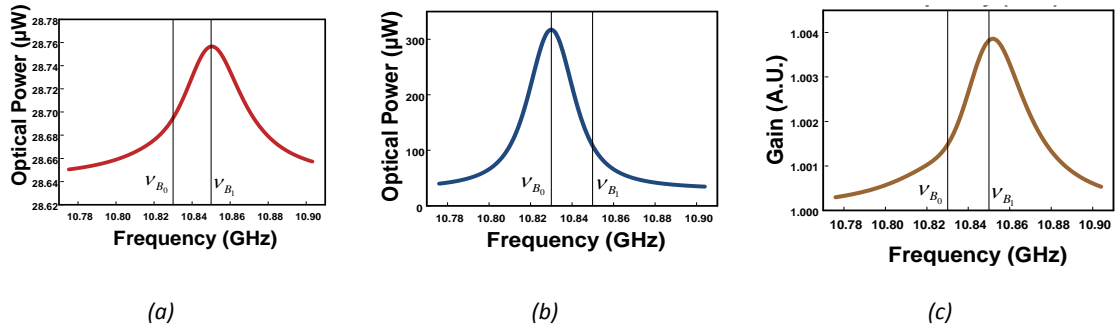
Figure 2.4: Simulated spectra for the final section of a 50-km long fiber with 10.830GHz Brillouin frequency shift in the first 49.7Km and 10.850GHz in the last 0.3Km measured with 10ns pulses of 30dBm keeping the probe to -5.5dBm. In (a) the ER of the pulse was fixed to 80dB while in (b) and (c) the ER was set to 25dB. The difference between (b) and (c) is that correction (2.4) was only performed in the later.

(a) *(b)*
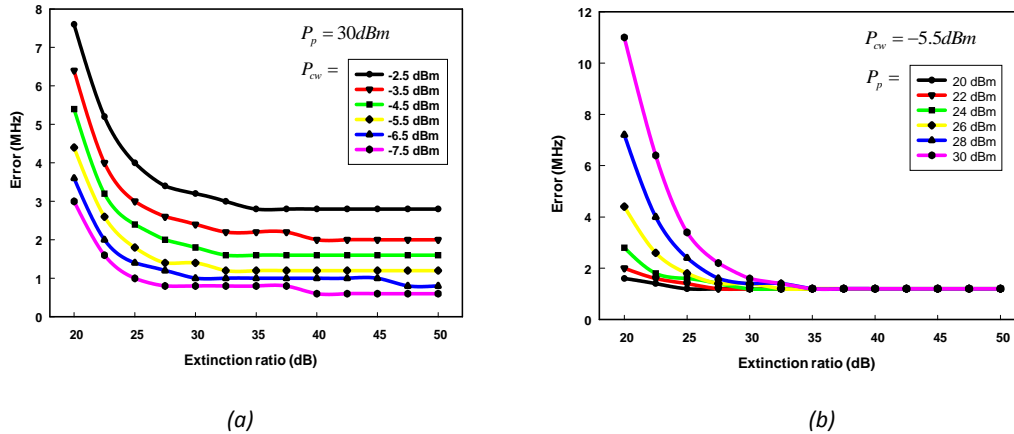
Figure 2.5: Error in the measurements for the final section of a 50-km long fiber with 10.830GHz Brillouin frequency shift in the first 49.7Km and 10.850GHz in the last 0.3Km measured with 10ns pulses of 30dBm and variable probe power (a) or a fixed value of -5.5dBm for the probe power while varying the pump pulse power (b).

2.3   RF SHAPING OF PUMP PULSES THEORY

In microwave photonics, it is usual to take advantage of devices and technology other than photonic and fiber optic devices, such as microwave or radio frequency (RF)

devices. What it is more, between optics and RF technology there are punctual applications in which is better to take advantage from one or the other technology. Therefore, although there are aspects, like propagation loss or electro-magnetic immunity, that make fiber optics a more interesting technology, there are applications more suited for RF devices. In RF technology, there are many devices that have a better and more stable behavior at a lower cost compared to the ones available in fiber optics technologies. For example RF switches can generate RF pulses with up to 80dB isolation or ER, values which are not possible modulating directly in the optical domain and are very interesting in BOTDA sensors [ZORNOZA 2010]. We can take advantage of this and obtain high performance pulses by translating such signals from the electrical to the optical domain with devices such as electro-optic modulators (EOM), which translate the shape of an RF signal directly from the electrical to the optical domain.
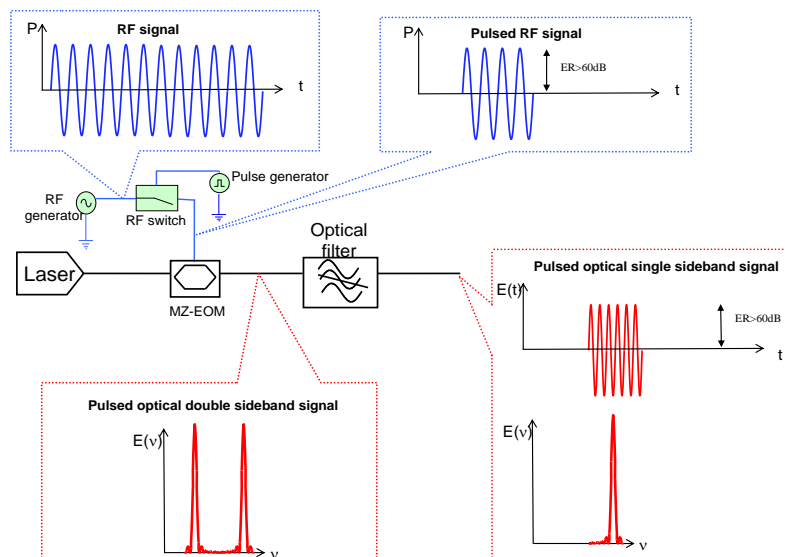
Figure 2.6: Fundamentals of the RF shaping of optical pump pulses.

The RF shaping of pump pulses technique consists in this: pulsing an RF continuous signal using a microwave switch and then translating this pulse to the optical domain so the characteristics of the RF pulse are also present after the electrical to optical conversion.

Commercial RF switches are low cost, available with very fast responses (up to 1ns) and extremely high isolation. An RF single-pole/single-throw switch has two inputs and an output. The output signals must be a continuous RF signal of a given power and a pulsed signal with a usually higher amplitude that TTL. When the pulsed signal is greater than the pulse (a "1") the output of the signal equals the input RF signal (with the insertion losses). But when the pulsed signal is lower than TTL (a "0") the output

signal is near none, of up to 80dB lower than the output when it is a "1". Therefore, it is possible to obtain fast pulses of RF energy with extremely high extinction ratio.

As depicted in figure 2.6, these signals can be applied to a MZ-EOM operating at the minimum of its transfer curve so as to generate an ODSB-SC modulation. The sidebands of this modulation will have the same shape and frequency (from the carrier) than the RF signal. The RF pulse shape is directly translated to the optical domain by the modulator; thus two sidebands pulsed with very high extinction ratio are generated. Then, since just a single optical pulse is needed, this pulsed optical double sideband suppressed carrier modulation (ODSB-SC) is filtered with an optical filter to select one of the sidebands. Therefore, we end up having an ultra-high extinction ratio pulsed pump wave with a frequency difference from the carrier given by the RF signals frequency.

Moreover, since these pulses have a frequency shift from the carrier given by the RF signal used for the generation of the RF pulses, this frequency can be swept near the Brillouin frequency shift of the fiber. Consequently we can deploy this technique in a regular BOTDA setup in order to generate pump pulses with high extinction ratio and the frequency shift and frequency sweep in the same step.

2.4   EXPERIMENTAL SETUP AND MEASUREMENTS

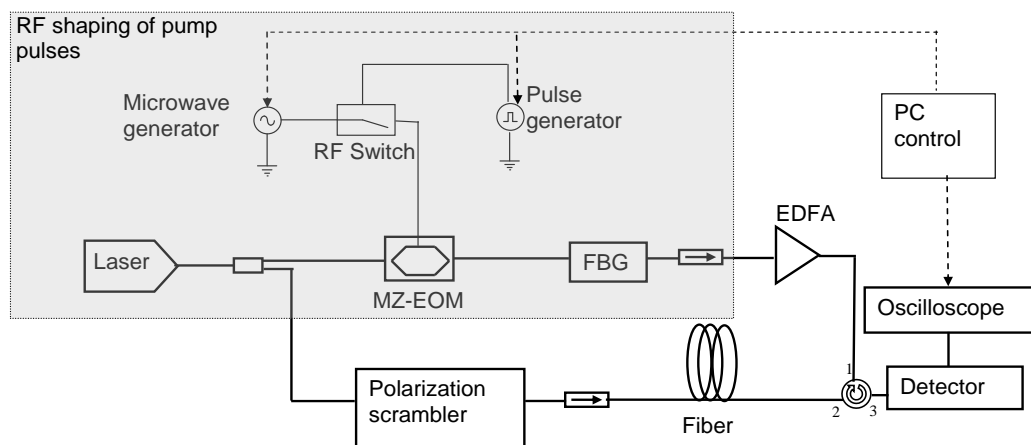*Figure 2.7: Experimental setup of the proposed high-extinction-ratio and simplified BOTDA sensing scheme.*

So as to implement the RF-shaping scheme in a BOTDA setup, we propose the scheme shown in figure 2.6 [ZORNOZA 2010]. It can be seen that in the upper part, the same RF-shaping setup explained in figure 2.5 is present. In the following paragraphs a detailed explanation of the rest of the setup working principle is given.

The output of a single mode laser is first divided in two branches by an optical coupler, so that the same light source is used for pump and Stokes generation. In the upper branch the RF shaping of pump optical pulses is performed, achieving the pulsing and frequency shifting in a single step, as explained in the previous section. The optical filter that we use is a narrow FBG centered near the unwanted sideband of the modulation. An Erbium-doped fiber amplifier (EDFA) is used to amplify the pulses to the desired level. Finally we direct them to the fiber under test using a circulator.

In the lower branch the laser output is directly used to provide the probe wave. Just a passive polarization scrambler is used to compensate the polarization sensitivity of SBS [DIAZ 2008]. The BOTDA signal is directed to a 125-MHz detector by a circulator and is visualized in a digital oscilloscope. A computer is used to control all the instruments by GPIB bus, so it performs the frequency sweep of the RF generator, defines the pulse width and period, captures the BOTDA traces from the oscilloscope and makes the measurement reconstruction.

In the conventional BOTDA setups two electrical to optical converters are usually needed: one to create the CW as a sideband of an ODSB-SC, and another one to pulse the pump wave. Furthermore, in order to generate high ER pulses specialty MZ-EOMs or SOAs are used, with 45dB ER [LI 2008, DIAZ 2008], much more expensive or complex respectively than telecom grade MZ-EOMs, with 20 to 30dB ER. So notice that the presented scheme is different to conventional BOTDA setups: although the pulsing and frequency shift are performed in two steps, only the second one is made in the optical domain, while the pulsing is achieved in the electrical domain. This enables us to create ultra-high extinction ratio pump pulses at low cost, with a RF switch and a single telecom-grade MZ-EOM. Moreover, as the CW probe comes directly from the laser with no modulation at all, thus no additional deleterious spurious signals are present in the detected optical spectra and there is no need for additional optical filtering in the receiver.

We assembled an experimental setup following the scheme in figure 2.6 for a proof-of-concept demonstration of our system. The only microwave switch that we had available was a model limited to 65ns pulses, which set the maximum spatial resolution of the measurements to approximately 6m. However, as it was mentioned before, faster switches are commercially available so that even sub-meter resolution measurements should be possible with this system. As depicted in figure 2.8 (a), the RF pulsed signal was measured in a 20GHz oscilloscope. However we could not measure the ER because the leakage level was too small for the available scales. Consequently we measured in an electrical spectrum analyzer (ESA) at zero span as shown in figure 2.8(a). The ER level is found to be larger than 50dB. However, the measurement was

limited by the ESA's noise floor. The extinction ratio given by the switch specifications is 60dB. In figure 2.8(a) the pulse shape is broadened due to the ESA's intermediate frequency filter bandwidth, 10MHz. An additional measurement was performed to check that clean, square optical pulses were been generated by using an optical detector and oscilloscope to measure the optical signal after FBG filtering. This is shown in figure 2.8(c), where a square pulse of 65ns duration is perfectly seen.
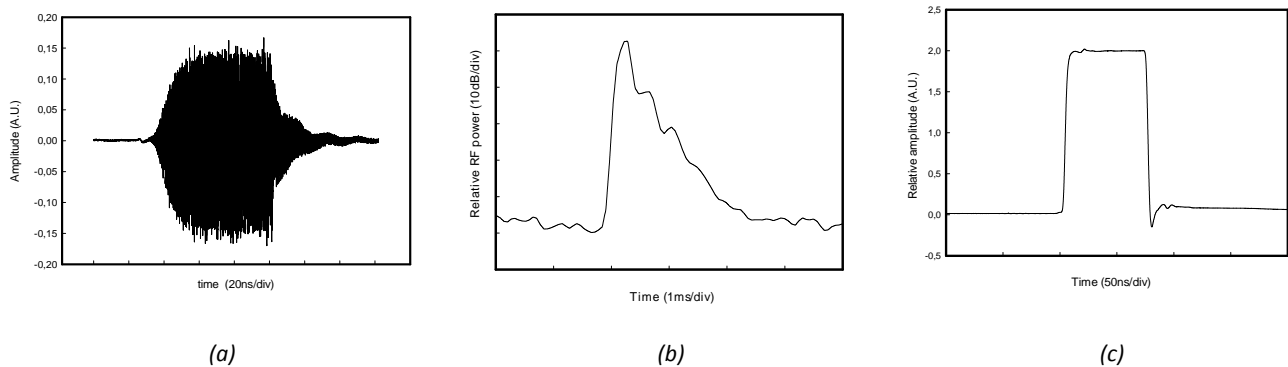

(a) *(b)* *(c)*

Figure 2.8: (a) Measured RF pulse in a 20GHz oscilloscope, (b) in the ESA at zero span and (c) the optical pump pulse measured in an oscilloscope.

The ODSB-SC signal measured with an optical spectrum analyzer after the MZ-EOM is shown in figure 2.9. Also highlighted is the use of the FBG filter to obtain an optical single-sideband suppressed-carrier (OSSB-SC) signal for the gain configuration of the setup. The suppression of carrier and unwanted sideband relative to the wanted sideband were 38dB and 18dB, respectively. It is important to suppress the carrier as much as possible because it leads to Rayleigh scattering in the fiber in the same direction and at the same wavelength as the probe wave, which could have increased noise in detection. We checked that there was no problem with this in the measurement shown in figure 2.10. The received optical spectra with and without probe wave were measured to verify that spurious signals power could be neglected and further optical filtering in detection was unnecessary. The unwanted sideband suppression was also found to be enough to avoid the generation of Brillouin loss in the Stokes signal.
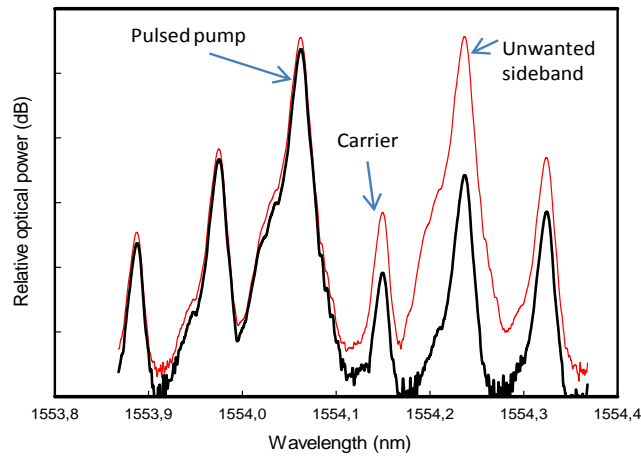
Figure 2.9: Effect of the FBG filtering of the OSDB-SC spectrum. The red line corresponds to the signal before filtering and the dark line after.
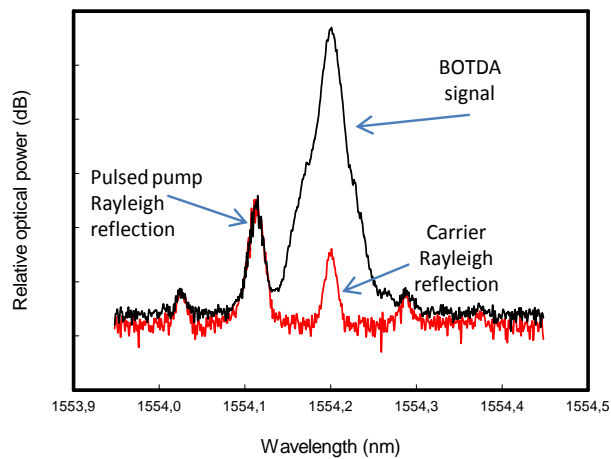
Figure 2.10: BOTDA signal spectra in detection measured is in grey. The dark line corresponds to Rayleigh scattering of the pump when the probe is switched off.

2.4.1   MEASUREMENTS

We performed distributed temperature measurements in a 25-km length of standard single-mode fiber at 6-m resolution with 20-dBm pump pulses and -10-dBm CW. 200 m of the fiber were placed loose in a climatic chamber at 47ºC while the rest were held at room temperature in a reel. The RF was swept at 1-MHz steps.

64
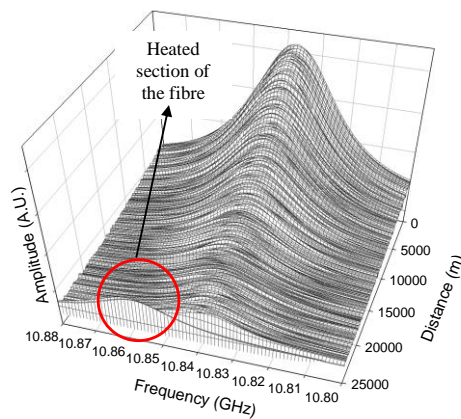
Figure 2.11: Evolution of the Brillouin spectra in the FUT. The heated section is clearly visible at the end and there is no measurement distortion due to the low leakage pulses.
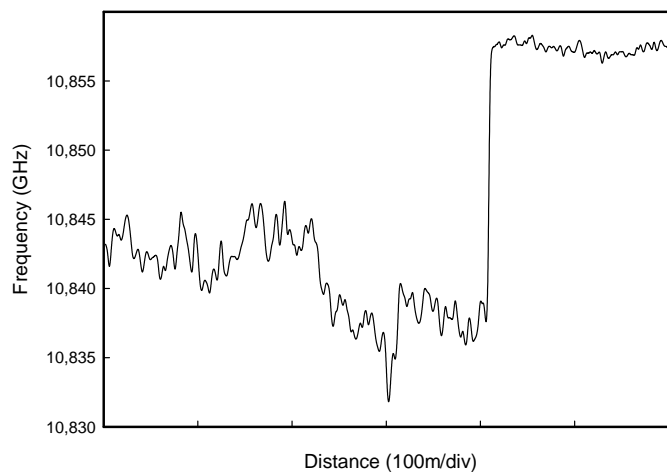
Figure 2.12: Evolution of the measured Brillouin frequency shift in the end of the fiber. The last 200m correspond to the heated section of the fiber, where the measurement is very uniform.

The distributed measurement of the Brillouin spectra is shown in figure 2.11 after data processing (a Lorentzian fit). As explained previously, correction (2.4) is unnecessary in these measurements because the ER is so large that the interaction between leakage and CW is completely negligible. The heated section of the fiber is clearly distinguishable due to the shift in the Brillouin frequency. After processing the temperature measurement uncertainty was estimated to be 0.44ºC in the worst case scenario with the heated section of the fiber at the end of the FUT, and was calculated with the standard deviation of the temperature measured in the heated section of the fiber shown in figure 2.12. The measurement of the frequency shift in the reel is not uniform because the fiber suffers random strain generated by the spool winding. The

65

spatial resolution was confirmed to be 6m by measurements of rise time between two adjacent sections of fiber at different temperatures.

2.4.2 COMPARISON OF THE SYSTEM MEASUREMENTS WITH CONVENTIONAL SYSTEMS WITH LOWER ER

We also compared the setup with 60dB ER pulses to the system working with pulses with lower ER. In order to emulate lower ER ratio pulses the RF switch was replaced with a RF mixer. The mixers have a worse performance while pulsing RF signals. Apart from having greater insertion losses, their isolation is much worse, of up to 29dB. This means that in the best cases, 29dB ER pulses are obtained. Varying the DC level of the pulses the ER of the pulses can be varied, but always for worse values than 29dBs.

We performed measurements with pulses of the same optical power but with different ERs: 21dB, 28dB and 60dB. The first two pulses, with 21dB and 28dB ER, were generated deploying the mixer, while for the last pulse, with 60dB ER, the microwave switch was used. The spatial resolution was modified to 19m in order to increase SBS gain. This is because of the interaction between CW and leakage, which adds a noisy DC level to the BOTDA signal. It is attributed to the polarization scrambler, because it makes the interaction between leakage and CW change for each polarization state. The gain of the EDFA was modified for every case so the pump pulse amplitude launched to the FUT was always the same, while the CW power was kept at -5dBm. The CW was also larger than in the previous measurements so as to gain some dynamic range.
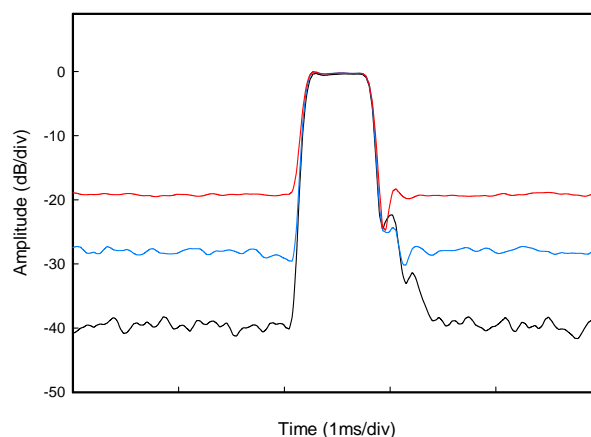
Figure 2.13: RF pulses with different ER level measured in the ESA at zero span. 21-dB ER in red line, 28-dB ER in blue line and 60-dB ER in solid dark line. The pulse shapes are broadened because of the intermediate frequency of the ESA, the same as happens in figure 2.8(a). The measurement for the pulse with 60dB ER is limited by the ESA's dynamic range too, so the measured ER, 40dB, is worse than the given by the RF switch specifications, 60dB.

In figure 2.14 we observe the Brillouin spectra in the heated section of the fiber for different ER values of the pump pulses. In figure 2.14(a) to (c) no correction has been applied to the measurements. The model predicted that only when we use 60-dB extinction ratio pulses the temperature is properly measured because the maximum of the gain corresponds to the frequency shift of the heated part. However, when correction (2.4) is performed, in figures 2.14(d) to (f), we are able to measure the temperature shift with 21-dB and 28-dB ER. There is no need for correction (2.4) when 60dB ER pulses are used. This is because the spectrum of the interaction between leakage and CW is completely flat. So applying correction (2.4) is the same as dividing by a constant as has been previously explained. However this correction is also performed and the resulting trace is shown in figure 2.14(d) so as to compare with the measurements with lower extinction ratios.

(a)   *(b)*   *(c)*

(d)   *(e)*   *(f)*
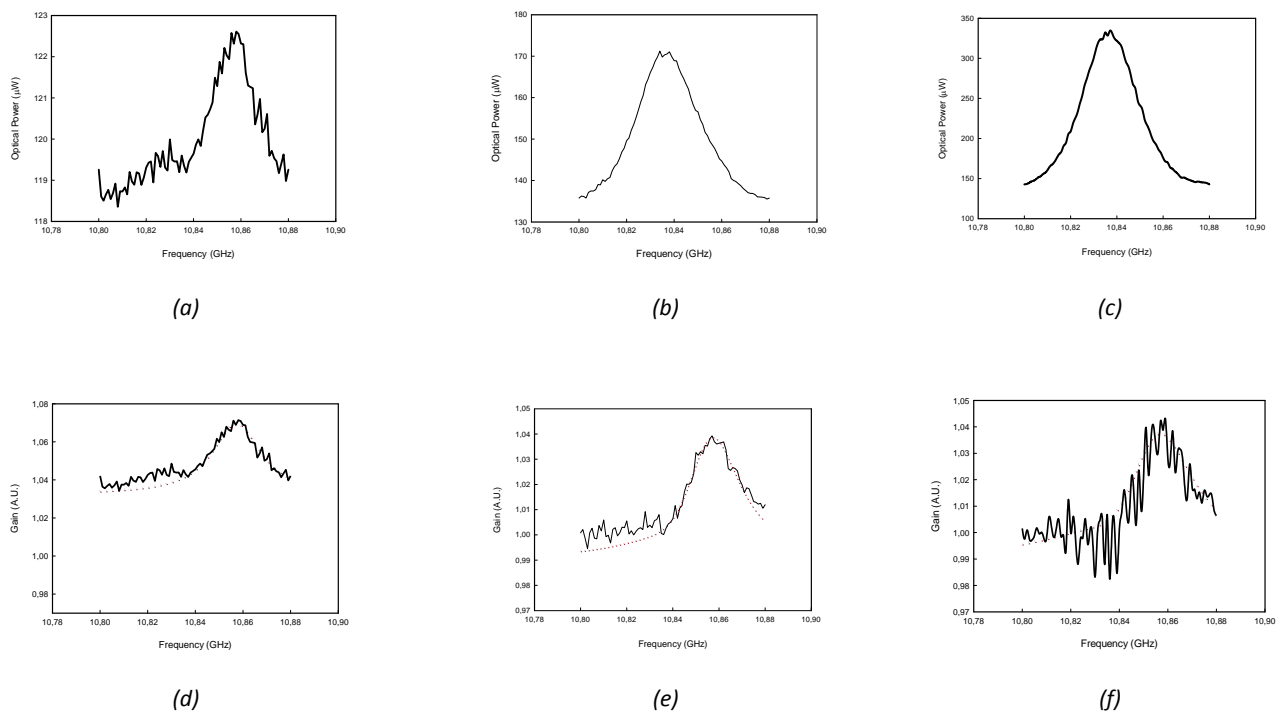
Figure 2.14: Reconstructed spectra in the heated section for ER values of ER=60dB (a) without correction and (d) with correction; ER=28dB (b) without correction and (e) with correction; and ER=21dB (c) without correction and (f) with correction. The solid lines correspond to experimental measurements, while the dotted lines correspond to theoretical data calculated with the model described in section 2.

In all three cases the traces match the theoretical model previously developed. Thus, the measurements show a 3MHz error for 21dB ER and 1.5MHz error for 28dB ER due

to non-local effects. However, in the case of using the 60-dB ER pulses provided by our enhanced setup the error is lower than the frequency accuracy of the setting.

The standard deviation of the experimental traces relative to the theoretical model was calculated. It grows as the leakage level increases: the larger leakage level, the greater the noise. This is attributed to the noisy DC level caused by the leakage-CW interaction due to the polarization scrambler, and cannot be suppressed with the correction. Using other kind of polarization scrambling this noise could be minimized [DIAZ 2008].

Therefore, it is clearly beneficial to use our proposed scheme in long range BOTDA sensing shaping RF pulses in the electrical domain with a RF switch, since it avoids errors caused by non-local effects.

2.5 CONCLUSIONS

In this chapter we have studied the importance of leakage in long range BOTDA measurements and presented a setup that minimizes the leakage at least 2 orders of magnitude compared to existing technologies. We have proved the validity of the technique with measurements.

A theoretical model has been developed to study in detail the behavior of a long range BOTDA system without ideal ER pulses. From the study we clearly see that the effect of the leakage is detrimental in long range measurements. First by an increase on the quantification noise because of needing larger scales digitalizing BOTDA signals, second by the increase on computational cost by performing correction (2.4) when a considerable level of leakage is present. And finally the most important problem we must deal with: the increase of non-local effect induced error. The interaction of the leakage with the CW raises the level of the second; hence a greater depletion of the pump pulse occurs, increasing the measurement error. Consequently there is an important need to suppress or minimize the leakage in long range BOTDA sensing.

The solution presented to minimize leakage, a BOTDA setup based on RF shaping of pump pulses, is simpler and cheaper than other state of the art setups [2009 ZORNOZA]. Just one electrical to optical device is needed, a single EOM, while other setups need two EOMs [BERNINI 2011] or one EOM and a SOA [DIAZ 2008]. This is because the pulsing, the frequency shift and the frequency sweep are made in a single electrical-to-optical step, taking advantage of the RF pulse shaping technique, while other setups separate the pulsing and the frequency shift in two different steps.

REFERENCES

[BERNINI 2011] Bernini, R., Minardo, A. & Zeni, L. 2011, "Long-range distributed Brillouin fiber sensors by use of an unbalanced double sideband probe", *Optics Express,* vol. 19, no. 24, pp. 23845-23856.

 [DIAZ 2008] Diaz, S., Mafang, S.F., Lopez-Amo, M. & Thévenaz, L. 2008, "A high-performance optical time-domain brillouin distributed fiber sensor", *IEEE Sensors Journal,* vol. 8, no. 7, pp. 1268-1272.

[KALOSHA 2006] Kalosha, V.P., Ponomarev, E.A., Chen, L. & Bao, X. 2006, "How to obtain high spectral resolution of SBS-based distributed sensing by using nanosecond pulses", *Optics Express,* vol. 14, no. 6, pp. 2071-2078.

 [LECŒUCHE 1998] Lecœuche, V., Webb, D.J., Pannell, C.N. & Jackson, D.A. 1998, "Brillouin based distributed fiber sensor incorporating a mode-locked brillouin fiber ring laser", *Optics Communications,* vol. 152, no. 4-6, pp. 263-268.

[LI 2008] Li, Y., Bao, X., Ravet, F. & Ponomarev, E. 2008, "Distributed Brillouin sensor system based on offset locking of two distributed feedback lasers", *Applied Optics,* vol. 47, no. 2, pp. 99-102.

[RAVET 2007] Ravet, F., Bao, X., Li, Y., Yu, Q., Yale, A., Kalosha, V.P. & Chen, L. 2007, "Signal processing technique for distributed Brillouin sensing at centimeter spatial resolution", *Journal of Lightwave Technology,* vol. 25, no. 11, pp. 3610-3618.

[THEVENAZ 2004] Thévenaz, L., Le Floch, S., Alasia, D. & Troger, J. 2004, "Novel schemes for optical signal generation using laser injection locking with application to Brillouin sensing", *Measurement Science and Technology,* vol. 15, no. 8, pp. 1519-1524.

[ZORNOZA 2009] Zornoza, A., Olier, D., Sagues, M. & Loayssa, A. 2009, "Distortion-free Brillouin distributed sensor using RF shaping of pump pulses", *Proceedings of SPIE - The International Society for Optical Engineering*, 75036D.

[ZORNOZA 2010] Zornoza, A., Olier, D., Sagues, M. & Loayssa, A. 2010, "Brillouin distributed sensor using RF shaping of pump pulses", *Measurement Science and Technology,* vol. 21, no. 9, 094021.

CHAPTER 3

WAVELENGTH SWEEP BASED BOTDA SENSOR

3.1 INTRODUCTION

Brillouin distributed sensors rely on the spectral characterization of this nonlinear effect along an optical fiber in order to measure temperature and strain. This is typically implemented using a pump and a probe wave in which their frequency difference is swept so as to scan the spectral response of the interaction. The pump or the probe wave is at a fixed wavelength, while the other wave is swept with controlled steps of 1MHz or less resolution, as it has been explained in chapter 1 [NIKLES 1997]. In most proposals this tuning of the wavelength separation is ultimately controlled by a synthesized microwave generator [THEVENAZ 2004, DIAZ 2008, ZORNOZA 2010]. Different types of scan types, like the previously explained offset locking [LI 2008] technique have been presented as alternatives to using synthesized microwave generators in BOTDA sensing setup design.

In this chapter we take one more step in this research trend: we introduce and experimentally demonstrate an alternative spectral scan technique for Brillouin distributed sensing based on the wavelength dependence of the Brillouin frequency shift. It allows the use of a low-cost coarse tunable laser instead of the synthesized microwave generators that are deployed in most setups to sweep the frequency difference between pump and probe waves, or the fine tuning of lasers needed in

offset locking. So it derives in different experimental setup introducing a new degree of freedom to BOTDA sensor design [ZORNOZA 2011].

3.2   DESCRIPTION OF THE TECHNIQUE

The Brillouin frequency shift in a single mode optical fiber is dependent on the acoustic velocity, v_a, via Doppler effect, of the travelling acoustic wave responsible of the energy transfer between probe and pump wave. But not only this, the frequency shift also depends on the wavelength of the pump wave. The equation that describes such relationship is:

$$v_B = \frac{2nv_a}{\lambda_p} = v_p \cdot \frac{2nv_a}{c} \tag{3.1}$$

where n is the effective group refraction index at the pump wavelength λ_p and v_p the optical frequency of the pump wave. We can see that there is an explicit relationship with v_p, and also another implicit via the wavelength dependence of n. So, for every pump wave wavelength, the Brillouin frequency shift is different. Consequently, taking advantage of this phenomenon, a new sweeping method could be potentially achieved.
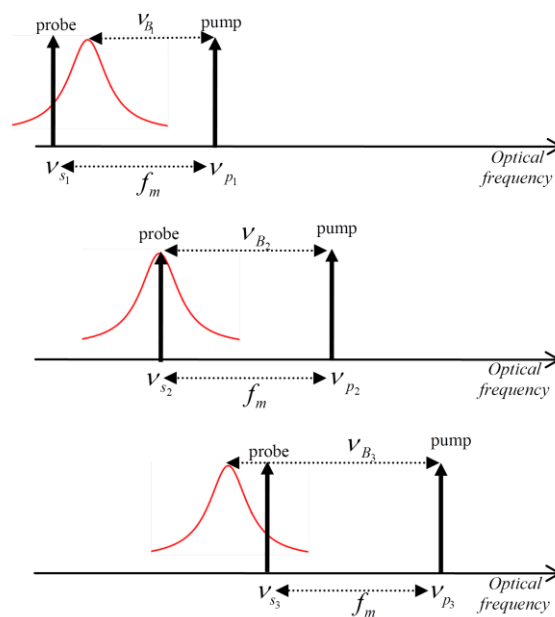

Figure 3. 1: Fundamentals of the Brillouin spectral scanning

Figure 3.1 highlights how this wavelength dependence of v_B can be exploited to scan the Brillouin spectra. The basic idea is to change the wavelength of the pump and probe waves simultaneously while their optical frequency difference, f_m, is held

constant. v_B varies with pump wavelength according to (3.1); thus a different detuning from Brillouin resonance is experienced by the probe wave at each wavelength. This detuning is given by:

$$\Delta v_i = v_{S_i} - v_{P_i} + v_{B_i}$$

(3.2)

where v_S is the optical frequency of the stokes wave. In conventional pump and probe schemes, Δv_i is scanned by modifying ($v_{Si} - v_{pi}$), while in the method explained it is scanned via v_{Bi}. Note that this spectral scanning method is compatible with any of the three Brillouin distributed sensor families: BOCDA, BOFDA and of course BOTDA. From now on we will center in the application of this method to BOTDA.

A wavelength tunable laser is required to implement this spectral scanning concept. Typical measured variations of v_B with pump wavelength in standard single mode fiber (SSMF) are of the order of 7 MHz/nm at 1550nm [SAGUES 2007]. Therefore, fine wavelength tuning is not needed since Brillouin distributed sensors require spectrum scanning at around 1-MHz resolution, i.e. 0.15-nm steps. A low-cost wavelength-agile monolithic tunable laser of the type been deployed for wavelength division multiplexing (WDM) networks is sufficient to provide this tuning. A scan from 1530nm to 1565nm would be equivalent to a 245MHz span in a regular BOTDA sweep. Therefore, in order to measure the complete Brillouin spectrum, a less than full C-band tunable laser is required. The effective group refraction index, n, has a slope of ~2.083e-6/nm [CORNING 2002, CAPMANY 2001], corresponding to a variation of ~7.29e-5 in the whole C-band. Then, the effective group refraction index contribution in the whole C-band span is less than 1MHz in (3.1), what we consider negligible. So n could be taken as constant in (3.1). A variation of ~2MHz in the Brillouin bandwidth [AZUMA 1988] is also present in the measuring range. However, since the measurement of Brillouin bandwidth is much less accurate than the Brillouin frequency shift, this 2MHz can be noticeable only in very high SNR measurements, which are not usually the case of long range measurements.

In this type of spectral measurements, the pump wavelength or optical frequency at which the Brillouin gain is maximum is the parameter to be taken into account to obtain the strain or the temperature variation applied to the optical fiber. This wavelength is obtained by applying a Lorentzian fit to the distributed measurement of the Brillouin spectra in terms of wavelength. The linear dependence of the Brillouin frequency shift Δv_B on the applied strain $\delta\varepsilon$ and temperature change δT can be expressed as [ZOU 2008]:

$$\Delta v_B = (A' \cdot \delta\varepsilon + B' \cdot \delta T) \cdot v_{B0} = v_B - v_{B0}$$

(3.3)

73

Where *A'* and *B'* are the normalized strain and temperature coefficients respectively and v_{B0} the Brillouin frequency shift with no strain applied to the fiber at reference temperature. Then, when substituting v_{B0} with (3.1), the relationship of the Brillouin frequency shift with $\delta\varepsilon$ and δT is:

$$\upsilon_B = \left(A'\cdot\delta\varepsilon + B'\cdot\delta T + 1\right)\cdot\frac{2nv_a}{c}\cdot v_p \tag{3.4}$$

In our case the frequency between pump and probe is fixed to the value given by the oscillator, f_m, and v_{max} is the value of the optical frequency v_p when $v_B = f_m$:

$$f_m = (A'\cdot\delta\varepsilon + B'\cdot\delta T + 1)\cdot\frac{2nv_a}{c}\cdot\upsilon_{max} \tag{3.5}$$

So the dependence of the gain maximum in wavelength with the applied strain and temperature variation is:

$$\lambda_{max}\left(\delta\varepsilon,\delta T\right) = \left(A'\cdot\delta\varepsilon + B'\cdot\delta T + 1\right)\cdot\frac{2\cdot n\cdot v_a}{f_m} \tag{3.6}$$

A', *B'* and *$2nv_a/f_m$* are obtained characterizing the optical fiber under test. So finally by substituting λ_{max} with the maximum obtained in the Lorentzian fit, the applied strain or the temperature change in the fiber is measured.

3.2.1 EFFECT OF CHROMATIC DISPERSION

We have seen that the variation of *n* with wavelength does not affect the BFS in the spans we are using. However the variation of *n* affects the group velocity of the fiber. Since the propagation velocity in the fiber varies for different wavelengths, signals with different wavelength take different times to travel the same distance in the fiber. This phenomenon is called chromatic dispersion. In BOTDA the interaction between pump and probe is based in the timing of Brillouin interaction. So, chromatic dispersion needs to be taken into account in a system taking advantage of the wavelength sweep. The pulses of different wavelength travel at different velocities in the fiber. Particularly, the time spent by a pulse traveling through a fiber of length *L* is:

$$\tau(\lambda) = \frac{L}{v_g(\lambda)} = \frac{L}{c/n_g(\lambda)} = \frac{Ln_g(\lambda)}{c} \tag{3.7}$$

where v_g is the group velocity of the fiber at the operating wavelength λ, and n_g the effective refractive index at the operating wavelength. As depicted in figure 3.2, given that at a reference wavelength the time needed to travel the whole fiber is t_1, at different wavelengths, pulses will suffer a delay, $\Delta\tau$. Note that depending on the fiber

and the wavelength, it could be an advance instead of a delay. The maximum delay for a pulse travelling in a fiber of length *L* is given by:

$$\Delta\tau(\lambda) = L(\lambda_n - \lambda_1)D = L\Delta\lambda D \tag{3.8}$$

where λ_1 *and* λ_n are the shortest and longest wavelengths of the sweep, $\Delta\lambda$ the measuring wavelength span, and *D* the dispersion parameter of the fiber. However, *D* has a weak wavelength dependence which cannot be neglected for long measuring spans. So the maximum delay or advance suffered by a pulse taking into account the wavelength dependence of *D* is given by:

$$\Delta\tau(\lambda) = L\sum_{i=1}^{n} D(\lambda_i)(\lambda_i - \lambda_{i-1}) \tag{3.9}$$

This last equation, which actually is a Riemann sum, if λ_i-λ_{i-1} is very small, it is equivalent to:

$$\Delta\tau(\lambda) = L\int_{\lambda_1}^{\lambda_n} D(\lambda)d\lambda \tag{3.10}$$

As a consequence of the different travelling time for each wavelength, the duration of the signal received is different for each wavelength too. To calculate the length of the signal we must take into account that it is given by twice the traveling time of the signals: the time needed for the pulse to travel to a specific section, and the time needed of the generated signal to go back to the beginning of the fiber. Subsequently, taking into account the previous considerations, the duration of a given signal at a wavelength equal to λ is:

$$T(\lambda) = 2\frac{L}{c/n} + 2\Delta\tau(\lambda) = 2\frac{L}{c/n} + 2L\int_{\lambda_1}^{\lambda} D(\lambda)d\lambda \tag{3.11}$$

Where the shortest wavelength of the sweep, λ_1, has been taken as the reference wavelength and *n* is referred to that. Since *D* is different for every fiber, these equations are different for each type of fiber too. For the specific case of SMF-28 fiber, we have that the dispersion slope of the fiber is given by [CORNING 2002]:

$$D(\lambda) = \frac{S_0}{4}\left(\lambda - \frac{\lambda_0^4}{\lambda^3}\right) \tag{3.12}$$

So we can calculate the maximum delay of the pulse in the fiber:

75

$$\Delta\tau(\lambda) = L\int_{\lambda_1}^{\lambda}\frac{S_0}{4}\left(\lambda - \frac{\lambda_0^4}{\lambda^3}\right)d\lambda = L\frac{S_0}{8}\left[\lambda^2 - \lambda_1^2 + \frac{\lambda_0^4}{\lambda^2} + \frac{\lambda_0^4}{\lambda_1^2}\right] \tag{3.13}$$

where S_0 is the zero dispersion slope at the zero dispersion wavelength λ_0. Then, the total duration of the signal generated with BOTDA interaction would be given by:

$$T(\lambda) = 2\frac{L}{c/n} + L\frac{S_0}{8}\left[\lambda^2 - \lambda_1^2 + \frac{\lambda_0^4}{\lambda^2} + \frac{\lambda_0^4}{\lambda_1^2}\right] \tag{3.14}$$

For example, for a 25-km long SMF-28 fiber, the duration difference of the interaction between the longest and shortest wavelength in the whole C-band implies a difference of ~28.04ns, which is not negligible for spatial resolutions near 1m. Moreover, it could cause an error in the spatial localization of up to 2.8m. Consequently Chromatic dispersion can play an important role when performing wavelength sweeps in BOTDA. However, this influence of chromatic dispersion can be calibrated out, because dispersion is a stable, deterministic effect. So a correction must be performed for an accurate localization of each point in the fiber. This correction should consist on converting each BOTDA signal from the temporal to the spatial domain taking into account the propagation time difference and grouping correctly the points at the same localization as it is explained in detail below.
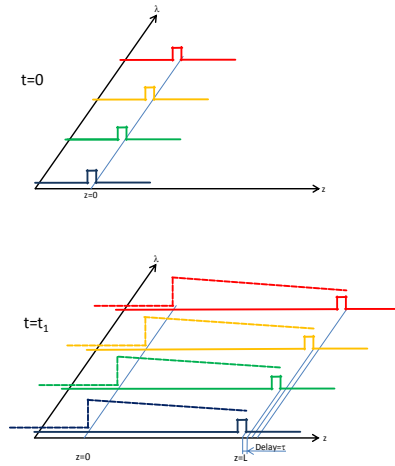
Figure 3.2: delay for pulses of different wavelength travelling in fiber of length L.

We propose the following steps, depicted in figure 3.3, to convert the received signals from the temporal to the spatial domain, which are depicted in figure 3.3. Once the acquisition is done, we can see that the traces have different duration. Note that even if the duration of the signal is different, the length of the fiber interrogated and the spatial resolution are the same. The first step consists in converting time, t, to spatial

localization, z, taking into account expression (3.4). As an alternative to using (3.4), since we know that the different duration of the signals corresponds to the same length of the fiber, a known parameter, we can perform the conversion by normalizing the temporal axis. At this stage, although every point in each trace is correctly localized in space, they correspond to different localizations at each wavelength, as depicted with dark dots in the second step of figure 3.3. So we cannot reconstruct the spectra correctly neither. There are two options at this point. The first one is performing an interpolation in z so we have points at the same spatial localization. Note that for a correct interpolation at least 2 points per spatial resolution unit are needed according to the Nyquist-Shannon sampling theorem. Once the interpolation is done, with grey dots in the last step of figure 3.3, we can proceed with the fit for each spectrum. In the second option, instead of interpolating, but also only if the Nyquist-Shannon theorem is satisfied, we can group the spatially adjacent samples to reconstruct the spectra.
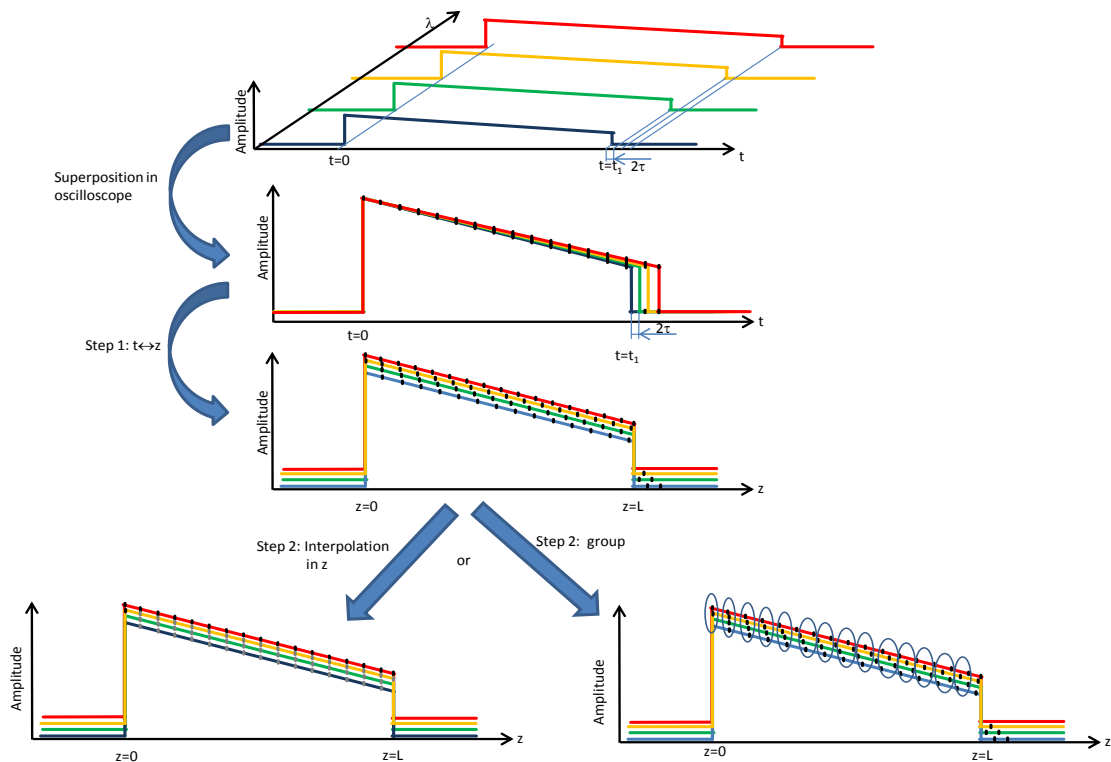
Figure 3.3: steps to avoid positioning error in long range high resolution BOTDA.

3.3   EXPERIMENTAL SETUP AND RESULTS

Figure 3.4 schematically depicts the BOTDA setup that performs wavelength sweep measurements. It is based on the RF shaping method explained in chapter 2. Note that it is important to choose devices with negligible wavelength dependent behavior, otherwise it should be carefully taken into account. The output of a full C-Band tunable

laser source is first divided in two branches. High extinction ratio RF pulses are generated using a fixed-frequency microwave oscillator, a baseband pulse generator and a single-pole single-throw microwave switch. Then, the RF pulse shape is directly translated to the optical domain employing an optical single-sideband modulator (OSSB). The simplest way to achieve an OSSB modulation is employing a MZ-EOM configured taking advantage of the technique developed by smith [SMITH 1997]. However the carrier of the modulation is not suppressed this way. Since a powerful carrier would alter the measurement performance because its Rayleigh scattering has the same wavelength as the probe wave in this setup, we propose to filter it. Nevertheless, it is not possible to use wavelength selective filters in this system, because the wavelength of the carrier is changed in every step of the sweep.
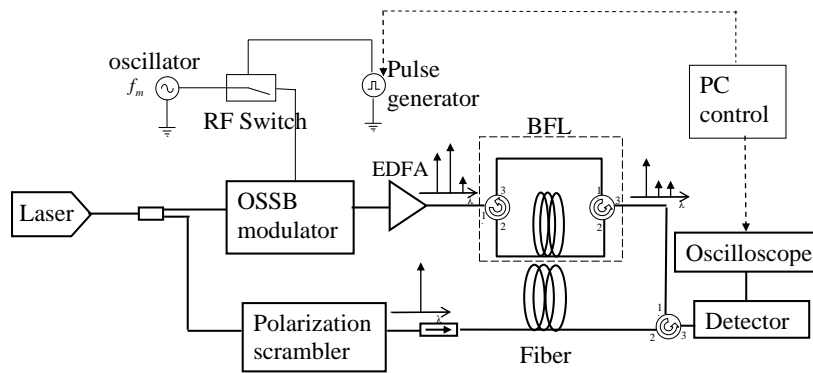

Figure 3.4: BOTDA experimental setup that performs wavelength Brillouin spectral scanning

Therefore, we propose using a Brillouin fiber laser (BFL) as a power selective filter [LOAYSSA 2000]. This device can control the carrier of a modulated signal without affecting the sidebands. The main working principle is that the carrier is depleted while pumping the Brillouin amplification of a Stokes wave. The BFL is a resonant ring structure with a gain media, a section of single mode fiber, based on Brillouin gain. Therefore, if the optical carrier power is injected to the BFL, a narrow-band gain is generated by SBS for optical signals traveling in the opposite direction in the ring. This causes the laser signal of the BFL to appear at an optical frequency shifted from the frequency of the optical carrier by the Brillouin frequency shift of the fiber. This laser signal is the Stokes wave that is amplified with stimulated Brillouin scattering in the section of fiber. Then, the carrier is depleted, provided that the source laser's linewidth is less than the bandwidth of the SBS. Meanwhile, the peaks that do not have enough power to start the lasing exit the BFL unaltered, so we only filter the carrier. Note that the operation of the BFL is the same regardless of the operating wavelength. So, after modulation and amplification with an Erbium doped fiber amplifier (EDFA), the BFL suppresses the optical carrier of the pulsed OSSB modulation. Finally we end up applying a pulsed pump wave with negligible DC base to the sensing fiber.

78

In the lower branch the laser output is directly used to provide the probe wave after polarization scrambling. Finally, the Brillouin spectra distributed along the fiber are measured by tuning the laser wavelength, as it was described above.

We assembled an experimental setup following the scheme in figure 3.2 for a proof-of-concept demonstration of our system. Especial care was taken while choosing every device, so their behavior was independent from the wavelength in the measuring range. That means that the EDFA amplification was flat in the entire measuring range, and no wavelength selective optical filters were used. In figure 3.5 we show the shape of the microwave pulse modulating the MZ-EOM. We used this pulse to perform the RF pump pulse shaping technique. Since the only microwave switch that we had available at the moment of this measurements was a model limited to 240ns, the maximum spatial resolution was set to approximately 24m. The extinction ratio of the switch was specified to be 80dB, so the ratio of ~60dB measured in figure 3.6 is because of the noise floor measured in the ESA. The OSSB modulation was performed with a single MZ-EOM, taking advantage of the technique developed by smith [SMITH 1997].
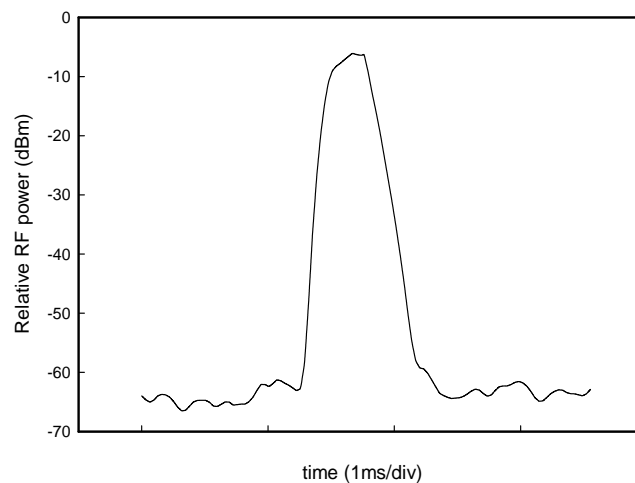
Figure 3.5: shape of the microwave pulse modulating in the MZ-EOM to perform the RF pulse shaping technique. The measurement was taken in the electrical domain with an ESA at zero span.

In the BFL, using 2km of DCF fiber, 37dB suppression of the carrier is obtained, as shown in figure 3.6. In the gray trace we can see the output of the BFL when a continuous microwave signal is modulating the MZ-EOM. Note that the sidebands are also depleted a few dB in the BFL. However, when pulsed, they are not, because they do not have enough average power to start the lasing, and depletion only occurs for the carrier. We can observe that there are some spurious signals generated in the BFL. These are generated in the lasing cavity as further order Brillouin scattering combined

79

with FWM. It is important to choose a fiber for the BFL with a different BFS than the fiber under test. Otherwise, these spurious signals may have the same frequency as the pulses and interact with the probe seriously compromising the measurements.
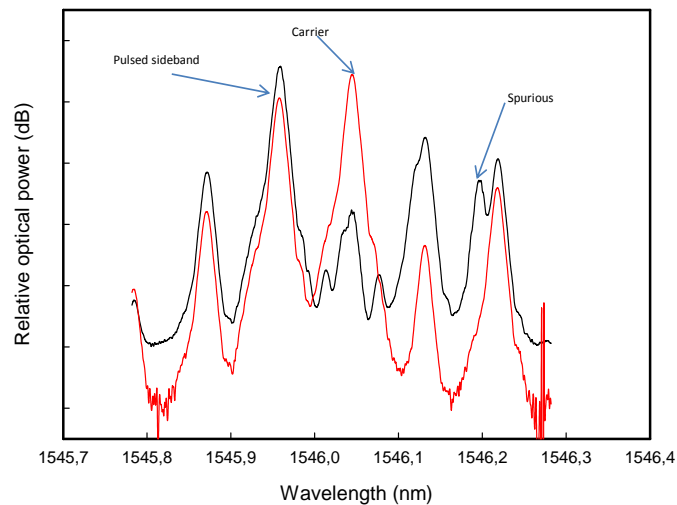
Figure 3.6: OSSB modulation before (red line) and after the BFL (dark line). We can observe a 37dB suppression of the carrier. In discontinuous line the trace for the carrier without modulation is shown.

The input signal at the receiver, depicted in figure 3.7, shows that the Rayleigh scattering of the pump signals is present in reception. However these signals are more than 27dB lower than the probe, and are not found destructive for the system.

Figure 3.7: signal at detection measured in an OSA turning on the probe wave (dark line) and turning off the probe wave (red line).

80

Figure 3.8: measured spectra at the final section of the 10km of fiber.

Figure 3.9: Comparison of the measured spectra using the wavelength sweep (dark line) and the conventional sweep

(red line).

81

Figure 3.10: Temperature measured in the final section of the 10 km fiber.

We performed distributed temperature measurements in a 10-km length of standard single-mode fiber with the last 200m of fiber placed in a climatic chamber at 42ºC while the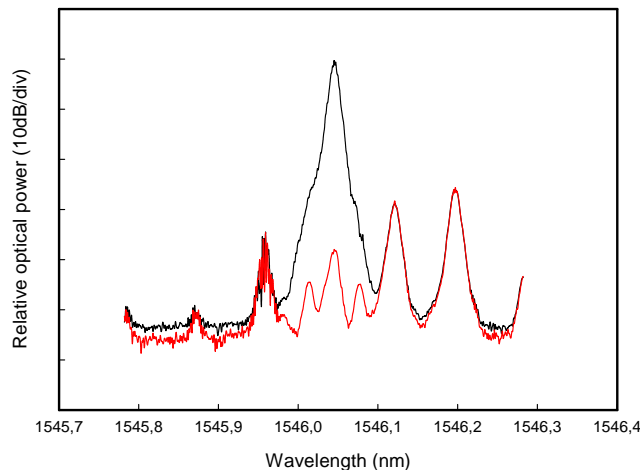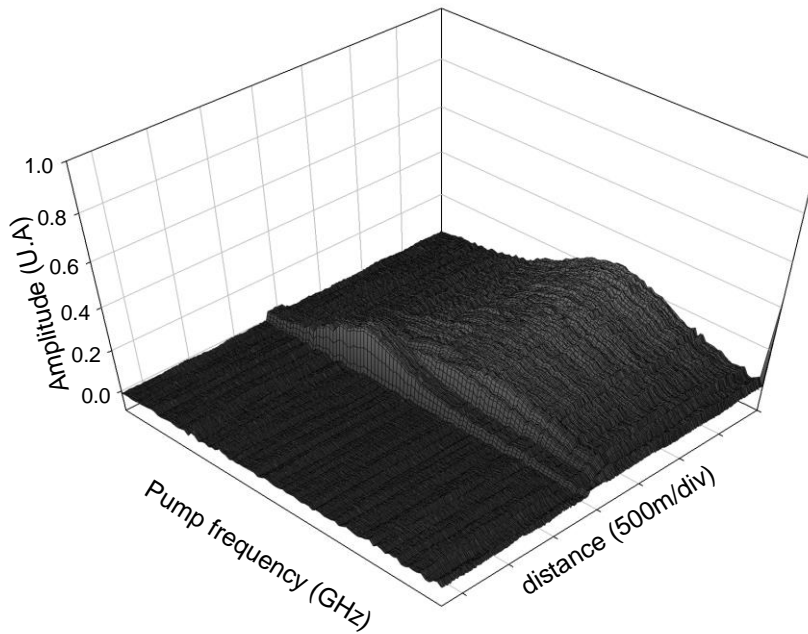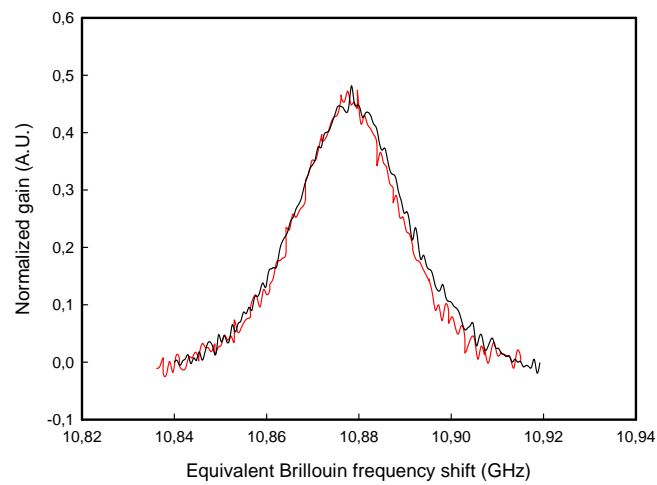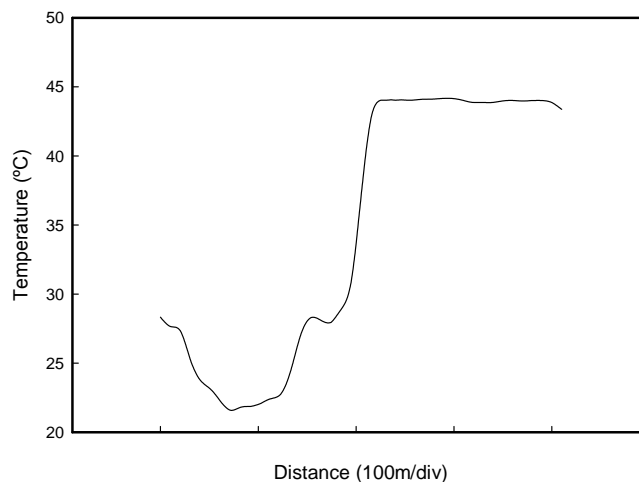 rest was at room temperature. The chosen wavelength span was between 1540.3nm and 1551.5nm, and we swept at 0.13nm steps. The pump pulse power was set to 20dBm and the probe power to -7dBm. The duration difference between the shortest and longest wavelengths in these measurements was calculated to be ~3.5ns with expression (3.8) (equivalent to ~35cm error), so it was negligible for the spatial resolution employed. Therefore, there was no need to perform the correction previously described.

Figure 3.8 depicts the Brillouin spectra measured along the last section of the fiber, including the section heated. We can see that the Brillouin spectra are perfectly reconstructed and the frequency shift difference due to the temperature change is noticeable. Furthermore, in order to be sure of the equivalence between our novel wavelength sweeping system and the regular sweep, we also performed these measurements. We did so by employing the same setup of figure 3.4, but fixing the laser wavelength and sweeping the frequency of the microwave pulses, as in the scheme described in chapter 2. In figure 3.9 the comparison of two measured spectra in the same section of the fiber are depicted, first using the conventional frequency sweep and second using the novel wavelength sweep. We can see that there is no noticeable difference between them.

So as to calculate the exact temperature of the fiber, we need the parameters for (3.6) that were obtained from a previous calibration of the fiber under test. Their values were measured to be *A'=4.6648 10^{-6} nm µε/MHz, B'=9.8954 10^{-5} nm ºC/MHz,* and *2nv$_a$=16767 nm MHz*. Therefore, from (3.3) we can directly calculate δT. Figure 3.10

82

depicts the distributed temperature calculated from our measurement data. The variation between 22ºC and 28ºC previous to the heated section are due to strain variations in this section, which were applied while winding the spool of fiber. The actual temperature measured in the heated section was 43.8ºC with a standard deviation of 0.32ºC. The error of 1.8ºC was related to non-local effects because of a too powerful probe signal. Note that when measuring with the heated section at the beginning of the fiber, the measurement was of 41.9ºC.

3.4 CONCLUSIONS

In this chapter we have demonstrated a new method to characterize the Brillouin spectrum. It is based on the linear dependence the Brillouin frequency shift exhibits with the pump wavelength. The characterization method can be applied in any of the Brillouin distributed sensing families based on SBS: BOCDA, BOFDA or BOTDA. We have focused our efforts in designing a BOTDA sensor taking advantage of wavelength sweeps. In this case, care must be taken, because chromatic dispersion can cause a spatial localization error in long range high resolution measurements. This error, which is a deterministic and predictable error, can be easily avoided with a correction method we have presented. We have shown the validity of the wavelength sweep based BOTDA with experimental measurements performed in the laboratory. However, the available RF-switch, limited the measurements spatial resolution considerably, not allowing us show the real performance of the sensor. Using a faster switch, higher resolution measurements could be achieved, so the real performance of the sensor could be demonstrated.

Any application can take advantage of this alternative sweeping method for Brillouin spectrum characterization, and it is not limited to sensors. Therefore, a new degree of freedom for future setups has been added. For instance, taking advantage of the dependence between wavelength and Brillouin frequency shift has afterwards been used for several applications. It has been applied to the generation of optical variable delay lines [LI 2011], where a continuous and full phase shift up to 360º at 18 GHz is achieved when the wavelength of the optical carrier is scanned from 1549 to 1554 nm using stimulated Brillouin scattering (SBS) in a 1.2-km length of dispersion-shifted fiber (DSF). It has also been exploited in optically Tunable Frequency-doubling Brillouin optoelectronic oscillators with carrier phase-shifted double sideband modulation [YANG 2012] where no high-Q electrical filter is required.

3.5   REFERENCES

[AZUMA 1988] Azuma, V., Shibata, N., Horiguchi, T. & Tateda, M. 1988, "WAVELENGTH DEPENDENCE OF BRILLOUIN-GAIN SPECTRA FOR SINGLE-MODE OPTICAL FIBRES.", *Electronics Letters,* vol. 24, no. 5, pp. 250-252.

[CAPMANY 2001]   Capmany, J., Fraile-Peláez, F.J., Martí, J., "Fundamentos de comunicaciones ópticas", Editorial Sintesis, 2001.

[CORNING 2002] Corning ® SMF-28™ optical fiber product information, 2002.

[DIAZ 2008] Diaz, S., Mafang, S.F., Lopez-Amo, M. & Thévenaz, L. 2008, "A high-performance optical time-domain brillouin distributed fiber sensor", *IEEE Sensors Journal,* vol. 8, no. 7, pp. 1268-1272.

[LI 2008] Li, Y., Bao, X., Ravet, F. & Ponomarev, E. 2008, "Distributed Brillouin sensor system based on offset locking of two distributed feedback lasers", *Applied Optics,* vol. 47, no. 2, pp. 99-102.

[LI 2011] Li, W., Zhu, N.H. & Wang, L.X. 2011, "Photonic phase shifter based on wavelength dependence of brillouin frequency shift", *IEEE Photonics Technology Letters,* vol. 23, no. 14, pp. 1013-1015.

[LOAYSSA 2000] Loayssa, A., Benito, D. & Garde, M.J. 2000, "Optical carrier-suppression technique with a Brillouin-erbium fiber laser", *Optics Letters,* vol. 25, no. 4, pp. 197-199.

[SAGUES 2007] Sagues, M., Loayssa, A. & Capmany, J. 2007, "Multitap complex-coefficient incoherent microwave photonic filters based on stimulated Brillouin scattering", *IEEE Photonics Technology Letters,* vol. 19, no. 16, pp. 1194-1196.

[SMITH 1997] Smith, G.H., Novak, D. & Ahmed, Z. 1997, "Technique for optical SSB generation to overcome dispersion penalties in fibre-radio systems", *Electronics Letters,* vol. 33, no. 1, pp. 74-75.

[THEVENAZ 2004] Thévenaz, L., Le Floch, S., Alasia, D. & Troger, J. 2004, "Novel schemes for optical signal generation using laser injection locking with application to Brillouin sensing", *Measurement Science and Technology,* vol. 15, no. 8, pp. 1519-1524.

[YANG 2012] Yang, B., Jin, X., Chi, H., Zhang, X., Zheng, S., Zou, S., Chen, H., Tangdiongga, E. & Koonen, T. 2012, "Optically tunable frequency-doubling brillouin

optoelectronic oscillator with carrier phase-shifted double sideband modulation", *IEEE Photonics Technology Letters,* vol. 24, no. 12, pp. 1051-1053.

[ZORNOZA 2009] Zornoza, A., Olier, D., Díaz, S. & Loayssa, A. 2009, "Simplified Brillouin distributed sensing scheme using ultra-high extinction ratio RF Pulses", *Proceedings of IEEE Sensors*, pp. 433.

[ZORNOZA 2010] Zornoza, A., Olier, D., Sagues, M. & Loayssa, A. 2010, "Brillouin distributed sensor using RF shaping of pump pulses", *Measurement Science and Technology,* vol. 21, no. 9, 094021.

[ZORNOZA 2011] Zornoza, A., Olier, D., Sagues, M. & Loayssa, A. 2011, "Brillouin spectral scanning using the wavelength dependence of the frequency shift", *IEEE Sensors Journal,* vol. 11, no. 2, pp. 382-383.

[ZOU 2008] Zou, W., He, Z. & Hotate, K. 2008, "Investigation of strain- and temperature-dependences of Brillouin frequency shifts in GeO2-doped optical fibers", *Journal of Lightwave Technology,* vol. 26, no. 13, pp. 1854-1861.

CHAPTER 4

TIME DIVISION MULTIPLEXING BOTDA

4.1   INTRODUCTION

One of the main applications of BOTDA sensors is the monitoring of large structures such as pipelines or railways that can be hundreds of kilometers long. Therefore the extension of the maximum sensing length is an important research trend in BOTDA sensors [SOTO 2009, ANGULO 2012, MINARDO 2009]. However, this is not a simple issue, since the signals in BOTDA are weak and detrimental nonlinear phenomena appear easily. Modulation instability, self-phase modulation or non-local effects must be taken into account, as discussed in chapter 1, and they increase with fiber length. Among these, non-local effects manifest themselves as an error in the Brillouin frequency shift (v_B) measurement at a section of the fiber due to the influence of the rest of the fiber. The origin of this error is the SBS-induced frequency-dependent pump depletion, causing a distortion in the acquired Brillouin gain spectra (BGS), and eventually, an error in the v_B estimation. Consequently, when enlarging the measuring length of a BOTDA sensor, especial care must be taken.

There are some possibilities to minimize the error induced by non-local effects. These include the minimization of the leakage of the pump pulses taking advantage of the RF shaping of pump pulses presented in chapter 2 [ZORNOZA 2010]. Also using two spectral lines with a single probe beam [BERNINI 2011], as presented in chapter 1, is a

proved solution. Note that the last two cases, RF-shaping of pump pulses and using two spectral lines, present some compatibility problems, since the later needs two probe waves with an equal frequency shift from the pulse. Also a computationally complex algorithm can be used [MINARDO 2005] although the measuring time can increase considerably.

In this chapter we propose and demonstrate a simple solution that consists in pulsing the probe wave, so as to restrict the SBS interaction over a fiber section shorter than the total fiber length. As non-local effects arise from the cumulative energy exchange between the pump and probe waves, reducing the interaction length reduces the amount of depletion suffered by the pulse, leading to a reduction of non-local effects. In order to measure the whole fiber, different sections are measured at different moment by changing the delays of the pulsed signals [ZORNOZA 2011]. Consequently this technique is called time division multiplexing BOTDA.

This work was developed in the Second University of Naples in Aversa, Italy, during a 3 month research stay under the supervision of Prof. Luigi Zeni and Prof. Aldo Minardo.

4.2   THEORETICAL BACKGROUND

In order to introduce the theory of the time division multiplexing BOTDA let's remember the limitations of a typical BOTDA due to non-local effects presented in chapter 1. In the classical BOTDA approach, the pump pulse optical current is given by:

$$I_P(v,z) = I_P(0) \cdot Exp\left[\int_0^z - g_B(v,z) I_{CW}(v,z) dz - \alpha \cdot z \right] \tag{4.1}$$

where we can see that the first term of the integral is due to the energy transfer to the probe wave, and cause of non-local effects, while the second is because of the fiber loss. In figure 4.1 we depict the pump pulse and a continuous probe powers while they are counter propagating. The pulse power and probe powers along the fiber are supposed to decay exponentially because of the fiber loss, as depicted in the discontinuous blue and continuous red lines. However if the interaction with the probe is very long and the probe power is strong enough, the contribution of the first term of equation (4.1) is noticeable. In this case the pulse suffers an extra depletion due to the interaction with the probe and it is depicted in continuous blue line in figure 4.1. This eventually causes non-local effects and an error in the measurements, because the gain at a given point in the fiber is influenced by the interaction in previous sections, as it has been explained in detail in chapter 1.
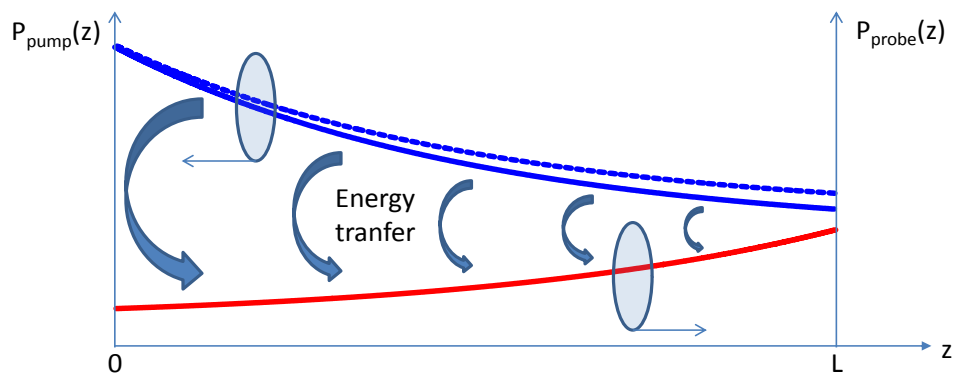
Figure 4.1: Pulse and probe power depletion in a conventional BOTDA system.

In order to avoid non-local effects, probe power cannot exceed the threshold value in which non-local effects become noticeable. In figure 4.2(a) the maximum launchable probe power for a less than 1MHz error is depicted. Note that it is the same figure as in chapter 1, repeated here for clarity. We can see that the probe power we can introduce in the fiber is very low, up to -14dBm in very long fibers. Furthermore, the power of these signals in detection, depicted in figure 4.2(b), is still lower for longer distances. Less power in detection means a lower signal to noise ratio level, as explained in chapter 1. Therefore, if we want to avoid non-local effects, the SNR of the system is greatly compromised.

(a)

(b)

Figure 4.2: maximum probe power we can handle to have a maximum of 1MHz non-local effect induced error

depending on the length of a SMF fiber (a) and power of the probe wave at detection in the same cases (b).

Figure 4.3: Pulse and probe power depletion in a TDM BOTDA system.

However, if the interaction section is shortened while keeping the overall sensing distance the same, the pump depletion is reduced:
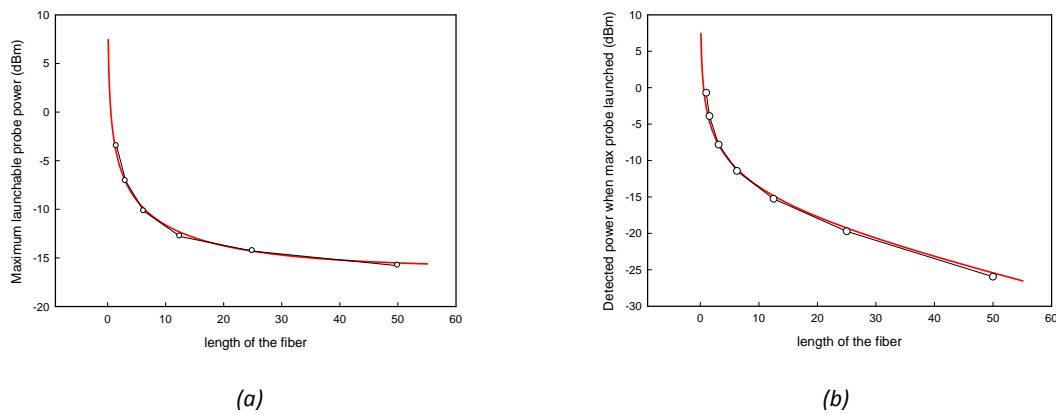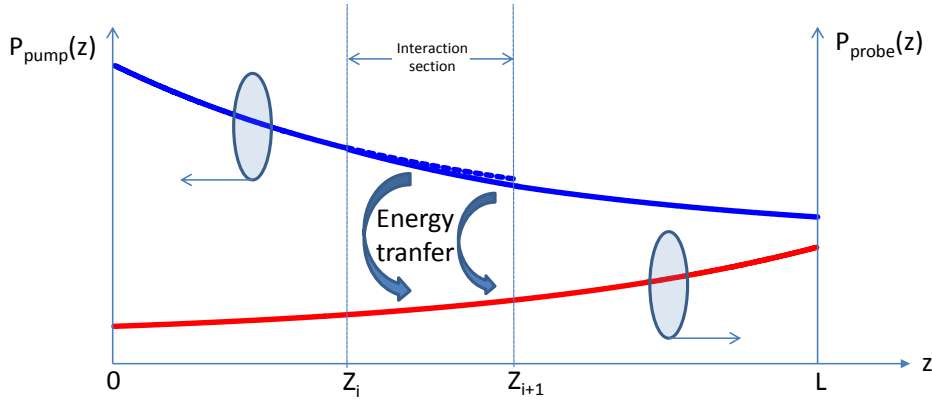
$$I_P(v,z) = I_P(0) \cdot Exp\left[\int_{Z_i}^{z} -g_B(v,z) I_{CW}(v,z) dz - \alpha \cdot z \right] \qquad (4.2)$$

Where Z_i is where the interaction section starts. So the threshold power to avoid non-local effects is given by the length of the section, and not the length of the fiber. Some techniques exploit this concept using different fibers with a significant difference in the BFS so that the maximum of the interaction is different along the fiber [DONG 2012]. In that case (4.2) can be written as follows:

$$I_P(v,z) = I_P(0) \cdot Exp\left[\sum_{k=1}^{i} \left(-\int_{Z_{k-1}}^{Z_k} g_B(v,z) I_{CW}(v,z) dz - \alpha_k Z_k \right) + \int_{Z_i}^{z} -g_B(v,z) I_{CW}(v,z) dz - \alpha_i(z - Z_i) \right]$$

$$(4.3)$$

Where there are n_S different fibers, each starting at position Z_k. Note that the BFS of each section must be different and they cannot be too close. This can cause design limits such as measuring strain and temperature range reduction. Consequently, since the Brillouin gain in all the other section can be negligible because we are near to the BFS of the section i, we can simplify the expression to:

$$I_P(v,z) \approx I_P(0) \cdot Exp\left[\sum_{k=1}^{i} -\alpha_k Z_k + \int_{Z_i}^{z} -g_B(v,z) I_{CW}(v,z) dz - \alpha_i(z - Z_i) \right] \qquad (4.4)$$

In TDM- BOTDA we physically limit the Brillouin interaction length to a section of the fiber by just pulsing the probe power. This way, the interaction occurs just in the section of fiber where the probe pulse and the pump pulse coincide. So the pump pulse power is given by:

$$I_P(\nu,z) = I_P(0) \cdot Exp\left[-\alpha z + \int_{Z_i}^{z} -g_B(\nu,z) \cdot I_{CW}(\nu,z)dz\right] \qquad (4.5)$$

In this case there is no range limitation since there is not interaction in any other section. In order to measure different sections of the fiber, the time delay between pump and probe pulses should be controlled so they coincide in different sections. The whole fiber length can be then covered with successive measurements. This is why this technique is called time division multiplexing of BOTDA.

In figure 4.3 we graphically show the behavior of the pump probe for an interaction in a fiber of length *L* that takes place only between Z_i and Z_{i+1}, being Z_i-Z_{i+1}<*L*. We can clearly see that the pump depletion only takes place in this section of the fiber, so the probe power could be as great as the threshold value for a fiber of length equal to Z_{i+1}-Z_i. So, this technique can be used to enhance the SNR of the system by increasing the probe power. Specifically, if we want to have the same non-local effect induced error in a measurement by dividing the fiber in *n* sections instead of performing a single measurement [THEVENAZ 2011], the maximum probe power to be used is:

$$P'_{S0} = P_{S0} \frac{1 - e^{-\alpha L}}{1 - e^{-\frac{\alpha L}{n_s}}} \qquad (4.6)$$

For example, for a fiber of 100km, if we want to keep the non-local effect induced error less than 1MHz, the maximum launchable probe power is depicted in figure 4.4. Given that the SNR is proportional to the square of the detected power, the improvement using a greater probe power obtained using TDM-BOTDA is remarkable.
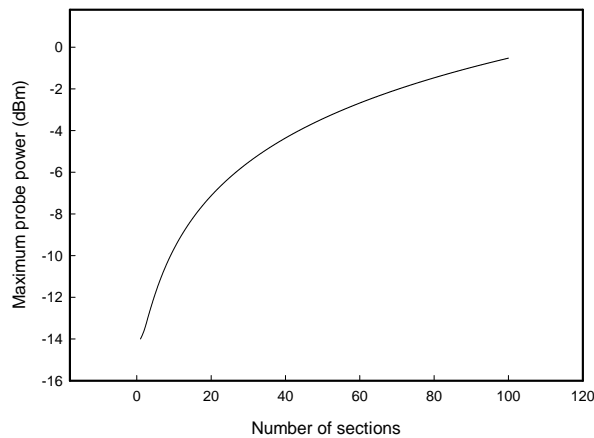

Figure 4.4: Maximum launchable probe power to have a less than 1 MHz non-local effect induced error in a 100Km SMF fiber.

91

However, since we need to perform more than one measurement to cover the whole fiber, we benefit from controlling non-local effects at expenses of the measuring time. The increase of the measuring time though is not necessarily linear with the number of sections. The time needed for a whole scan of the sensing fiber in the conventional system can be described by:

$$T_m = 2\tau N \frac{\Delta f}{f_{step}} \tag{4.7}$$

where τ is the time needed by the pulse to travel the whole fiber, N is the number of averages performed in each acquisition, Δf is the span of the RF sweep and f_{step} the separation of each step in the sweep. Note that the 2 factor is because the signal length is the double of the propagation time in the fiber: when the pulse exits the fiber, the signal that has just interacted with it must reach the other end of the fiber to be detected. When TDM-BOTDA is used, this duration is also multiplied by the number of sections interrogated, n. So we have:

$$T_m' = 2\tau N \frac{\Delta f}{f_{step}} n_s \tag{4.8}$$

We have previously seen that we can use a higher probe power than in a conventional system for the same non-local effect induced error, therefore we can decrease the number of averages keeping the SNR at the same level:

$$SNR_D = \frac{4R_D{}^2 P_{S0}^2 g_{SBS}^2 \sqrt{N}}{\sigma_D^2} = \frac{4R_D{}^2 P'_{S0}{}^2 g_{SBS}^2 \sqrt{N'}}{\sigma_D^2} \tag{4.9}$$

with P'_{S0} and N' the new levels of power and averages respectively. In this case we have that the duration of the measurement is given by:

$$T_m' = 2\tau N' \frac{\Delta f}{f_{step}} n = 2\tau \frac{P_{S0}^4 N}{P'_{S0}^4} \frac{\Delta f}{f_{step}} n = 2\tau N \left(\frac{1-e^{-\frac{\alpha L}{n_s}}}{1-e^{-\alpha L}} \right)^4 \frac{\Delta f}{f_{step}} n_s \tag{4.10}$$

However, the number of averages cannot be less than one: we always need at least one acquisition at each section in every step of the sweep, so care must be taken while using (4.9) and (4.10). We can divide (4.10) over (4.8) and we get:

$$\frac{T_m'}{T_m} = \left(\frac{1-e^{-\frac{\alpha L}{n_s}}}{1-e^{-\alpha L}} \right)^4 n_s \tag{4.11}$$

From this equation we can calculate the measuring time increase or decrease for a fiber of length *L* measured in a given number of sections *n*. For example, for a 100-km long fiber, four sections would decrease the measuring time %11, while five sections would decrease the measuring time %34. For shorter fibers (<20km) the improvement given by (4.11) is very big, however, care must be taken while interpreting these results: if we introduce the probe power given by (4.6), the signal arriving to the detector would be too high, generating saturation. Therefore the improvement given by (4.11) could not be taken into account, since the probe power must be reduced. From now on we will concentrate in the non-local effect induced error reduction and the application to long fibers.

4.3   EXPERIMENTAL SETUP AND RESULTS
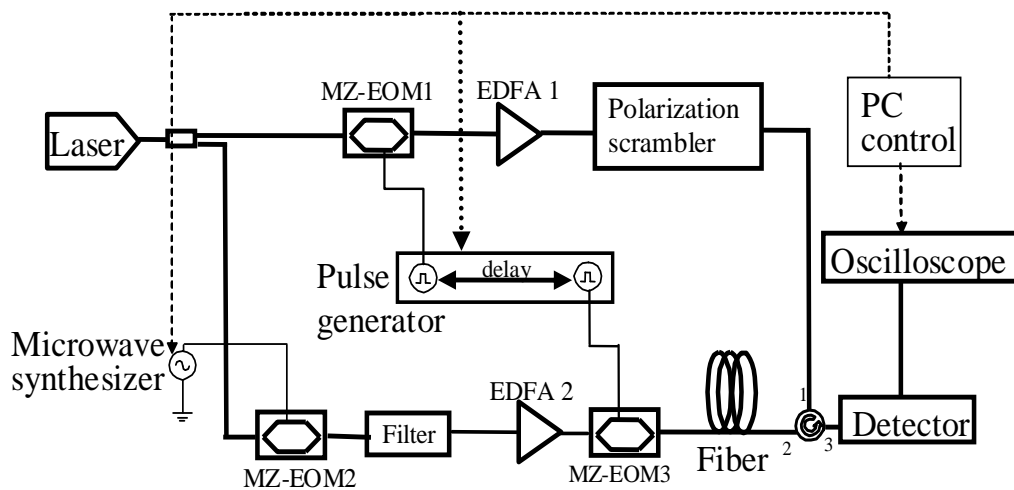
Figure 4.5: schematic setup of the TDM-BOTDA.

We assembled an experimental setup based on the schematic of figure 4.5 for a proof of concept demonstration of the TDM-BOTDA. It closely resembles the typical BOTDA set-up based on the sideband technique [NIKLES 1997], with an extra electro-optic intensity modulator (MZ-EOM3) aimed to pulse the probe beam. The output of the laser is divided in two branches, for the generation of pump pulses in the upper branch and probe pulses in the lower branch respectively. This is performed as follows.

In the upper branch the beam coming from the laser is pulsed in MZ-EOM1 polarized in minimum transmission driven with electrical pulses of amplitude near the V_π of the modulator. The shape of the electrical pulses is translated to the optical domain in the MZ-EOM1, therefore, at the output of the MZ-EOM1 we have optical pulses. So, the length of the electrical pulses gives the length of the optical pulses, and thus, the measurements spatial resolution. However, the leakage level of the pulses is given by the ER of MZ-EOM1. In order to reach the desired level of pump pulses, an Erbium

93

doped fiber amplifier (EDFA1) is employed. The optical pump pulses are directed to the fiber under test by a circulator after being affected by a polarization scrambler (PS) to mitigate the polarization dependence of the Brillouin gain.

In the lower branch MZ-EOM2 is deployed to have a double sideband with suppressed carrier modulation. The modulation frequency is chosen to be near the BFS of the fiber under test. Moreover, in order to reconstruct the whole Brillouin spectrum, this frequency must be swept in a range of over 300MHz. An optical filter is used so only one of the sidebands of the modulation interacts with the pump pulse. Then, this signal is amplified in the EDFA2 to reach the desired level of probe power. The last step is performed in MZ-EOM3, where we pulse the probe wave. The electrical pulse that drives this last modulator, longer than the pump pulse, defines the portion of the fiber to be interrogated.

4.3.1 MEASUREMENTS

A first set of measurements was taken along an 8km-long, standard, single-mode fiber spool. We used different probe powers in two different cases: measuring the whole fiber in one step or in two steps, measuring just half the fiber at each step. Therefore, probe pulse duration was set to either 80µs (probe pulse covering the whole fiber length) or 40µs (probe length equal to half fiber length). Meanwhile, the pump pulse duration and power were kept constant, with the output power of EDFA1 fixed to 15dBm and the pulse length set to 500ns (50m spatial resolution). This relatively poor spatial resolution chosen for the measurements was due to the high continuous wave component (leakage) of the pulses, given by the low extinction ratio (ER) of MZ-EOM1, which was near 20dB. In fact, in the performed measurements, we verified that the contribution of the leakage of the pump pulse was predominant over the pulsed component when using shorter pulses. A higher spatial resolution could be possible by using pump pulses with a higher ER (>30dB) [ZORNOZA 2010]. All in all, it should be noted that it has been proven that pump pulse length, and thus spatial resolution, has a negligible effect in non-local effects [FOALENG 2011]. So even if these measurements are not at the level of current commercial BOTDA setup performances, they are perfectly valid to prove the capability of the proposed TDM-BOTDA technique.

Due to the winding tension, the strain (and thus ν_B) is not uniform along the fiber; rather it exhibits some variation, especially along the last 300 meters of the spool. A number of measurements were performed with different probe powers, while keeping the output power of EDFA1 fixed to 15dBm. Fig. 4.6 shows that, when interrogating the whole fiber simultaneously (τ_{probe} = 80µs), the ν_B estimation in the final part of the fiber is affected by an error that increases with the probe power. On the other hand,

for τ_{probe} = 40μs, the ν_B estimation is less influenced by the probe power, thanks to the reduced cumulated pump depletion. Note that for τ_{probe} = 40μs the whole ν_B profile is obtained by merging two successive measurements. With τ_{probe}= 80μs the error on the estimated ν_B in the last measuring point was up to $\approx$ 12MHz, while being always <2MHz with τ_{probe}= 40μs (the reference value was measured by interrogating the fiber in the opposite direction, that is, by inverting the pump and probe launching sections).
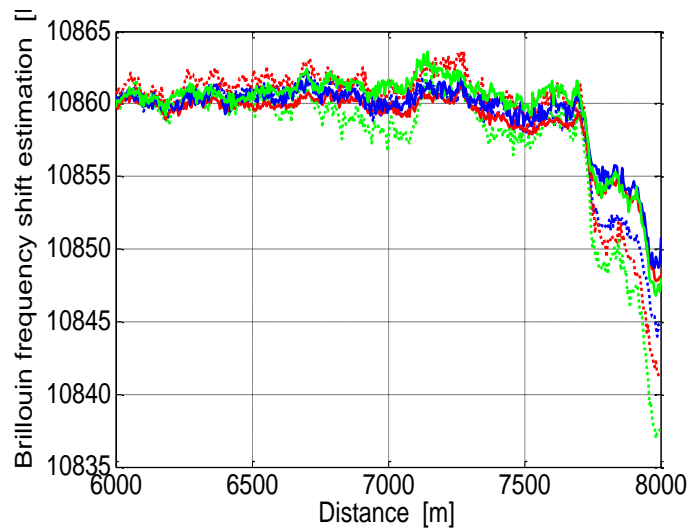
Figure 4.6: ν_B profile estimation along the last 2km of an 8km-long fiber. τ_{probe}= 40μs (solid lines) or 80μs (dashed lines). Output power from EDFA2 was set to 5dBm (blue lines), 8dBm (red lines) or 11dBm (green lines).

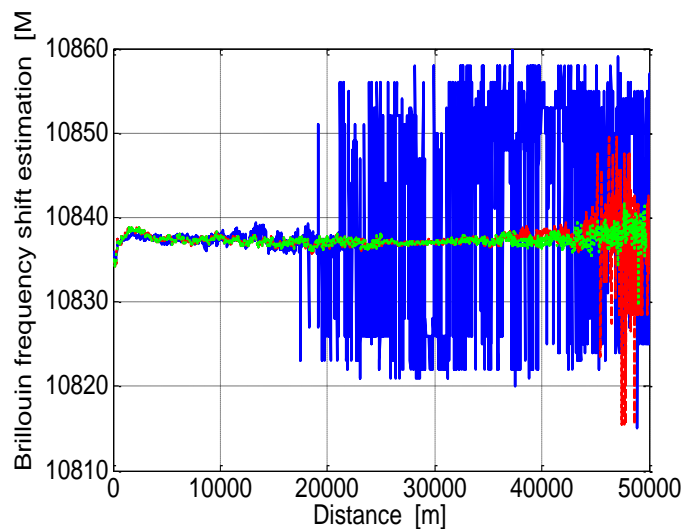*Figure 4.7: ν_B profile estimation along the 50km-long fiber spool. τ_{probe}=500μs (solid blue line), τ_{probe}=250μs (dashed red line) τ_{probe}=125μs (dotted green line). Output power from EDFA2 was set to 15dBm.*

The second set of measurements was taken along a standard, single-mode 50km-long fiber spool. These measurements were mainly aimed to investigate the potential extension of the maximum measuring range offered by the probe pulsing technique. Actually, when analyzing fiber lengths of several km with a nearly uniform ν_B distribution, the SBS-induced pump depletion leads to a progressive decrease of the Brillouin gain for a frequency detuning near the BFS as we move along the fiber.

The final consequence is a bad fitting of the BGS spectra in the final kilometers, as it is evident from the ν_B profile, shown in Fig. 4.7, obtained by interrogating simultaneously the whole fiber length (τ_{probe}=500μs, solid blue line). Moreover, we can see that in this case the correct fit, and consequently a correct measurement of the BFS, is only possible interrogating 4 segments separately.

The limits of the available BOTDA setup at the time of the measurements restricted our proof of concept demonstration without showing the high performance possibilities of the TDM-BOTDA technique. However, other state of the art setups, in which pulse leakage was completely negligible, have shown to enhance the performance characteristics of the measurements with TDM-BOTDA [DONG 2011]. Particularly a 0.6m spatial resolution over a 75-km fiber and a 2m resolution over a 100-km fiber have been demonstrated.

4.4   CONCLUSION

In this chapter the TDM-BOTDA technique has been presented as a solution to improve SNR while controlling non-local effects in long range measurements. The technique is named after its working principle, because different sections of the fiber are measured at different moments. This is simply obtained pulsing the probe wave, so the interaction takes place only in the section of the fiber where the pump pulse and the probe meet.

Since the interaction length is shortened, non-local effects are minimized, and a greater probe power can be used. Consequently the SNR in detection is enhanced. However, the time needed for a scan of the whole fiber is greater. So, when taking advantage of TDM-BOTDA, a trade-off between measuring time, SNR and non-local effect induced error is present. Therefore the TDM-BOTDA sensor can be designed depending upon the specific application it is supposed to suit.

The validity of TDM-BOTDA has been proved in long range measurements by the results presented in this thesis and by the measurements presented in [DONG 2011]. So the TDM-BOTDA technique introduces a new degree of freedom in long range BOTDA measurements, so the quality of the measurements can be improved and non-

local effect induced error can be further controlled. Moreover this technique can be mixed with other techniques tailored to minimize non-local effects and extend the measuring range, such as the RF-shape of pump pulses, using two spectral lines with a single probe beam etc. So a yet higher performance BOTDA sensing setup can be built taking advantage of TDM-BOTDA.

4.5   REFERENCES

[ANGULO 2012] Angulo-Vinuesa, X., Martin-Lopez, S., Corredera, P. & Gonzalez-Herraez, M. 2012, "Raman-assisted Brillouin optical time-domain analysis with sub-meter resolution over 100 km", *Optics Express,* vol. 20, no. 11, pp. 12147-12154.

[BERNINI 2011] Bernini, R., Minardo, A. & Zeni, L. 2011, "Long-range distributed Brillouin fiber sensors by use of an unbalanced double sideband probe", *Optics Express,* vol. 19, no. 24, pp. 23845-23856.

[DONG 2011] Dong, Y., Chen, L. & Bao, X. 2011, "Time-division multiplexing-based BOTDA over 100 km sensing length", *Optics Letters,* vol. 36, no. 2, pp. 277-279.

[DONG 2012] Dong, Y., Chen, L., Bao, X., 2012,"Extending the sensing range of Brillouin optical time-domain analysis combining frequency-division multiplexing and in-line EDFAs", Journal of Lightwave Technology, vol. 30, no, 8, art. no. 6035939, pp. 1161-1167.

[FOALENG 2011a] S. M. Foaleng and L. Thévenaz, "Impact of Raman scattering and modulation instability on the performances of Brillouin sensors," Proceedings of SPIE 7753, paper 77539V, 2011.

[MINARDO 2005] Minardo, A., Bernini, R., Zeni, L., Thevenaz, L. & Briffod, F. 2005, "A reconstruction technique for long-range stimulated Brillouin scattering distributed fibre-optic sensors: Experimental results", *Measurement Science and Technology,* vol. 16, no. 4, pp. 900-908.

[MINARDO 2009] Minardo, A., Bernini, R. & Zeni, L. 2009, "A simple technique for reducing pump depletion in long-range distributed brillouin fiber sensors", *IEEE Sensors Journal,* vol. 9, no. 6, pp. 633-634.

[NIKLES 1997] Niklès, M., Thévenaz, L. & Robert, P.A. 1997, "Brillouin gain spectrum characterization in single-mode optical fibers", *Journal of Lightwave Technology,* vol. 15, no. 10, pp. 1842-1851.

[SOTO 2009] Soto, M.A., Bolognini, G., Di Pasquale, F. & Thévenaz, L. 2010, "Simplex-coded BOTDA fiber sensor with 1 m spatial resolution over a 50 km range", *Optics Letters,* vol. 35, no. 2, pp. 259-261.

[THEVENAZ 2011] Thévenaz, L., Foaleng Mafang, S. & Lin, J. 2011, "Impact of pump depletion on the determination of the Brillouin gain frequency in distributed fiber sensors", *Proceedings of SPIE - The International Society for Optical Engineering*, 775322.

 [ZORNOZA 2010]   Zornoza, A., Olier, D., Sagues, M. & Loayssa, A. 2010, "Brillouin distributed sensor using RF shaping of pump pulses", *Measurement Science and Technology,* vol. 21, no. 9, 094021.

[ZORNOZA 2011] Zornoza, A., Minardo, A., Bernini, R., Loayssa, A. & Zeni, L. 2011, "Pulsing the probe wave to reduce nonlocal effects in brillouin optical time-domain analysis (BOTDA) sensors", *IEEE Sensors Journal,* vol. 11, no. 4, pp. 1067-1068.

CHAPTER 5

HYBRID NETWORK WITH POINT AND DISTRIBUTED BRILLOUIN SENSORS

5.1   INTRODUCTION

Structural health monitoring has attracted much attention in both research and development in recent years. This reflects an increasing need to control the continuous deterioration conditions of important civil infrastructures, such as buildings, tunnels, dams, bridges, piles and pipelines [LI 2004]. Brillouin distributed fiber optic sensors are particularly suitable for large structural monitoring applications since all the segments of an optical fiber act as sensors and therefore the perturbations within various segments of the structure can be sensed [ROGERS 2002]. Their electromagnetic immunity and their dielectric structure also make them ideal for use in harsh environments, like those in the oil, gas and electrical industries [JONES 1998].

Therefore, by wrapping or embedding a fiber inside a structure and using distributed Brillouin scattering sensing, users can detect when an structure is being abnormally strained or heated/cooled, e.g. because of leakage in a pipe, allowing problems to be corrected before catastrophic failure occurs. However, many other measurements apart from strain and temperature are needed in the practical monitoring of large infrastructures, for instance, gas concentrations or vibrations. Particularly, the detection of low frequency vibrations (from 50Hz to 0.1Hz) needs to be monitored in pipelines, civil structures, buildings, etc. [LI 2004, BARIAIN 1999]. Distributed fiber optic sensing systems carry out these last mentioned measurements, but with a

limited performance, whereas local (or point) fiber optic sensors are well suited for these tasks. For example, fiber-optic-taper based sensors employed as transducers are able to measure a number of environmental parameters [DATTA 1996, ARREGUI 1998, BARIAIN 1999] or gases [DIAZ 2008]. They show distinct advantages such as their simple fabrication process, low-cost and versatility in the number of measurable parameters. Furthermore, long-range sensing networks for point sensors are now possible using Er-doped fiber or Raman optical amplification [ELOSUA 2006]. For instance, taper-based point temperature sensors using fiber Bragg gratings as wavelength reference elements have been multiplexed at distances of up to 35 km [DIAZ 2005].

In this chapter we show another step in the development of long-range sensing networks: the integration of point and distributed sensors in a hybrid consolidated long multiplexing network. This offers obvious advantages as the fiber lengths that are anyway needed to interconnect and multiplex point sensors also serve as distributed sensors. However, there are significant challenges to overcome in order to implement these networks.

The complexity of the sensor system is greatly increased, with many different signals travelling simultaneously in the fiber. This can lead to problems such as crosstalk, Rayleigh backscattering or overlapping the sensors signals. Also we can have limitations in the sensor range imposed by the interplay of the different signals present. Another thing to be taken into account is the total accumulated loss due to multiplexing devices. Moreover, in any case it becomes necessary to optimize the operating parameters of all sensors involved so that satisfactory performance is obtained for all of them simultaneously.

We experimentally study and demonstrate two hybrid sensor networks integrating point vibration sensors based on fiber optic tapers with distributed temperature sensing based on stimulated Brillouin scattering. The Brillouin distributed sensing sub-system is specially tailored for long distance sensing, utilizing the RF-shaping of pump pulses technique to generate the sensing signals that minimizes systematic measurement errors discussed in chapter 2. Furthermore, Raman distributed amplification is deployed to simultaneously amplify both the Brillouin sensing and the interrogation signals of the point sensors. This simultaneously increases the range of the Brillouin distributed sensor and enhances the optical signal to noise ratio (OSNR) of the point sensor system [ZORNOZA 2010a, FERNANDEZ 2012].

5.2   DESCRIPTION OF THE NETWORKS

Two different topologies are studied, a single bus topology and a double bus topology. Although the first one is the simplest, the range of the measured signals for the point sensors is worse. In the second, the double bus topology, the OSNR of the point sensor signals is enhanced, and thus the performance of the sensor. Moreover, since the architecture of the sensing network has considerable losses, we use distributed Raman amplification to supplement the low power and noise and enhance the sensors capability, opening the path for Raman assisted Brillouin sensors.
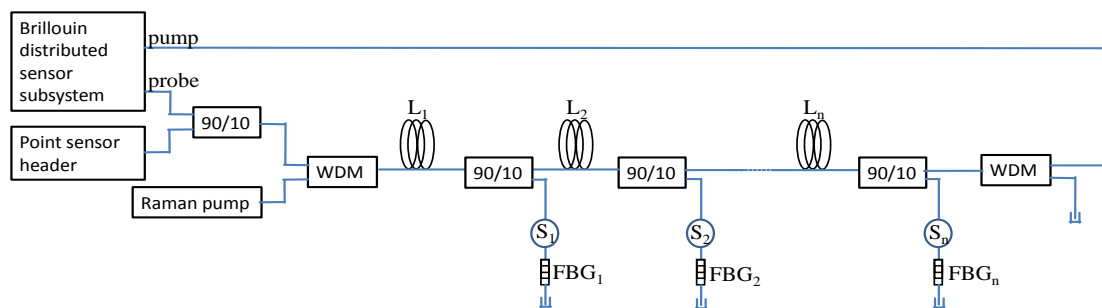
5.2.1   SINGLE BUS TOPOLOGY

Figure 5.1: schematic of the proposed hybrid sensor network of Brillouin distributed and point sensors.

Figure 5.1 schematically depicts the hybrid sensor network that we propose. The system can be separated in two parts: the sensor network itself and the monitoring station equipment. The monitoring station is where the signals needed for interrogation of the point sensors and for the Brillouin distributed measurements are generated, received and processed. The Brillouin measurement system is based on the Brillouin optical time-domain analysis (BOTDA) principle in which a pulsed pump and a continuous (CW) probe waves counter-propagate in the fiber under test. Note that the sensing fiber for the BOTDA system would be the whole bus, of length $L_1+L_2+...+L_n$.

The sensor network has a bus topology with a total length of $L_1+L_2+...+L_n$ of standard single mode fiber (SSMF). Individual point sensors are introduced in the network by the use of fiber couplers. A dual-ended approach is proposed because of the BOTDA distributed sensing scheme deployed in the network. However, the network could be transformed to single-ended measurements by deploying well known techniques [LECŒUCHE 1999].

The bus topology proposed was used for wavelength-division multiplexing (WDM) of the point sensors. We propose the use of n sensors. Each one incorporates a narrow-bandwidth FBG at a unique wavelength. The launched signals are ultimately incident

on all of the sensors but the gratings ensure that each sensor returns only its characteristic channel towards the launching point (the head end) after passing through the sensor a second time. The specific sensors used, S_1, S_2... and S_n in figure 5.1, can be any kind of fiber optic point sensors, from vibration sensors to gas concentration sensors. The BOTDA operating wavelength must be different from the sensors wavelength in order to avoid crosstalk. Note that employing different wavelengths in each interrogation system, filtering is of the essence. Otherwise, crosstalk between the different signals can occur in detection.

Note that with such architecture, the total loss of the bus is not given just by the total length of the fiber. The loss of each coupler must be taken into account. Then, if a considerable number of point sensors are used, the cumulated loss of the bus can be destructive for the system, where very weak signals are used. One way to enhance the measurement range in BOTDA sensors is by increasing the pulse pump power so as to increase the CW probe signal gain. However, as explained in chapter 1 of this thesis, it is limited by the onset of the modulation instability (MI) effect [ALASIA 2005], which limits the maximum usable power. Recently the use of optical pulse coding has been proposed to increase the measurement dynamic range; thus avoiding the need for high pump powers [LINZE 2009, GONG 2007]. Another method to enhance the length of Brillouin distributed sensors is by using Raman amplification. This has the main advantage that the gain is distributed along the fiber so that the pump pulse does not reach at any position the high power that causes the MI effect. The use of Raman amplification has been demonstrated for the Brillouin optical time-domain reflectometer type sensor [ALAHBABI 2005]. However, it had never been experimentally demonstrated in BOTDA sensors at the time this work was performed although its use had been proposed [SOTO 2009]. In our system, we deploy Raman distributed amplification for backward pumping of the pump pulses and forward pumping of the probe. Moreover, this would enhance the performance of the point sensors, since it amplifies the interrogating signals too.

Consequently, a Raman pump laser is also deployed at one of the fiber outputs of the monitoring station in order to generate distributed amplification in the sensor bus extending the fiber sensor network range. This pump laser is injected into the fiber bus by using a fiber wavelength division multiplexer (WDM). Another wavelength division multiplexer should be used at the other end of the bus to prevent the residual Raman pump from re-entering the monitoring station. The Raman pump, signals and receiver are co-located in one head end. This strategy would remove the logistical inconvenience of electrical power feeds in remote locations. The Raman pump propagates co-directionally with the launched signal but counter-directionally with the returned signals from the gratings. Pumping from the opposite end of the bus (or even

bi-directional pumping) is also possible. It is better to amplify counter directionally to the pump pulses. This way the pump pulses are amplified when approaching the end of the fiber, where their amplitude is lower, and so is the Brillouin interaction. Furthermore, when counter-propagating, the RIN noise transference between the Raman pump and the signals is reduced compared to the two other schemes [ANGULO 2012].

5.2.1.1 EXPERIMENTAL RESULTS AND DISCUSSION

We assembled a proof-of-concept experiment in order to demonstrate the hybrid network concept following the design explained in the previous section. The schematic of the whole experiment is shown in figure 5.2. This setup is based in the bus topology shown in [DIAZ 2005].
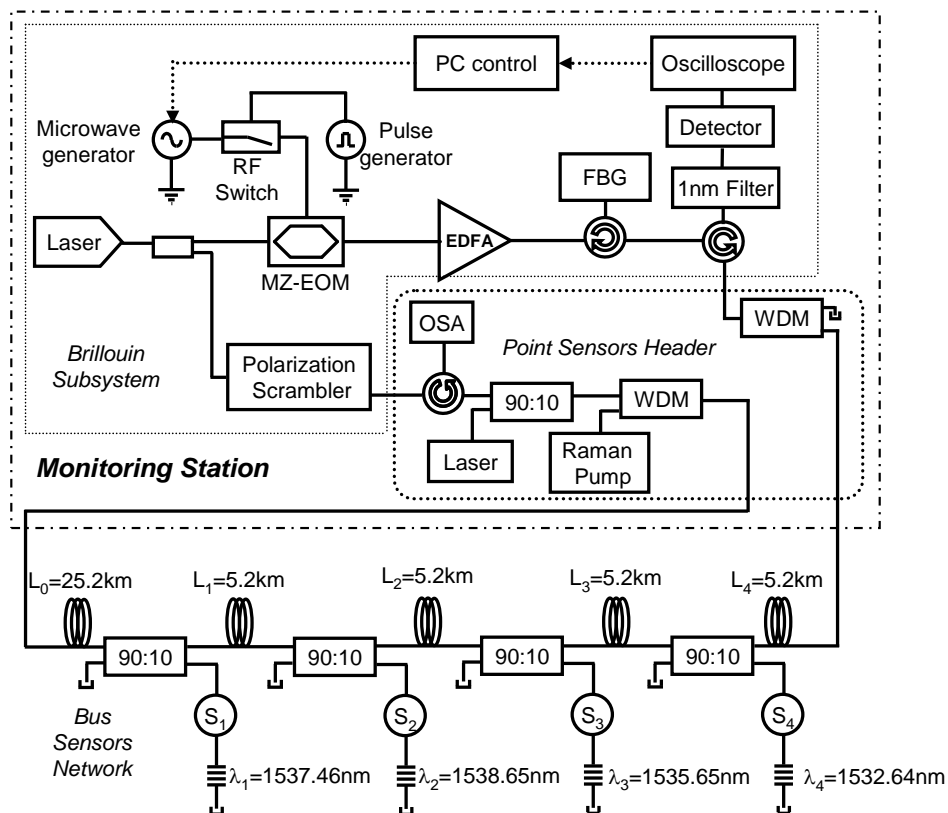
Figure 5.2: Hybrid sensor network with point and distributed optical sensors. The monitoring station includes the Brillouin subsystem and the point sensors header.

The 46-km bus length was implemented in the experiments using SSMF: one 25.2-km reel plus four 5.2-km reels. This fiber, although it has a relatively low Raman efficiency (due to its large effective area), it is widely used in telecommunication networks, where the influence of impairments such as nonlinear cross-talk and Rayleigh back-

scatter is low, as well as its cost. Four point sensors were located at 5.2-km intervals at the end (from the point of view of the interrogation system) of the fiber bus in order to simulate a worst case scenario in order to measure vibrations. These sensors were developed and implemented by the researchers of our group that are experts in this area. The sensors are based on fiber-optic taper sensors employed as transducers to measure mechanical vibrations. They show some advantages, as their simple fabrication process, low-cost and versatility in the number of measurable parameters [MATIAS 2003]. The fiber-optic point sensors were fabricated using a splicing machine with a modified program to move one of the arms trapping the fiber while the fusion happens. The arc fusion power and the splicing time were fixed to have tapers with different elongations, depending on the moveable arm length. Obviously, as the length increased, the sensor would have higher loss and sensitivity, and consequently, it would be more fragile. The main design parameter of the point sensors is the loss induced by the taper, which determines the sensitivity and the dynamic range. It is optimized so that the maximum losses induced by the sensors is 1.75dB, which is doubled in the experimental set up because the signal passes through each sensor twice. The transmitted optical power of the taper depends on its bending radius: as it decreases, the transmitted power decreases as well [DATTA 1996]. When vibration is applied to these taper sensors, the fiber is bent in the stretched area, giving a curvature's change, and then, a variation in the transmitted power. So, it can be used to detect vibrations just by monitoring the power variations of the signal across the taper [MATIAS 2003]. In this case, the optical signal crosses the taper back and forth, because the sensors are used in reflective configurations. Thus, they have double sensitivity, although the losses are also doubled. So, there must be a compromise between the sensors' sensitivity, the induced losses and the maximum measuring length.

Directional couplers (90:10 $\pm$ 0.3% ratios) at the pump and all signal wavelengths are shown in figure 5.3 to perform power distribution among the sensors. Their insertion losses vary from 10.4dB to 10.8dB in the 10% branch for the pump and the signal wavelengths and from 0.5dB to 0.7dB in the 90% branch for the pump and the signal wavelengths. 5.2-km fiber spans are placed between the couplers. However, there is no strict constraint on the lengths. All the free terminations on the bus are refractive-index-matched to eliminate unwanted reflections. This is of particular importance to minimize multi-path interference [BROMAGE 2004]. The signal source used to interrogate the point sensors is a tunable laser (1460-1580nm) with a spectral linewidth of 5MHz. The Raman amplification is provided by a pump laser that it is able to couple up to 3.2 W into the single-mode fiber at 1445nm.
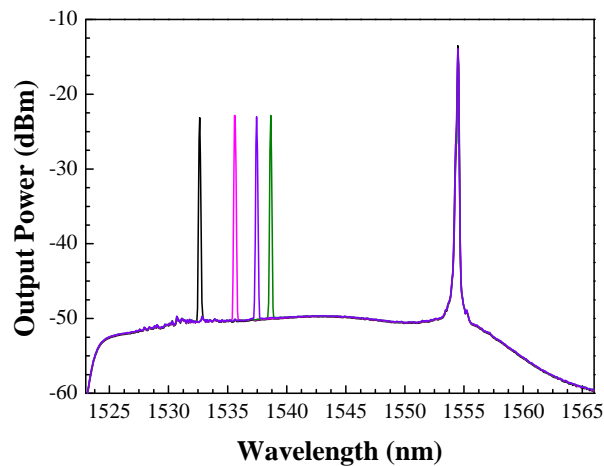
Figure 5.3: Measured optical spectrum for the four point sensors (black, pink Lela and green) and the Brillouin+Raman amplified transmitted signal (purple).

The peak wavelengths of the gratings are marked on figure 5.3. The grating wavelengths corresponded to frequency shifts from the pump ranging between 11.7 and 12.8THz. These values are selected so as to be on the short wavelength side of the peak of the Raman gain profile (which is ~13.2THz from the pump in the germano-silicate glass of standard single mode fiber). By making such a choice, the Raman gain profile increases with frequency shift. This property is used to obtain a degree of power equalization of the returned signals from the sensors.

It is known that Raman amplification is more efficient in long-range bus networks [GRUNER 2004]. Therefore, the first span of 25.2 km of standard single mode fiber acts as an amplification span to maximize the Raman gain in the bus. However, it is also possible to locate sensors closer to the header if necessary [DIAZ 2008].

In the sensor network used within this work the pump power to obtain equalization of the four sensors using Raman amplification is 1 W, which is also a good compromise for the amplification of the Brillouin signals as described below. The output reflected signals from the FBGs are equalized at -23 dBm, and the maximum peak difference between the four channels is approximately 0.29 dB. Figure 5.3 displays the complete measured spectrum for the four sensors using Raman amplification. It is also represented the peak power of the optical output signal, at the Brillouin amplified wavelength.

The BOTDA setup deployed in this network includes the novel method to generate pump pulses with ultra-high ER using standard low-ER EOM [ZORNOZA 2010b] described in chapter 2. It is based on shaping the pulses in the electrical instead of the optical domain. As it is shown in figure 5.2, the signals for Brillouin distributed sensing

105

are obtained from a common laser. The output of this laser is divided in two branches: upper branch, where the pump pulses are generated and lower branch, where the probe signal is obtained.

The pump pulses are first generated in the RF domain. The output of a microwave generator with operating frequencies close to the Brillouin frequency shift is applied to the input of an RF switch, which is driven by a pulse generator. At the output of the RF switch we get short pulses of RF energy with equivalently high extinction ratio. Next step is translating these pulses to the optical domain. This is performed by using optical single-sideband (OSSB) modulation. A Mach-Zehnder electro-optic modulator (MZ-EOM) is driven by the RF pulses and biased at minimum transmission in order to generate optical double-sideband suppressed-carrier (ODSB-SC) modulation. Then, a fiber Bragg grating filter is used to remove one of the sidebands; hence, we end up having a pulsed optical single-sideband suppressed-carrier modulation. The characteristics of the RF pulse are directly translated to the optical domain by this modulation format and consequently optical pump pulses with 60-dB to 80-dB extinction ratio and tunable wavelength are obtained. The Brillouin spectra along the fiber are scanned by tuning the microwave generator frequency. Finally the pump signal is injected in the sensor bus.

In the lower branch of the setup the polarization of the probe signal is scrambled so as to avoid Brillouin polarization dependencies and then it is also injected in the sensor network. The probe signal counter-propagates with the pump pulses in the network and finally arrives back to the detection system, where it is captured using a photo-receiver and digital high-speed scope. The photo-receiver is preceded by a 1-nm wide optical filter tuned to the wavelength of the Brillouin signals that is inserted to avoid any crosstalk from the point sensors interrogation system. The operation of the microwave and pulse generators is controlled by a computer that is also used to acquire and process the measured signals.

5.2.1.1.1 BRILLOUIN DISTRIBUTED TEMPERATURE MEASUREMENTS

In the Brillouin distributed system we deployed a 1554-nm laser with a 100-KHz line-width and 0.5-pm stability. The pump power before Raman amplification was 18dBm and the CW probe was -20dBm. 130-ns pump pulses were used; hence the spatial resolution of the measurements was ~13m.
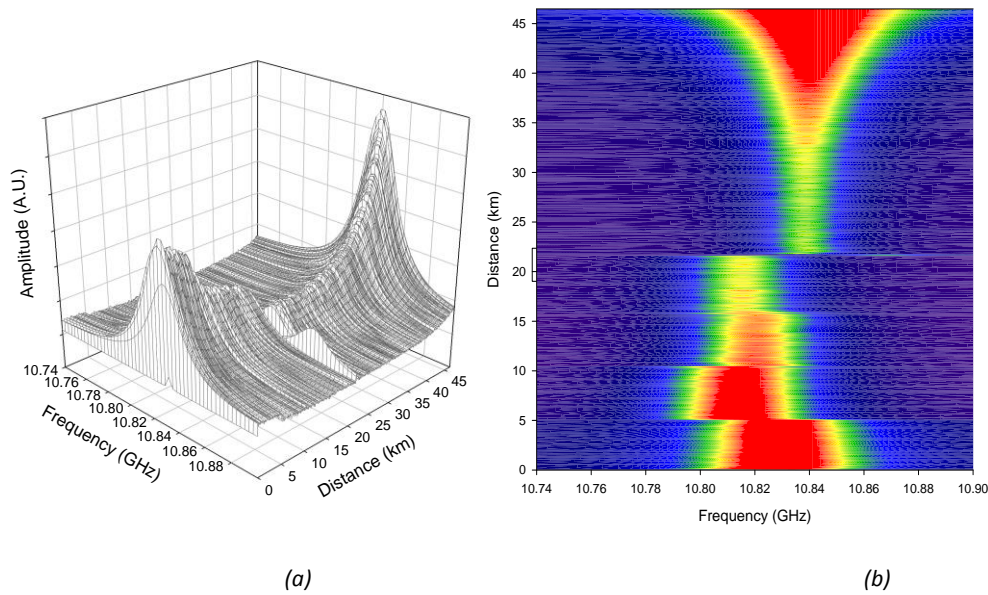
(a)   *(b)*

Figure 5.4: Measurement of Brillouin gain spectra along the fiber network. (a) 3D representation, (b) intensity plot representation.

Figure 5.4 displays the complete characterization of the Brillouin spectra along the fiber. Figure 5.3(b) depicts an intensity plot in which higher amplitude of the spectra is depicted with brighter colors. It can be appreciated that the five fiber reels that make the bus have slightly different intrinsic Brillouin frequency shift. This is attributed to different compositions (as they come from 2 different vendors) and winding tensions. The heated fiber in the middle of the bus is also distinguished. Figure 5.4(a) depicts a 3D view of the Brillouin spectra that highlights their amplitude evolution along the fiber, which is directly linked to the pump pulse amplitude that the probe wave finds at each location. The amplitude of the pulses start to decay due to fiber attenuation as they start to travel through the fiber, but around the middle of the bus the trend is inverted and the amplitude progressively increases until the fiber bus ends. This behavior is due to Raman distributed amplification. We analyzed various pumping configurations to find that backward Raman pumping of the pump pulses was optimal. The reason is that in this way the pump pulses get maximum amplification when it is most needed, i.e., at the end of their journey through the fiber. This explains the observed trend-change at the middle of the fiber bus. With this configuration the worst case location for Brillouin measurements is the middle of the fiber sensor bus. Therefore, as it is shown below, we referred our measurement resolution results to that location. The optimum Raman pump was found to be 1W. The use of higher pumps increased the probe wave amplitude too much leading to significant saturation of Brillouin gain and depletion of the pump, which introduced systematic measurement errors. In a network with more point sensors the Raman pump would be increased accordingly to compensate the additional coupler losses.

A section of 200 m of fiber around the middle of the fiber bus (at 25.2-km distance from the Brillouin pump input) is inserted in a temperature-controlled climatic chamber at 60ºC. This short fiber section was used to simulate a worst case scenario where the Brillouin signal is weaker. Figure 5.4 depicts the measurements of Brillouin frequency shift along the fiber that was obtained by post-processing the data in figure 5.4. Figure 5.5 highlights the four initial 5.2-km reels with slightly different Brillouin frequency shift, then the temperature-controlled 200-m length and finally the rest of the 25.2-km reel. In the middle section, the heated fiber is clearly visible. The Brillouin frequency shift in this area was measured to be 10.868GHz which agreed with a previous calibration of the fiber that had given a temperature coefficient of 0.9MHz/ºC. The standard deviation of the measurement in the 200-m heated fiber was approximated to be 0.6MHz. Hence the temperature precision of the measurements was estimated to be ~0.7ºC.
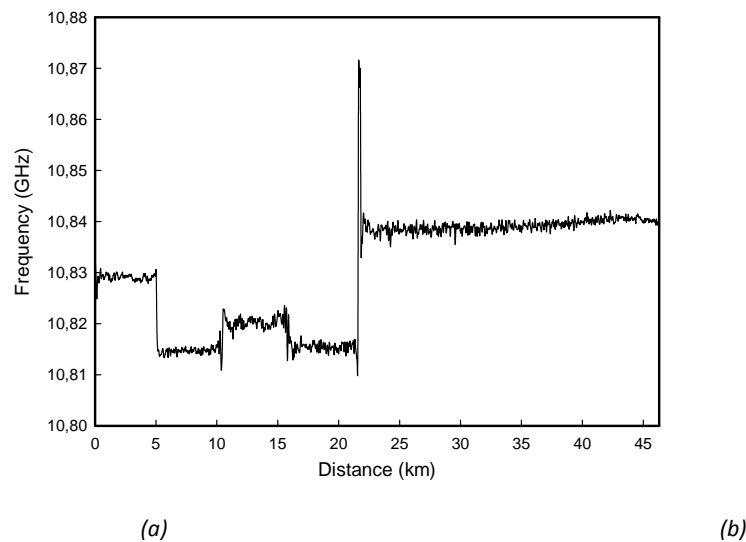

(a) *(b)*

Figure 5.5: Brillouin frequency shift distribution along the fiber.

5.2.1.1.2   POINT SENSORS MEASUREMENTS

Figure 5.6 shows the losses present in the remote sensing network, a total of 12dBs. Note that although the couplers lose between 0.5 and 0.7dBs, there are extra loss coming from each connector. The dynamic range (the measurable optical power variations) was improved using Raman amplification, giving a value of 3dB in the worst case. For the nearest sensor, the dynamic range was higher than 10dB. The OSNR of the sensors, which can be measured in figure 5.3, is of 27dB. By using Raman amplification, the limitation in the maximum sensing length is not due to signal attenuation, but because of backward amplified spontaneous scattering (ASS). When a sensor is located further from the head of the network, the noise level increases, and

108

the signal coming from the sensor is attenuated by the length travelled, the taper's loss, the 90:10 coupling ratios and the grating's reflectivity. The most critical measurement corresponds to the sensor located in the further position, because of both the attenuation suffered and the backward ASS. For a better behavior of the system, the ASS should be minimized, something really difficult with the current architecture of the network.
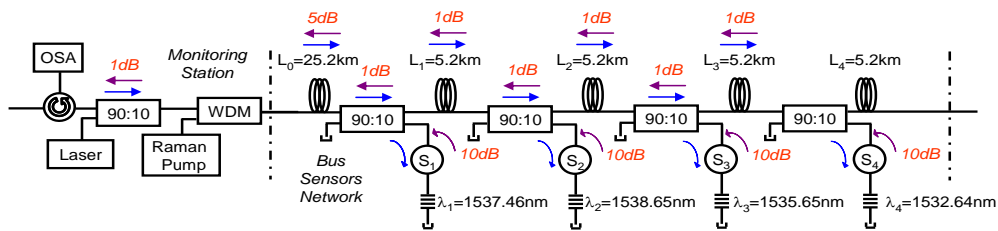

Figure 5.6: Insertion losses present in sensors network.
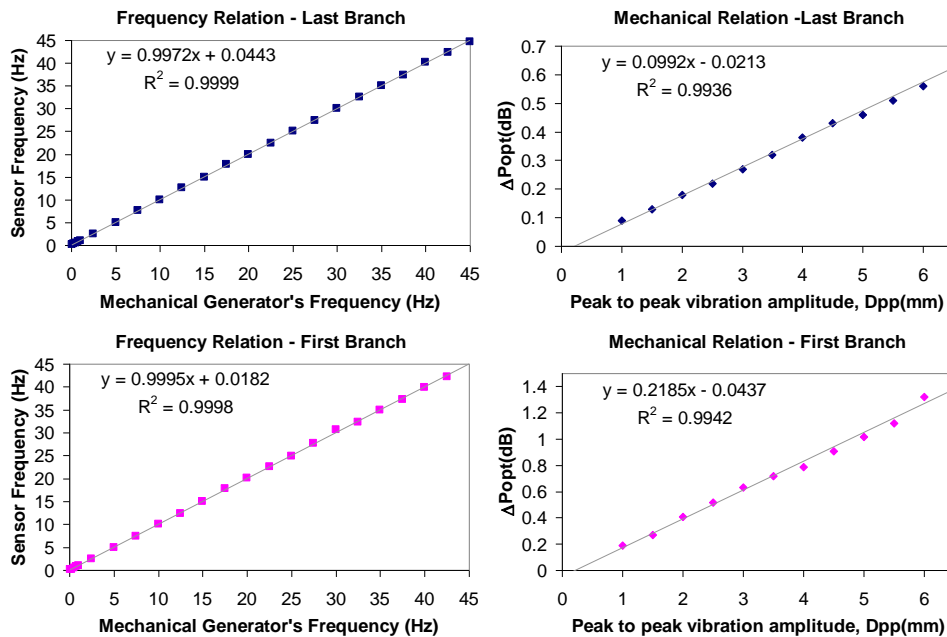
Figure 5.7: Sensor's frequency and amplitude responses (first and second column respectively) for the first and last vibration sensors.

We applied vibrations of different frequency, amplitude and waveform. The applied frequencies ranged from 0.1Hz to 100Hz and the amplitudes varied from 0.5mm to 3.25mm (limited by the variable frequency mechanical wave driver from Pasko, mod. SF-9324 utilized in our experiments). To measure the frequency response, a sinusoidal wave with 6.5mm peak-to-peak variation at different frequencies was applied, aiming to check if the returned signal from the sensor had the same shape and frequency than the excitation signal. Figure 5.7 displays the results obtained. In both cases, the

109

sensor's frequency equals the mechanical generator's frequency. To analyze the amplitude response, a 45Hz vibration frequency was used and the amplitude was varied from 6.5mm peak-to-peak to 1mm peak-to-peak. As in the previous, there was a lineal relation between the vibration amplitude applied and the returned sensor's optical power amplitude (figure 5.6). The vertical axis of the right column charts are not the same. The difference between these ranges is due to the effect of Rayleigh back scattering. While increasing the distance, the backscattered Rayleigh signal is more powerful, and it overlaps with the signal coming from the sensor, affecting the dynamic range of the sensor. This lowers the final sensibility of the last sensor, but anyway, the system is able to measure the same amplitude range as the sensor placed in the first branch.

5.2.2 DOUBLE BUS TOPOLOGY

In the previous section we have demonstrated a long-range hybrid network with point and distributed Brillouin sensors using Raman amplification. This offered a great advantage: the fiber length deployed to interconnect and multiplex point sensors also serves as distributed sensor. Nevertheless the point sensor network with a simple bus topology presents high noise levels coming from ASS. This limits the performance of the system considerably, since the further the point sensors are, the noisier the signals are. In this section we propose and experimentally demonstrate an improved sensor network for multiplexing the point sensors based on a double bus topology that minimizes the ASS. The low noise configuration offers a great improvement in the signal to noise ratio, thus, the number of point sensors to be multiplexed could increase or we could reach further distances. Meanwhile, the BOTDA sensor remains unaltered.
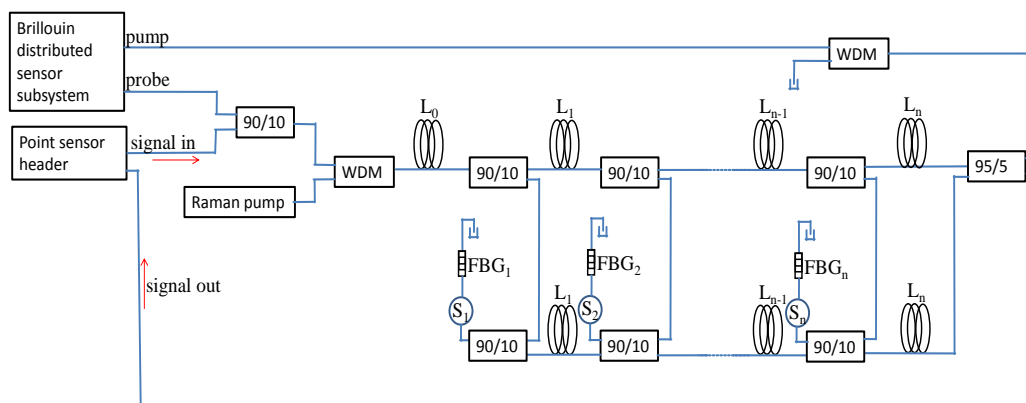

Figure 5.8: schematic of the proposed hybrid sensor network of Brillouin distributed and point sensors.

The experimental setup for the hybrid sensor network is shown in figure 5.8. It is very similar to the setup of the previous section, but with some improvements in order to

enhance the quality of the signals of the point sensors. The same as the single bus set up, the setup can be divided in two different parts: the sensor network itself and the monitoring station equipment. It is in the monitoring station where both, the signals needed for interrogation are generated and the outputs of the networks are processed, as in the single bus topology.

The proposed WDM network is composed of a double-bus topology, each bus of $L_1+L_2+...+L_n$ km long with an extra section L_0 to reach the first point sensor. The upper bus is used for interrogation of the point sensors and distributed sensing.

N point sensors are wavelength-division multiplexed (WDM) along the bus. Each sensor is addressed by a narrow-bandwidth FBG at a unique wavelength and it is accessed with optical couplers, as in the single bus topology. The access, however, is quite different. In each coupler, a portion of the incident light is directed to another coupler. In this second coupler, a portion of the signal is directed to the point sensor, and after crossing the point sensor, just the carrier with the same wavelength as the following FBG is reflected. So, although the launched signals reach all the sensors, the FBG ensures that each sensor returns only its information to the point sensor header after passing through the sensor a second time. While crossing the sensor, the carrier of the same wavelength as the FBG will be modulated by the sensor, depending on the parameters it is capable of measuring. Then, the signal is directed to the lower bus, until it reaches the point sensor header input.

Since in this setup we are supposed to have an important loss from the couplers, Raman distributed amplification is proposed to mitigate this effect, the same as in the single bus topology. So, the Raman pump and the signal are located at one end of the fiber outputs of the monitoring station. Another WDM is used at the other end of the bus to prevent the residual Raman pump from re-entering the monitoring station. Also note that the output of the lower bus located in the other head end. All the free terminations on the double-bus are refractive-index-matched to eliminate undesirable reflections.

5.2.2.1 EXPERIMENTAL SETUP AND RESULTS

In figure 5.9 the experimental setup implemented for a proof of concept demonstration of the double bus setup is depicted. The Brillouin subsystem runs under the same operating principle as the setup of the previous section. The only difference is that the pulsed optical single sideband modulation with suppressed carrier is generated with a dual parallel Mach-Zehnder electro-optic modulator instead of a regular Mach-Zehnder electro-optic modulator combined with a narrow FBG.

The output of a tunable laser source is first divided in two branches, so that the same light source is used for pump and stokes generation. In the upper branch a Dual Parallel Mach-Zehnder (DPMZ) biased at minimum transmission generates a pulsed optical single side band suppressed carrier modulation (POSSB-SC). The pulsing is achieved in the electrical domain using the RF shaping proposed in [ZORNOZA 2010b] so as to avoid leakage. The POSSB-SC signal is then applied to the sensing fiber as pump pulse after an active polarization scrambler is used to compensate the polarization sensitivity of SBS. Then, a 1-nm wide optical filter tuned to the wavelength of the POSSB-SC signal is inserted to reduce the amplified spontaneous emission (ASE) noise from the erbium doped amplifier.
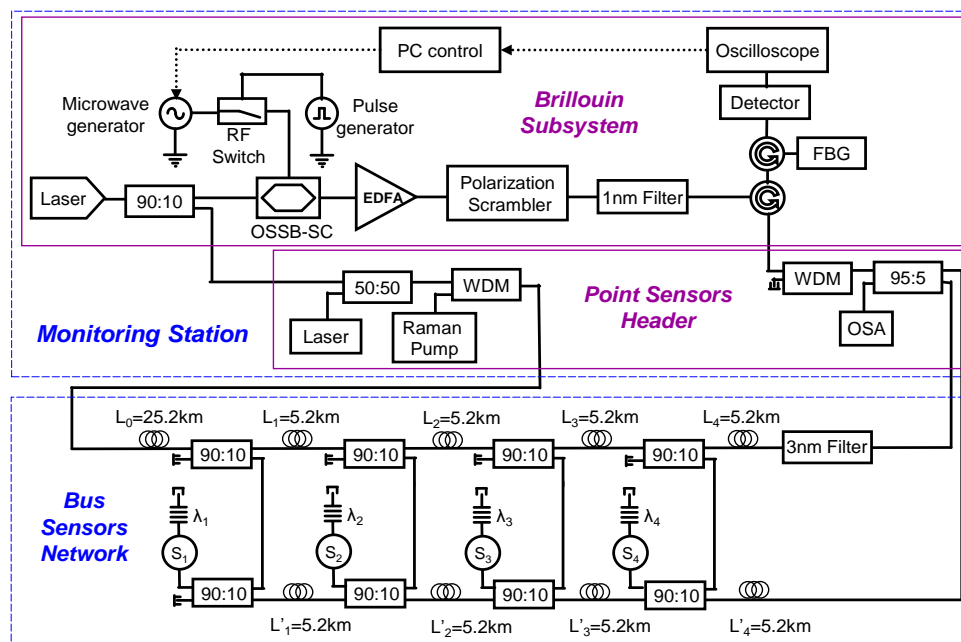

Figure 5.9: Hybrid sensor network with point and distributed optical sensors

In the lower branch the laser output is directly used to provide the probe wave. No modulation at all is needed in this branch. In order to avoid any crosstalk from the point sensors interrogation system a fiber Bragg grating filter is used before detection.

The point sensors network subsystem includes eight directional couplers (90:10 ± 0.3% ratios) to perform power distribution among the sensors. The distance between two adjacent couplers is about 5.2km SMF. Both buses are identical with four couplers each one in order to wavelength-division multiplexing (WDM) the point vibration sensors.

The fiber-optics sensors were the same four sensors used in the single bus topology. The sensors, addressed by four fiber Bragg gratings centered at λ_1=1539.8nm, λ_2=1538.47nm, λ_3=1533.9nm and λ_4=1535.36nm, are separated by 5.2km fiber spans.

The grating wavelengths are located on the short wavelength side of the peak of Raman gain profile.

The signal used to interrogate the point sensors is a tunable laser (1460–1580nm) with a spectral line-width of 5MHz. A Raman pump laser generates distributed amplification in the sensor bus using the first span of 25.2km SMF, thus Raman gain is maximized in the bus and the fiber sensor network range is extended. The Raman pump power is launched into the fiber bus by using a fiber wavelength division multiplexer (WDM). It is able to launch up to 3.2W into the single-mode fiber at 1445nm.

5.2.2.1.1   POINT SENSORS MEASUREMENTS

Figure 5.10(a) presents the spectrum for the four point sensors when Raman pump power is 1W. Amplification of the Brillouin signal and the signal used to interrogate the point sensors have been taking into account to select the optimum pump power. The output reflected signals reached -24dBm and an OSNR of 55dB.
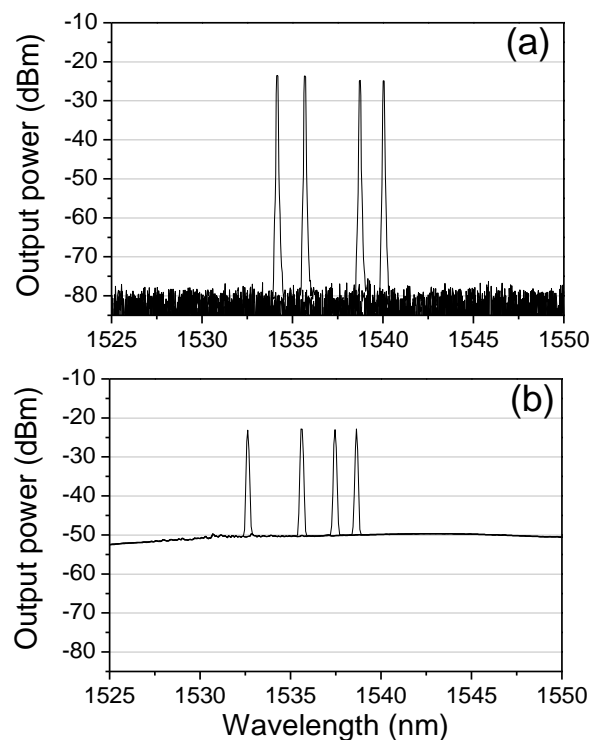
Figure 5.10: Optical spectrum for the four point sensors: (a) Double-bus topology; (b) Single-bus topology

Although the double bus topology is more complicated and expensive than the used in the previous section where the sensor network was composed by a single bus, a great improvement of 25dB in the OSNR has been attained (figure 5.10). This enhancement is reached because, in the single-bus topology, the backward ASS was co-propagating

113

with the modulated signal and both were coupled to the OSA; however, with the double bus topology the backward ASS is removed in the upper bus index-matching gel and only a bit amount of forward ASS reaches the OSA. Thus, with this low-noise configuration the number of sensors that could be multiplexed increases.
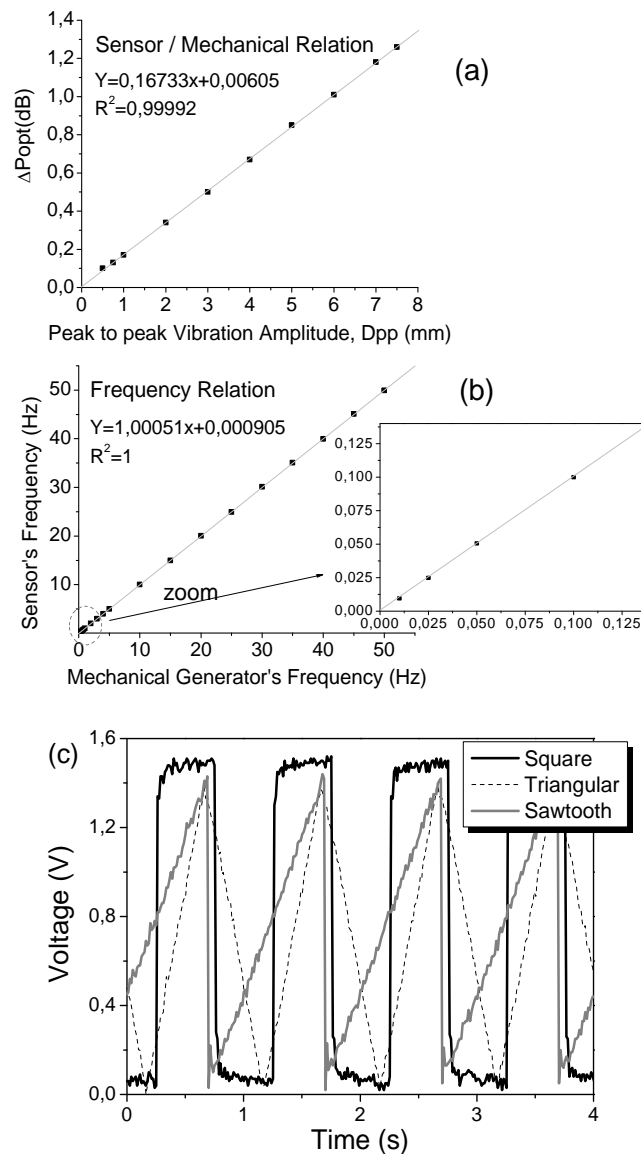
Figure 5.11: Sensor's amplitude (a), frequency (b), and waveform (c) responses for a sensor.

The double bus topology has the advantage of obtaining an improvement in signal to noise ratio and thus the dynamic range increases. The available dynamic range (the measurable optical power variations) reaches 24 dB for all the sensors with the double-bus topology although the actual dynamic range in these measurements is only 1.3 dB. For this reason, we could add more point sensors in the network or reach further distances.

114

To characterize the sensor's response, we applied vibrations of different frequency, from 0.01 Hz to 100 Hz; amplitude, from 0.025 nm to 3.25 nm and waveform, sinusoidal, square, triangular and saw tooth waves. So as to measure the frequency response, a sinusoidal wave with 6.5 mm peak-to-peak variation at different frequencies was applied, aiming to check if the returned signal from the sensor had the same shape and frequency as the excitation signal. In order to analyze the amplitude response, a 45 Hz vibration frequency was used and the amplitude was varied from 6.5 to 0.05 mm peak-to-peak. Figure 5.11(a) and (b) show that the returned signal from the sensor have the same shape and frequency than the excitation signal. Figure 5.11(c) depicted as different waveform can be deployed as excitation signal, the returned signal from the sensor has exactly the same shape.

5.2.2.1.2   BRILLOUIN DISTRIBUTED TEMPERATURE MEASUREMENTS

In the Brillouin distributed sensor we performed distributed temperature measurements along the fiber bus. Another RF-switch was available, which was faster than the one available for the single bus topology measurements. The shortest pulses that we could generate were 30ns long. This corresponds to a ~3m resolution. 200m of the fiber at a distance of 25Km of the beginning were placed in a climatic chamber at 55 ºC while the rest was held at room temperature. This heated section was placed at the end simulating the worst case scenario, where the amplitude of the BOTDA signal is weaker. The RF was swept at 1MHz steps. The distributed measurement of the Brillouin frequency shift of the whole fiber is shown in figure 5.12. Different types of fiber used in the bus sensors network and heated section are clearly distinguishable.
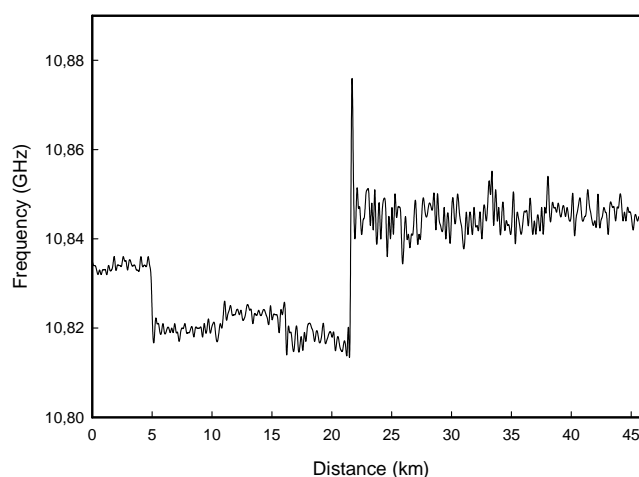

Figure 5.12: Distributed measurement of the Brillouin spectra; (b) Brillouin frequency shift of the whole fiber.

5.3   CONCLUSIONS

This work contributes to the development of the large scalable networks of sensors that are required to monitor extended infrastructures in many practical applications. Two hybrid networks that demonstrate a novel cost-effective architecture that integrates point and distributed Brillouin sensors and distributed Raman amplification have been implemented. The use of Raman amplification in BOTDA distributed sensors, serves to compensate branching and fiber losses in the network. The performance of the systems can be improved by fine tuning of the system; particularly the substitution of the RF switch with a faster device would provide meter or even sub-meter resolution. Furthermore, the simultaneous Raman amplification of the signals from the low-frequency (from 0,1 to 50 Hz) vibration point sensors allows them to be placed as far away as the end of the fiber bus, several kilometers away from the interrogation equipment overcoming low power levels or backscattering noise problems.

The maximum number of sensors that can be multiplexed and the maximum possible length of the network depend on the performance needed to achieve by the application. By adding point sensors, the total loss of the network increases, so the signals are weaker. We can overcome the SNR decrease consequent of weaker signals by increasing the Raman pump power. However this cannot be done arbitrarily, since too much Raman power may cause physical damage to the network and increase nonlinear phenomena. On the other hand, by increasing the sensing length, the signals get weaker too, so we have the same problem as when increasing the number of sensors. In addition, a longer fiber means an enhancement of nonlinear phenomena that are detrimental for the system such as non-local effects, modulation instability or four wave mixing between different signals.

The application of Raman distributed amplification to BOTDA sensors has supposed a big breakthrough in long range measurements, since it has allowed a significant SNR improvement. Note that in a regular BOTDA network, where a single fiber is deployed, no branching losses are present, so Raman amplification can be used to simply compensate fiber loss. Different configurations have been presented taking advantage of Raman amplification and it must be mentioned that they include some of the best performances achieved in BOTDA sensors. By combined co-propagating and counter-propagating Raman amplification with RIN transfer reduction techniques measurements in a 100-km at 0.5m spatial resolution with 2.5ºC uncertainty have been reported [ANGULO 2012]. Also, combining simplex coding, differential pulse width BOTDA and Raman amplification measurements in lengths of 93km at 0.5m

116

spatial resolution and 240km at 5m spatial resolution have been achieved [TAKI 2013, SOTO 2014].

5.4   REFERENCES

[ALAHBABI 2005] Alahbabi, M.N., Cho, Y.T. & Newson, T.P. 2005, "150-km-range distributed temperature sensor based on coherent detection of spontaneous Brillouin backscatter and in-line Raman amplification", *Journal of the Optical Society of America B: Optical Physics,* vol. 22, no. 6, pp. 1321-1324.

[ALASIA 2005] Alasia, D., Herráez, M.G., Abrardi, L., López, S.M. & Thévenaz, L. 2005, "Detrimental effect of modulation instability on distributed optical fibre sensors using stimulated Brillouin scattering", , pp. 587.

[ANGULO 2012] Angulo-Vinuesa, X., Martin-Lopez, S., Nuño, J., Corredera, P., Ania-Castañon, J.D., Thévenaz, L. & González-Herráez, M. 2012, "Raman-assisted Brillouin distributed temperature sensor over 100 km featuring 2 m resolution and 1.2 °c uncertainty", *Journal of Lightwave Technology,* vol. 30, no. 8, pp. 1060-1065.

[ARREGUI 1998] Arregui, F.J., Matías, I.R., Bariain, C. & López-Amo, M. 2003, "Experimental design rules for implementing biconically tapered single mode optical fibre displacement sensors", *Proceedings of SPIE - The International Society for Optical Engineering*, pp. 164.

[BARIAIN 1999] C. Bariáin, I. R. Matías, F. J. Arregui and M. López-Amo, "Experimental results towards development of humidity sensors by using a hygroscopic material on biconically tapered optical fibre" Proc. SPIE 3555, 95-105 (1999).

 [BROMAGE 2004] J. Bromage, P. J. Winzer and R. J. Essiambre, "Multiple path interference and its impact on system design", in Raman Amplifiers for Telecommunications 2, M. N. Islam, ed. (Springer, 2004), Chap. 15.

[DATTA 1996] Datta, P., Matías, I., Aramburu, C., Bakas, A., López-Amo, M. & Otón, J.M. 1996, "Tapered optical-fiber temperature sensor", *Microwave and Optical Technology Letters,* vol. 11, no. 2, pp. 93-95.

[DIAZ 2005] Diaz, S., Lasheras, G. & Lopez-Amo, M. 2005, "WDM bi-directional transmission over 35 km amplified fiber-optic bus network using Raman amplification for optical sensors", *Optics Express,* vol. 13, no. 24, pp. 9666-9671.

[DIAZ 2008] Diaz, S., Abad, S. & Lopez-Amo, M. 2008, "Fiber-optic sensor active networking with distributed erbium-doped fiber and Raman amplification", *Laser and Photonics Reviews,* vol. 2, no. 6, pp. 480-497.

[ELOSUA 2006] Elosua, C., Matias, I.R., Bariain, C. & Arregui, F.J. 2006, "Volatile organic compound optical fiber sensors: A review", *Sensors,* vol. 6, no. 11, pp. 1440-1465.

[FENRANDEZ 2012] Fernandez-Vallejo, M., Olier, D., Zornoza, A., Perez-Herrera, R.A., Diaz, S., Elosua, C., Bariain, C., Loayssa, A. & Lopez-Amo, M. 2012, "46-km-long raman amplified hybrid double-bus network with point and distributed brillouin sensors", *IEEE Sensors Journal,* vol. 12, no. 1, pp. 184-188.

[GONG 2009] Gong, Y.D. 2007, "Guideline for the design of a fiber optic distributed temperature and strain sensor", *Optics Communications,* vol. 272, no. 1, pp. 227-237.

[GRUNER 2004] L. Grüner-Nielsen and Y. Qian, "Dispersion-compensating fibers for Raman applications," in Raman Amplifiers for Telecommunications 1, M. N. Islam, ed. (Springer, 2004), Chap. 6.

[JONES 1998] J. D. C. Jones and R. McBride, Optical fiber sensor technology: Devices and technology, ed. K. T. V. Grattan and B. T. Meggit, (Chapman & Hall, London, 1998), vol. 2, p. 117.

[Lecœuche 1999] Lecœuche, V., Webb, D.J., Pannell, C.N. & Jackson, D.A. 1999, "25 km Brillouin based single-ended distributed fibre sensor for threshold detection of temperature or strain", *Optics Communications,* vol. 168, no. 1, pp. 95-102.

[LI 2004] Li, H.-., Li, D.-. & Song, G.-. 2004, "Recent applications of fiber optic sensors to health monitoring in civil engineering", *Engineering Structures,* vol. 26, no. 11, pp. 1647-1657.

[LINZE 2009] N. Linze, W. Li, and X. Bao, "Signal-to-noise ratio improvement in Brillouin sensing" Proc. SPIE 7503, 75036F (2009).

[MATIAS 2003] Matías, I.R., Fernández-Valdivielso, C., Arregui, F.J., Bariáin, C. & López-Amo, M. 2003, "Transmitted optical power through a tapered single-mode fiber under dynamic bending effects", *Fiber and Integrated Optics,* vol. 22, no. 3, pp. 173-187.

[ROGERS 2002] A. Rogers, "Handbook of fibre optic sensing technology", ed. J. M. Lopez-Higuera (John Wiley & Sons, Chichester, 2002), Chap. 14.

[SOTO 2009] Soto, M.A., Bolognini, G., Di Pasquale, F. & Thévenaz, L. 2010, "Simplex-coded BOTDA fiber sensor with 1 m spatial resolution over a 50 km range", *Optics Letters,* vol. 35, no. 2, pp. 259-261.

[SOTO 2014] Soto, M.A., Angulo-Vinuesa, X., Martin-Lopez, S., Chin, S.-H., Ania-Castañon, J.D., Corredera, P., Rochat, E., Gonzalez-Herraez, M., Thévenaz, L., 2014,

"Extending the real remoteness of long-range brillouin optical time-domain fiber analyzers", Journal of Lightwave Technology, vol. 32, no. 1, art. no. 6678536, pp. 152-162.

[TAKI 2013] Taki, M., Soto, M.A., Bolognini, G., Di Pasquale, F. 2013, "Study of Raman amplification in DPP-BOTDA sensing employing Simplex coding for sub-meter scale spatial resolution over long fiber distances", *Measurement Science and Technology*, vol. 24 no. 9, art. no. 094018.

[ZORNOZA 2010a] Zornoza, A., Pérez-Herrera, R.A., Elosúa, C., Diaz, S., Bariain, C., Loayssa, A. & Lopez-Amo, M. 2010, "Long-range hybrid network with point and distributed Brillouin sensors using Raman amplification", *Optics Express,* vol. 18, no. 9, pp. 9531-9541.

 [ZORNOZA 2010b] Zornoza, A., Olier, D., Sagues, M. & Loayssa, A. 2010, "Brillouin distributed sensor using RF shaping of pump pulses", *Measurement Science and Technology,* vol. 21, no. 9.

CHAPTER 6

BOTDA SENSORS USING COHERENT SELF-HETERODYNE DETECTION

6.1   INTRODUCTION

In field applications of BOTDA sensors, where high resolution and fast measuring times are required, having clean and low noise measurements can be really challenging. In this cases, the performance of BOTDA sensors is limited by the reduced gain or loss generated during the SBS interaction, which can be near the noise floor. The natural solution to this problem may seem to enhance the SBS interaction and the signal to noise ratio of the signals by increasing the probe and pump powers. Nevertheless, as we have explained in detail in chapter 1 of this thesis, the maximum usable power of these waves is limited by modulation instability and spontaneous Raman scattering in the pump pulse case [ALASIA 2005], and by non-local effects, for the probe power [MINARDO 2005]. Consequently, the overall performance of the sensor is deteriorated when using powers above certain threshold. There have been proposals of different solutions such as Raman amplification [ZORNOZA 2010] or pulsing the probe wave [ZORNOZA 2011, DONG 2011], to increase the threshold powers without affecting the sensor performance, although they can affect the setup cost or measurement time considerably. Other alternative solutions include the coding of the pump signal, and have been proven as key to improve the sensor performance without increasing the pump and probe powers [SOTO 2010].

121

In this chapter we demonstrate the benefits of applying coherent detection techniques in BOTDA systems to improve the SNR without the need of increasing the pump and probe powers [ZORNOZA 2012]. Furthermore we also show the possibility to obtain Brillouin phase-shift measurements, which further increase the accuracy of the sensor allowing fast dynamic distributed measurements in large strain ranges [URRICELQUI 2012a, URRICELQUI 2012b]. In our research, we have specifically concentrated in the application of self-heterodyne detection techniques to BOTDA sensors. In such systems the detected signal and the local oscillator are generated in the same laser source [OKOSHI 1980], so the phase noise is reduced. Furthermore we benefit from the fact that BOTDA setups architectures perfectly fit the implementation of self-heterodyne detection.

6.2   BOTDA SELF-HETERODYNE DETECTION THEORY

Coherent systems have been widely used in fiber optic communication and sensor systems in order to enhance the performance by increasing the sensitivity in detection [AGRAWAL 1997]. The basic idea is the coherent combination of the information carrying optical signal with a continuous wave, the local oscillator (LO). Then, the system benefits from the nonlinear operation of optical to electrical converters: the output current of a photo receiver is proportional to the square of the input optical field. So, the beating of the received optical signal with the LO improves the receiver performance.

There are two main types of coherent detection techniques: homodyne detection and heterodyne detection, depending on the wavelength of the LO. In the homodyne detection, the wavelength of the local oscillator is chosen to be the same as the optical signal carrying the information. If the two signals are in phase, the detected electrical power is increased by a factor given by the LO power. The heterodyne detection technique however, uses a different wavelength for the LO. So, during the detection operation the two different components, each of them at a different wavelength or optical frequency, are beaten and a new spectral component is generated in the electrical domain. The frequency of the new spectral component is given by the optical frequency difference between the LO and the signal. During the detection, the amplitude of each optical component is multiplied by the other one, so the weakest signal is amplified by the strongest, the same as in the homodyne case. Also, the phase difference of each of the peaks with the other will be present in the generated electrical signal, as the phase offset of the RF signal. Note that phase difference variation on time between the LO and the signals in any of both techniques would add phase noise to the electrical signal. To prevent from this phase noise, in the so-called self-heterodyne and self-homodyne techniques instead of having two different optical

sources for the signal and the LO, the same laser source for the generation of the two signals is used. Nevertheless in these cases, the optical network architecture must allow for such schemes, because the laser source and the receiver must be one next to the other.

In conventional self-heterodyne detection, the laser output is divided in two branches. One of the signals, the local oscillator, is delayed, and the other one is modulated. Finally, both signals are recombined before the photo-receiver for heterodyne detection [OKOSHI 1980]. Although this scheme is also possible, we propose a slight modification to apply in BOTDA. It consists in modulating the laser output and using the sideband as probe and the carrier as LO, without any division and recombination. This particular coherent technique fits perfectly the architecture of BOTDA. Since the probe power is limited by non-local effects, the LO can be increased for a greater performance in detection. Also, this scheme is simpler and has the benefit that the LO and the probe wave are coherent, so that we avoid phase noise that would appear in the conventional self-heterodyne scheme.
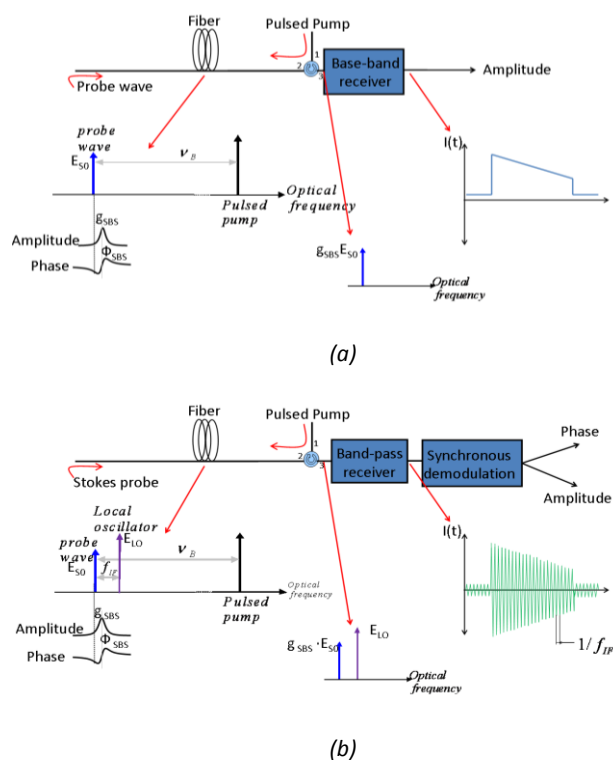

(a)

(b)

Figure 6.1: Step by step Schematic diagram of the BOTDA interaction and detection using common direct detection (a) and self-heterodyne detection with synchronous demodulation (b).

In figure 6.1(a) a conventional BOTDA's detection operation principle is shown, the same as in chapter 1, but repeated for clarity. As we have seen, after the optical to electrical conversion in a baseband photo-receiver, the detected current is:

123

$$I(t) = R_D P_{S0} \left(H_{SBS}(\nu_S, z) \right)^2$$
$$= R_D P_{S0} \exp\left(2g_{SBS}(\nu_S, z) \right) \approx R_D P_{S0} \left(1 + g_{SBS}(\nu_S, z) \right)^2 \tag{6.1}$$

where R_D is the detector responsivity and P_{S0} is the power of the probe at detection. We can see that the amplitude of the detected Brillouin interaction signal current is directly proportional to the received probe power.

In figure 6.1(b) the BOTDA scheme using self-heterodyne detection is depicted. Instead of a probe signal directly coming from the laser source, as in the common setup, we have two signals arriving to the detector: a local oscillator at an optical frequency of ν_{LO} and the probe wave at an optical frequency of ν_S. The SBS interaction occurs between the pump pulse and the probe wave. So, in this case, the total optical field received after Brillouin interaction is:

$$E_T(t,\nu) = E_{S0} H_{SBS}(\nu_S, z) \exp\left(j\left(2\pi \nu_S t + \phi_{SBS}(\nu_S, z) \right) \right) + E_{LO} \exp(j 2\pi \nu_{LO} t) \tag{6.2}$$

where E_{S0} is the complex amplitude of the probe wave, and E_{LO} is the complex amplitude of the local oscillator. Then, the detected optical power at the frequency difference between the probe and the local oscillator is:

$$P_T(t,\nu_S) = 2\sqrt{P_{S0} P_{LO} \exp\left(2g_{SBS}(\nu_S, z) \right)} \cos\left(2\pi f_{IF} t + \phi_0 - \phi_{SBS}(\nu_S, z) \right)$$
$$\approx 2\sqrt{P_{S0} P_{LO} \left(1 + g_{SBS}(\nu_S, z) \right)^2} \cos\left(2\pi f_{IF} t + \phi_0 - \phi_{SBS}(\nu_S, z) \right) \tag{6.3}$$

where ϕ_0 and f_{IF} are the phase and frequency difference between the probe and the local oscillator, P_{LO} the optical power of the local oscillator and P_{S0} the probe wave power. The detected current is then:

$$I(t) = 2R_C \sqrt{P_{S0} P_{LO} \exp\left(2g_{SBS}(\nu_S, z) \right)} \cos\left(2\pi f_{IF} t + \phi_0 - \phi_{SBS}(\nu_S, z) \right)$$
$$\approx 2R_C \sqrt{P_{S0} P_{LO} \left(1 + g_{SBS}(\nu_S, z) \right)^2} \cos\left(2\pi f_{IF} t + \phi_0 - \phi_{SBS}(\nu_S, z) \right) \tag{6.4}$$

where R_C is the detector responsivity. The current is not directly proportional to the Stokes signal, but to the square root of the product for the local oscillator and stokes powers. Then, if the stokes signal and local oscillator have the same power, the signal power is the same as in base-band detection. However if the local oscillator power is greater, the detected signal's current is greater than in the base-band detection. This supposes an increase in the SNR of the current, and hence in the measurement quality, because the current amplitude is amplified while the noise is kept at the same level. A detailed analysis of the improvement in SNR is performed in the next section. Furthermore, we can see that (6.4) is not only an amplitude modulated signal but a phase modulated signal, since the Brillouin phase shift contribution is not lost in the

optical to electrical conversion. Then, the Brillouin distributed phase shift can be measured.

6.3   STUDY OF THE SNR IN SELF-HETERODYNE BOTDA

After the description of the self-heterodyne scheme applied to BOTDA sensors, we perform a thorough analysis for the SNR of these systems comparing it to direct detection schemes. In figure 6.2 the noisy demodulation model for both systems self-heterodyne and conventional BOTDA, is presented. Note that the baseband demodulation model was already presented in chapter 1, and here is repeated for clarity. In both cases we assume the presence of white and Gaussian noise, *w(t)*, with a spectral density of $\eta/2$. So, for the commonly used base band detection technique, following the diagram of figure 6.2(a), the received current in presence of noise is then:

$$z(t) = I(t) + n(t) = R_D P_{S0} \exp\left(2 g_{SBS}(\nu_S, z)\right) + n(t) \approx R_D P_{S0}\left(1 + g_{SBS}(\nu_S, z)\right)^2 + n(t) \quad (6.5)$$

Where *n(t)* is the filtered noise *w(t)*, in the bandwidth of $I_S(t)$, *Δf*. So we can conclude that the signal to noise ratio of a conventional BOTDA setup is given by:

$$SNR_D = \frac{4 R_D^{\,2} P_{S0}^2 g_{SBS}^2}{2 \eta \Delta f} = \frac{4 R_D^{\,2} P_{S0}^2 g_{SBS}^2}{\sigma_D^2} \quad (6.6)$$

where σ_D^2 is the total noise of the system in the given bandwidth, and can be expressed as:

$$\sigma_D^2 = \sigma_{TD}^2 + \sigma_{RD}^2 + \sigma_{SD}^2 =$$
$$= \frac{4 \cdot K_B \cdot T}{R_L} \cdot F_n \cdot \Delta f + RIN \cdot \left(P_S \cdot R_D\right)^2 \cdot \Delta f + 2 \cdot q \cdot (R_D \cdot P_S + I_d) \cdot \Delta f \quad (6.7)$$

where σ_{TD}^2 is the thermal noise contribution, σ_{RD}^2 the relative intensity noise (RIN) contribution, σ_{SD}^2 the shot noise contribution, K_B the Boltzmann constant, *T* the photo-detector operating temperature, R_L the output resistance, F_n the photo-detector preamplifier noise figure, *RIN* the relative intensity noise of the laser source, *q* the electron charge and I_d the photo-detector dark current. The probe power is usually low (<-15dBm). Hence, RIN and shot contributions are negligible. Thus, in conventional BOTDA systems where direct detection is employed the noise is predominantly thermal.

As a consequence we can conclude that in conventional BOTDAs with direct detection, the SNR is directly proportional to the detected probe power. Accordingly, with a stronger P_S the SNR is increased. Nevertheless, if the probe power is increased,

non-local effects appear to be noticeable, which must be taken into account with powers as low as -14dBm in long range measurements [THEVENAZ 2011]. Therefore, the maximum probe power launched to the fiber in long range BOTDA measurements cannot exceed a certain level, limiting significantly the systems SNR.

Following the diagram in figure 6.2(b), in the self-heterodyne scheme, the pass band noise is [THOMAS 2006]:

$$n(t) = r(t)\cos\left(2\pi f_{IF}t + \varphi(t)\right) = n_I(t)\cos(2\pi f_{IF}t) - n_Q(t)\sin(2\pi f_{IF}t)$$
(6.8)

where *r(t)* is the amplitude of the pass band noise at center frequency f_{IF}, $\varphi(t)$ is the phase of the pass band noise, $n_I(t)$ the in phase component of the pass band noise and $n_Q(t)$ the quadrature component of the pass band noise. The current before demodulation depends on the format of the probe power. The easiest way to obtain a probe and optical oscillator with a known phase difference and with a fixed frequency shift between them is modulating the output of a laser source. However, depending on the modulation format, the detected current will be different. In this chapter we are going to concentrate in two different modulation formats. The first is OSSB, which matches perfectly the ideal self-heterodyne scheme previously described. Although the modulation can be complicated to achieve, since care must be taken while modulating, it has the advantage that in detection, the Brillouin gain and phase shift are perfectly translated from the optical to the electrical domain. The other format is phase modulation (PM), which is very easy to achieve experimentally, and has some other advantages such as a low average power after detection, thus simplifying the demodulation scheme. Other demodulation formats, such as amplitude modulation (AM), are not studied because they do not add any advantage or degree of freedom for the applications we propose in this chapter. The optical field in detection for an OSSB modulated probe is given by:

$$E_{OSSB}(t) = E_0 \exp(j2\pi v_0 t) + E_{SB}H_{SBS}(v_0 + f_{IF}, z)\exp(j2\pi(v_0 + f_{IF})t)$$
(6.9)

where E_0 is the complex amplitude of the carrier, and E_{SB} is the complex amplitude of the sideband. Note the similarity of this equation with equation (6.2), where only the suffixes are different. Therefore we can calculate the detected optical power and current the same as in equation (6.3) and (6.4) respectively. We can go one step further and write the electrical current after detection as a phasor, following figure 6.3:

$$z(t) = I_{OSSB}(t) = |A_{OSSB}(t)|\exp\left(j\phi_{OSSB}(t)\right) + |n(t)|\exp\left(j\varphi(t)\right)$$
(6.10)

where $A_{OSSB}(t)$ and $n(t)$ are the amplitude of the signal and noise respectively, with $\phi_{OSSB}(t)$ and $\varphi(t)$ their phases. We can particularize the phase and amplitude terms of the signal following the definition of the transfer function of Brillouin given in equation (1.13) to:

$$\left|A_{OSSB}(t)\right| \equiv 2R_D\sqrt{P_0 P_{SB}} \exp\left(\frac{g_1}{1+\left(2\dfrac{\Delta v(t,f)}{\Delta v_B}\right)^2}\right) \tag{6.11}$$

$$\phi_{OSSB}(t) \equiv \frac{-2\dfrac{\Delta v(t,f)}{\Delta v_B} g_1}{1+\left(2\dfrac{\Delta v(t,f)}{\Delta v_B}\right)^2} \tag{6.12}$$

where P_0 is the power of the carrier and P_{SB} is the power of the sideband.

When phase modulation is used, the optical field in detection is given by:

$$\begin{aligned}
E_{PM}(t) &= -E_{SB}\exp(j2\pi(v_0-f_{IF})t) + E_0\exp(j2\pi v_0 t)\\
&+ H_{SBS}(v_0+f_{IF},z)E_{SB}\exp(j2\pi(v_0+f_{IF})t)
\end{aligned} \tag{6.13}$$

Note that in this case we have two sidebands with opposite phases. So, the current after detection can be expressed as a phasor taking into account figure 6.3 as follows:

$$\begin{aligned}
z(t) = I_{PM}(t) &= R_D 2\sqrt{P_0 P_{SB}}\left(H_{SBS}(v_0+f_{IF},z)-1\right)\\
&= \left|A_{PM}(t)\right|\exp\left(j\phi_{PM}(t)\right) + \left|n(t)\right|\exp\left(j\varphi(t)\right)
\end{aligned} \tag{6.14}$$

where A_{PM} and n are the amplitude of the signal and noise respectively, with ϕ_{PM} and φ their phases. These terms are particularly:

$$\left|A_{PM}(t)\right| = \left|R_D 2\sqrt{P_0 P_{SB}}\left(H_{SBS}(v_0+f_{IF},z)-1\right)\right| \tag{6.15}$$

$$\phi_{PM}(t) = \angle\left(R_D 2\sqrt{P_0 P_{SB}}\left(H_{SBS}(v_0+f_{IF},z)-1\right)\right) \tag{6.16}$$

The reason behind the improvement on the sensitivity of the detector obtained in coherent detection is that the amplitude of this electrical signal is given by the product of the power of both optical signals. So the lower power signal is amplified considerably. Furthermore, the information for the phase of the signal is not lost, in opposition to a conventional BOTDA (6.1). $z(t)$ is then an amplitude and phase modulated signal that contains not only the conventional information of the Brillouin gain along the fiber, but also information of the Brillouin phase-shift along the fiber. Finally this signal must be demodulated so as to obtain the phase and amplitude

information. This last step can be easily performed in the electrical domain through synchronous demodulation, following the demodulation model in figure 6.2 (b). We will first concentrate in the SNR when the amplitude of the signal is measured, and after that, we will study the SNR in phase measurements.

Equations (6.9) and (6.13) show a simplified model of the BOTDA interaction. We must note that the carrier and other sidebands will be affected by the Brillouin interaction too. This influence however is very small for the signal to noise ratio analysis we are performing in this section, and can be neglected. However, when performing BOTDA measurements this effect distorts the measured spectrum by making it asymmetric, so the faddeeva function defined in chapter 1 is not accurate enough for the fitting. We can take into account the effects of the remaining spectral lines for the fitting function in order to easily avoid errors and perform accurate fitting of the measured spectra.
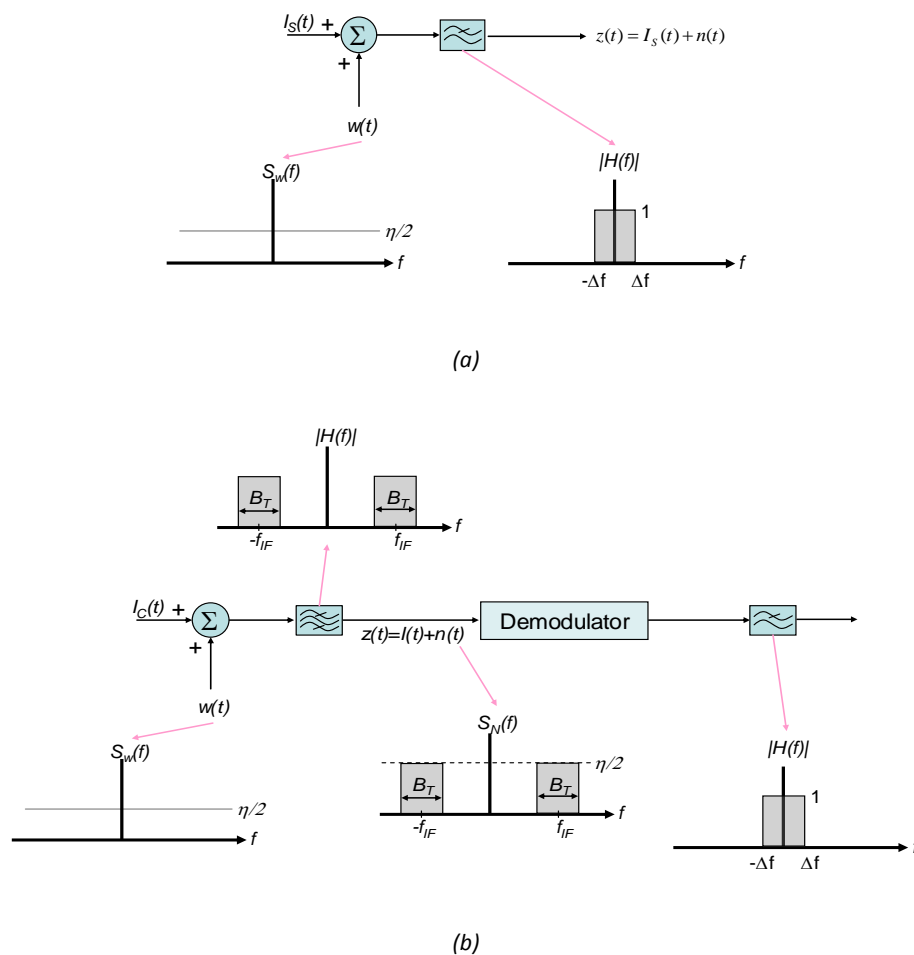

(a)

(b)

Figure 6.2: Schematic noisy demodulation model for the base band detection (a) and the phase or amplitude modulated signal (b).
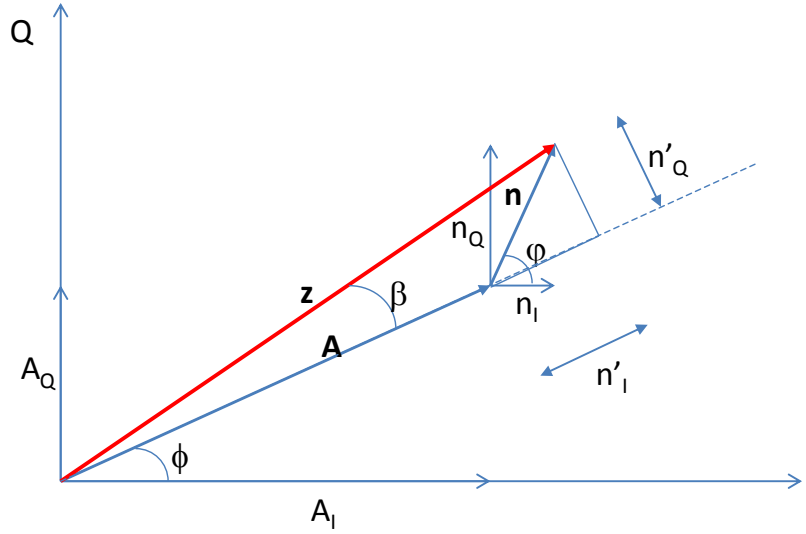
Figure 6.3: phasorial diagram of the noisy current at detection. Note that this diagram is valid for any modulation format, PM or OSSB, as long as the amplitudes and phases are substituted with their actual values.

6.3.1   SNR IN AMPLITUDE MEASUREMENTS

When g_B is a very small number, what usually happens in BOTDA, we can further approximate using $H_{SBS} \cong (1+g_{SBS})exp(j\phi_{SBS})$. Consequently, when performing OSSB modulation, (6.11) can be approximated to:

$$\left| A_{OSSB}(t) \right| \cong 2R_D \sqrt{P_0 P_{SB}} \left(1 + \frac{g_1}{1 + \left(2\dfrac{\Delta v(t,f)}{\Delta v_B} \right)^2} \right) \tag{6.17}$$

In the case of PM modulation, (6.19) can be approximated to:

$$\left| A_{PM}(t) \right| \cong \frac{2g_1 R_D \sqrt{P_0 P_{SB}}}{\sqrt{1 + \left(2\dfrac{\Delta v(t,f)}{\Delta v_B} \right)^2}} \tag{6.18}$$

We can observe two differences between the two profiles. The first one is the pedestal of the signal in OSSB, which is not present in PM. Since this pedestal does not contribute to the SNR, we can neglect it for this analysis. The second difference is the denominator, which is different in both cases. Therefore, the signal to noise ratio is

different for each modulation format, depending the frequency difference between pump and probe. For the OSSB case we have:

$$SNR_{OSSB\_amp} \approx \frac{\left(\dfrac{g_1}{1+\left(2\dfrac{\Delta\nu(t,f)}{\Delta\nu_B}\right)^2}\right)^2}{\dfrac{2\eta\Delta f}{4R^2{}_D P_0 P_{SB}}} \qquad (6.19)$$

While for the PM case we have:

$$SNR_{PM\_amp} \approx \frac{\left(\dfrac{g_1}{\sqrt{1+\left(2\dfrac{\Delta\nu(t,f)}{\Delta\nu_B}\right)^2}}\right)^2}{\dfrac{2\eta\Delta f}{4R^2{}_D P_0 P_{SB}}} \qquad (6.20)$$

However, for both cases, PM and OSSB, in the maximum interaction frequency, the SNR for the described self-heterodyne detection is the same, and it is given by:

$$SNR_C = \frac{4R_C{}^2 P_{S0} g^2_{SBS} P_{LO}}{2\eta\Delta f} = \frac{4R_C{}^2 P_{S0} g^2_{SBS} P_{LO}}{\sigma^2_C} \qquad (6.21)$$

Therefore with a self-heterodyne detection BOTDA, we can maintain the probe wave power to the limit in which non-local effects are negligible, and increase the SNR by using a stronger local oscillator without any penalization. Then, if the noise in the coherent system was the same as in the conventional system, the theoretical improvement of the SNR would be given by P_C/P_{S0}. However, this is a theoretical limit which is only true if the noise levels in both systems were the same, but with a powerful local oscillator the noise of the system is not only given by the thermal noise: relative intensity noise (RIN) and shot noise contributions must be taken into account, which can be negligible in direct detection. Actually, if the local oscillator is powerful enough, we could achieve the shot noise limit. Hence, in the coherent case, the noise is:

$$\sigma^2_C = \sigma^2_{TC} + \sigma^2_{RC} + \sigma^2_{SC} =$$
$$= \frac{4 \cdot K_B \cdot T}{R_L} \cdot F_n \cdot \Delta f + RIN \cdot (P_{LO} \cdot R_C)^2 \cdot \Delta f + 2 \cdot q \cdot (R_C \cdot P_{LO} + I_d) \cdot \Delta f \qquad (6.22)$$

Finally, comparing the two detection systems, the improvement achieved with self-heterodyne detection is given by:

$$\frac{SNR_C}{SNR_D} = \frac{R_C{}^2 P_C}{R_D{}^2 P_{S0}} \frac{\sigma_D^2}{\sigma_C^2}$$

(6.23)

The P_C/P_{S0} improvement is only true when the increase of the signal due to coherent detection is bigger than the increase of noise due to shot and RIN contributions. Now we are going to present some experimental measurements that validate the previous analysis.

6.3.1.1 EXPERIMENTAL SETUP AND MEASUREMENTS

As we have seen, the improvement of the SNR is notable using coherent self-heterodyne detection. So in this subsection we will present measurements so we can confirm the theoretical results. In order to generate the LO and stokes signals, we can use an OSSB modulation or PM modulation. However there is an experimental advantage when using PM: the signal after detection is only composed by the Brillouin interaction, without a carrier. Then, although the Brillouin signal amplitude is the same as in the OSSB case, the elimination of the carrier reduces the overall power. So the electronic devices that perform the demodulation handle less power, and can perform further away from saturation, simplifying the demodulation process considerably.

In figure 6.4 a schematic of the experimental setup is depicted. Note that it is based on the setup described in chapter 2, with some variations so as to generate the required signal for self-heterodyne detection. The output of the DFB laser is divided in two branches employing a 90:10 optical coupler. The signal in the upper branch, corresponding to the 10 percent of the couple output, is directed to a Mach-Zehnder electro-optic modulator (MZ-EOM), where we generate high extinction ratio optical pulses with the RF pulse-shaping technique [ZORNOZA 2010]. So the MZ-EOM is modulated with microwave pulses at near 11GHz so as to obtain a pulsed double-sideband with suppressed carrier modulation of the incident light. These pulses are generated in a microwave switch driven by a pulse generator and a microwave synthesizer. After the optical pulses are generated, they are amplified in an erbium doped fiber amplifier (EDFA) to acquire the desired power level. The ASE noise and the unwanted pulsed sideband are filtered in a narrow fiber Bragg grating (FBG). Then, so as to compensate the polarization sensitivity of SBS before the pump pulse is directed to the fiber by a circulator, a polarization scrambler is employed.

In the lower branch the probe wave is generated by modulating the output of the laser with an electro-optic modulator with an RF signal from an RF synthesizer. The

modulator can be a phase modulator or an amplitude modulator, depending if PM or OSSB is wanted. Then, the modulated optical signal goes directly to the fiber where it interacts with the pump pulse. After that, it is detected in a photo-receiver with enough bandwidth to detect the beat of the carrier with the sideband, and perform the self-heterodyne detection. The detected signal is subsequently demodulated in a synchronous demodulator. By using the same RF synthesizer source for the optical modulation and for the RF synchronous demodulation the phase noise is minimized [AGRAWAL 1997].

There is a trade-off between using a low or a high frequency in the RF synthesizer. If the frequency is too low, less than 500MHz, the pump pulse also interacts with the carrier which can be much stronger than the probe, and it must be taken into account. Also, if the frequency is too high, greater than 1.5GHz, the cost of the setup is more expensive since higher bandwidth devices are required in the setup.
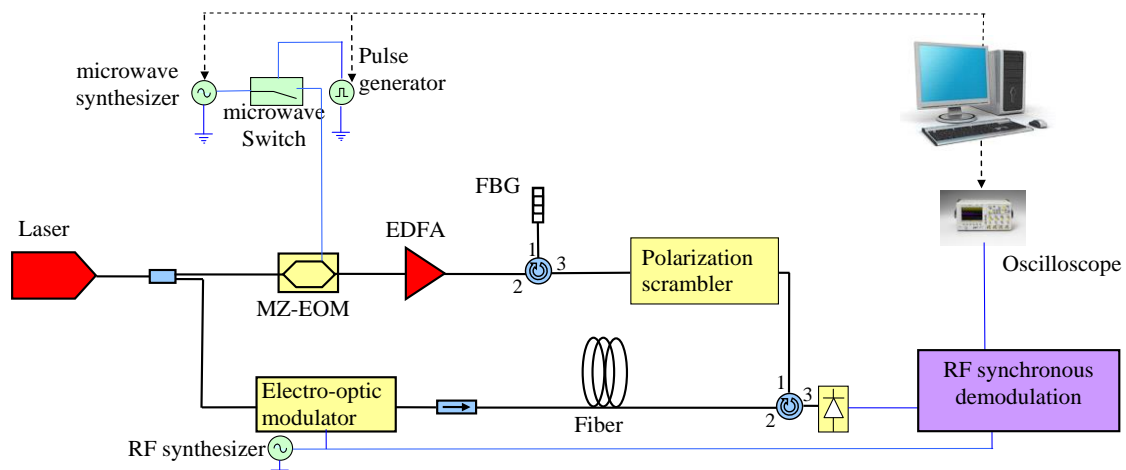

Figure 6.4: Scheme of the self-heterodyne detection BOTDA experimental setup.

Note that in this scheme the frequency sweep between pump and probe waves, which is of the essence to measure the Brillouin spectrum, can be made in two different ways. The first would be sweeping the microwave signal of the pump pulses, which is the typical in BOTDA setups. The second way would be sweeping the RF signal modulating in the probe signal. In the latter, since the RF signal is one order of magnitude lower than the microwave signal, the setup cost is reduced considerably. This is because a 1-MHz precision RF signal synthesizer (working at frequencies below 2GHz) is much cheaper than a 1-MHz precision microwave generator (working at frequencies around 11GHz). It also should be remarked that in the self-heterodyne scheme, since the photocurrent is in AC, the signal amplification is much simpler than when it has DC components, like in conventional BOTDAs.

We compared the performance of a conventional BOTDA sensor employing direct detection and our proposal of self-heterodyne detection and RF synchronous demodulation BOTDA setup under the same conditions. The experimental setup employing self-heterodyne detection was built following the scheme in figure 6.4. The modulation format chosen for self-heterodyne detection was phase modulation at a frequency of 850MHz. The power of the carrier to be used as local oscillator was limited because of spontaneous Brillouin scattering, so we fixed this parameter to the value of 5dBm [THEVENAZ 2011]. We measured the phase modulated signal in an ESA using heterodyne detection by combining the signal with another laser source. The result is shown in figure 6.5 and it was used to ensure that the modulation index was the required to have the desired probe power
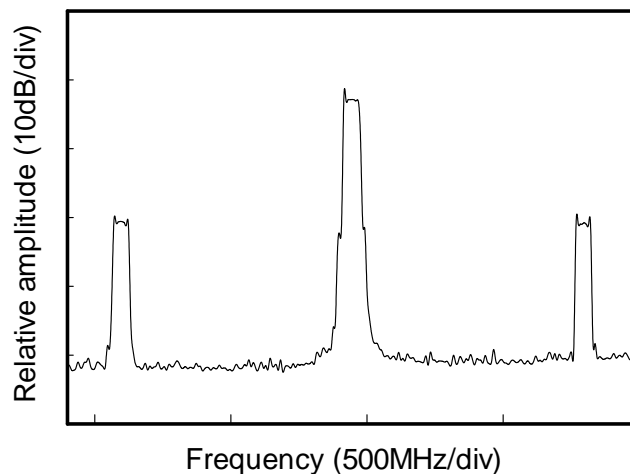

Figure 6.5: Phase modulation measured with heterodyne detection. The upper sideband is the probe wave for the BOTDA interaction.

The conventional BOTDA built for the comparison followed the scheme described in chapter 2. We equalized the values of all the operational parameters such as probe power, pump power, number of averages and spatial resolution in both systems. Note that in both systems we take advantage from the RF pulse shaping technique, so the pump pulses also have the same shape. The probe power, i.e. the side band of the modulation in the self-heterodyne setup and the unaltered laser output in the conventional setup, was set to -13dBm so as to avoid non-local effects. The pump pulse power was limited fixed to a value of 21.5dBm, because of the apparition of modulation instability. The photo-receivers employed in the two cases were different to fit the required bandwidth, power and coupling characteristics of the two systems. Nevertheless, the thermal noise levels in the two cases were similar. The spatial resolution was fixed to 1m and the averaging to 1024 acquisitions and we performed BOTDA measurements in a 20.6-km SMF fiber.

In figure 6.6 the distributed Brillouin gain trace in the maximum Brillouin interaction, with a near ν_B frequency difference between pump and probe, is shown. The trace using self-heterodyne detection is much cleaner than the trace using conventional direct detection. In order to quantify the improvement achieved, we calculated the SNR of each trace with:

$$SNR = \frac{V^2{}_{BOTDA}}{\sigma_v^2}$$

(6.24)

where V_{BOTDA} the amplitude of the BOTDA signal when the Brillouin gain is minimum (at the end of the fiber) and σ_v^2 the variance of the noise floor in the BOTDA trace. The improvement obtained using self-heterodyne detection is measured to be of 7.89dB, which is near the theoretical value calculated with (6.21), 7.1dB.

By sweeping the frequency of the pump wave in a span of 400MHz with steps of 4MHz we reconstruct the whole Brillouin spectra for each point of the fiber and measure the ν_B along the fiber. This measurement for both cases is represented in figure 6.7, and we can see that the measurement employing self-heterodyne detection is cleaner. In order to approximate the accuracy of the sensors we calculated the standard deviation of the measured ν_B along the fiber. So, after performing 5 consecutive measurements with the fiber under the same conditions, we depict the obtained standard deviation distribution in figure 6.8. Once again the measurements performed with coherent detection show to be better than the measurements performed with conventional BOTDA. Using the values from figure 6.8 we can also quantify the SNR in BOTDA sensors by the expression [HORIGUCHI 1995]:

$$SNR = \frac{\Delta\nu^4{}_B}{4 \cdot \delta\nu_B{}^4}$$

(6.25)

where $\delta\nu_B$ is the precision of the estimated frequency in the measurement. The improvement of SNR is of 14.3dB. However, we are using 10ns pulses for our measurements and (6.25) was defined taking into account the Lorentzian shape of the Brillouin spectrum. In our case the profile of the Brillouin gain spectrum is no more Lorentzian, it comes from the convolution between a Lorentzian and the pulse spectrum, as explained in chapter 1. Furthermore, equation (6.25) does not take into account parameters such as the measured frequency span or frequency step, which are very important parameters that affect measurement accuracy. Recently a new SNR analysis in BOTDA signals has proven that equation (6.25) is not a good model for BOTDA SNR estimation [SOTO 2013], and the following expression to quantify the figure of merit of BOTDA sensors is presented:

$$FoM = \frac{(\alpha L_{eff})^2 \exp(2\alpha L)\sqrt{f_{step}\Delta \nu_B}}{\delta \nu_B \Delta z \sqrt{N}}$$ (6.26)

where f_{step} is the step of the frequency sweep and L_{eff} the effective length of the fiber. Taking into account this equation, the figure of merit would be improved 2.27 times, which is a great improvement.
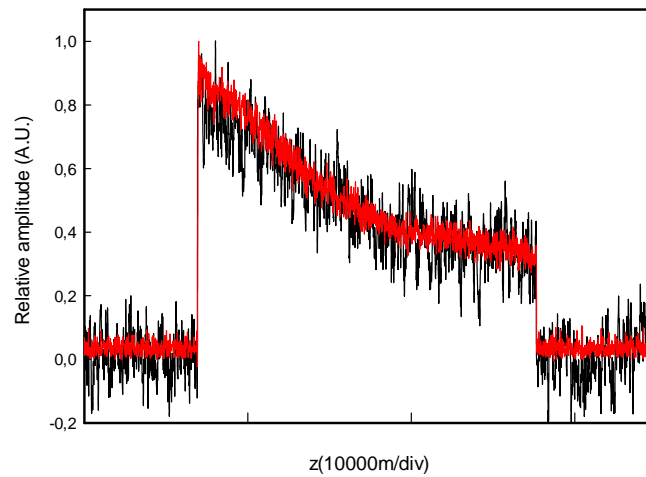

Figure 6.6: Amplitude BOTDA traces employing a conventional BOTDA system (black) and a coherent detection BOTDA (red) in equal power and resolution conditions in a 20-km long fiber.
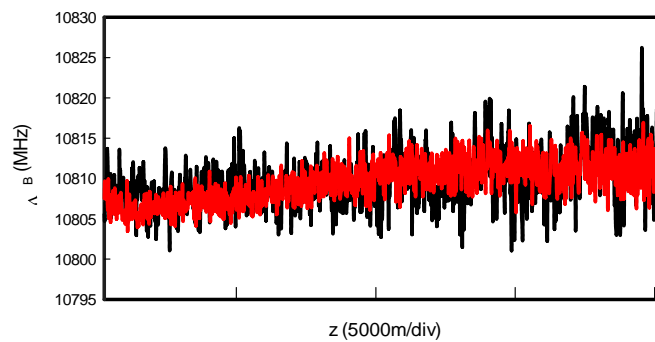

Figure 6.7: ν_B measured in a 20km fiber at 1m resolution, where the red trace was obtained employing the coherent BOTDA and the black trace with conventional BOTDA.
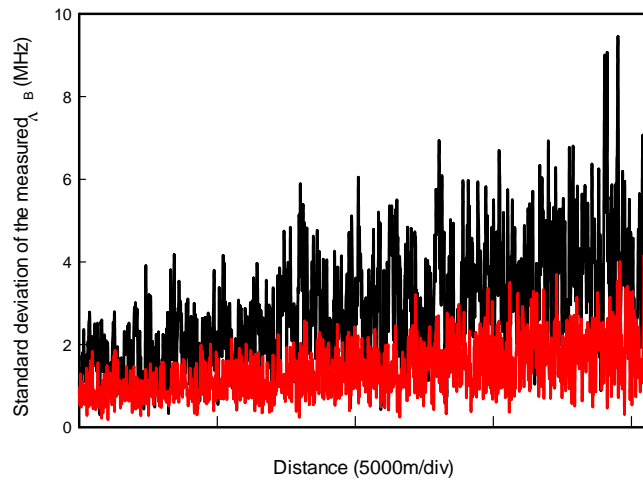
Figure 6.8: Standard deviation of 5 consecutive distributed measurement of the Brillouin frequency shift in black with self-heterodyne detection and in black with conventional BOTDA

In figure 6.9 we show the obtained ν_B of a measurement performed in a 25km fiber with 10ns pump pulses so as to ensure the systems capability. The last 36m of fiber were introduced in a thermal bath at a temperature of 50ºC, while the rest of the fiber was kept at room temperature (23ºC). We can measure the spatial resolution, which is below 1m.
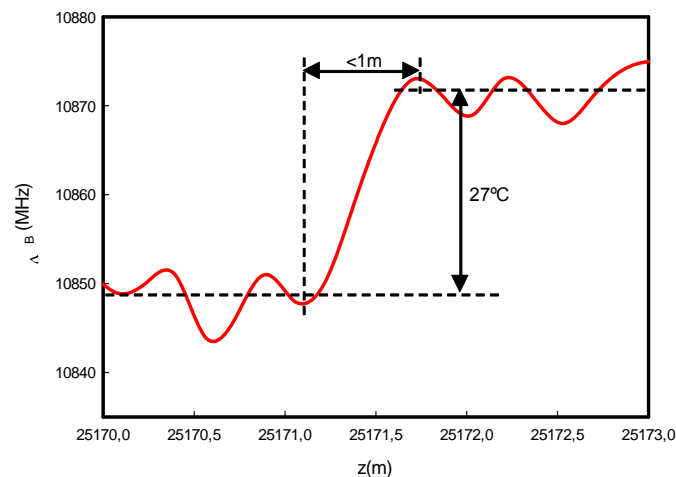

Figure 6.9: Zoom of the ν_B in the transition between the room temperature fiber section and the 36m section at the end of a 25.2km fiber that has been heated to 50ºC in a thermal bath.

6.3.2   SNR WITH BRILLOUIN PHASE SHIFT MEASUREMENTS

In section 6.1, expression (6.4), we have seen that with self-heterodyne detection the phase shift caused by the Brillouin interaction along the fiber is present in the detected current phase. So this information can also be studied instead of the amplitude to estimate the Brillouin frequency shift of the fiber. However the SNR analysis previously performed is not equivalent for phase measurements. So in this subsection we investigate phase measurements in terms of SNR. When measuring the phase we can notice that depending on the modulation format we use, the resulting measured phase is different. So, we will study the two cases, OSSB modulation and PM separately.

6.3.2.1 OSSB MODULATION FORMAT

Using OSSB modulation, the Brillouin phase shift is directly translated to the electrical domain, as seen in equation (6.4). From figure 6.3 and equation (6.4) we have that the phase, taking into account the noise, is given by:

$$
\theta_{OSSB} = \phi_{OSSB}(t,f) + \beta(t) = \frac{-2\frac{\Delta v(t,f)}{\Delta v_B}g_1}{1+\left(2\frac{\Delta v(t,f)}{\Delta v_B}\right)^2} + \arctan\left(\frac{n'_Q(t)}{\left|A_{OSSB}(t)\right|+n'_I(t)}\right) =
$$

$$
\frac{-2\frac{\Delta v(t,f)}{\Delta v_B}g_1}{1+\left(2\frac{\Delta v(t,f)}{\Delta v_B}\right)^2} + \arctan\left(\frac{\left|n(t)\right|\sin(\varphi-\phi)}{\left|A_{OSSB}(t)\right|+\left|n(t)\right|\cos(\varphi-\phi)}\right)
$$

$$
\approx \frac{-2\frac{\Delta v(t,f)}{\Delta v_B}g_1}{1+\left(2\frac{\Delta v(t,f)}{\Delta v_B}\right)^2} + \arctan\left(\frac{\left|n(t)\right|\sin(\varphi(t))}{\left|A_{OSSB}(t)\right|+\left|n(t)\right|\cos(\varphi(t))}\right)
$$

$$
= \frac{-2\frac{\Delta v(t,f)}{\Delta v_B}g_1}{1+\left(2\frac{\Delta v(t,f)}{\Delta v_B}\right)^2} + \arctan\left(\frac{n_I(t)}{2R_D\sqrt{P_0 P_{SB}}\exp\left(\frac{g_1}{1+\left(2\frac{\Delta v(t,f)}{\Delta v_B}\right)^2}\right)+n_Q(t)}\right)
\tag{6.27}
$$

And since $g_B \ll 1$ and $n_Q(t) \ll 2R_D\sqrt{P_0 P_{SB}}$, we can further approximate to:

$$
\theta_{OSSB} \approx \frac{-2\frac{\Delta v(t,f)}{\Delta v_B}g_1}{1+\left(2\frac{\Delta v(t,f)}{\Delta v_B}\right)^2} + \frac{n_I(t)}{2R_D\sqrt{P_0 P_{SB}}}
\tag{6.28}
$$

From there we can conclude that the signal to noise ratio can be approximated to:

$$SNR_{OSSB\_phase}(t,f) \approx \frac{\left(\dfrac{-2\dfrac{\Delta v(t,f)}{\Delta v_B} g_1}{1+\left(2\dfrac{\Delta v(t,f)}{\Delta v_B} \right)^2} \right)^2}{\dfrac{2\eta\Delta f}{4R^2{}_D P_0 P_{SB}}}$$

(6.29)

So we have the same noise level than in the amplitude cases, but with a different spectrum profiles. In figure 6.10 we can see these two spectra, for a value of g_B=0.001 and a BFS of 10500MHz. Although the amplitude spectrum is greater, the range of both signals (max-min) is actually the same. So, since the excursion of both signals is the same, this makes the SNR equal in both cases. Note that the excursion of the signal is taken as the amplitude when comparing it to the noise.
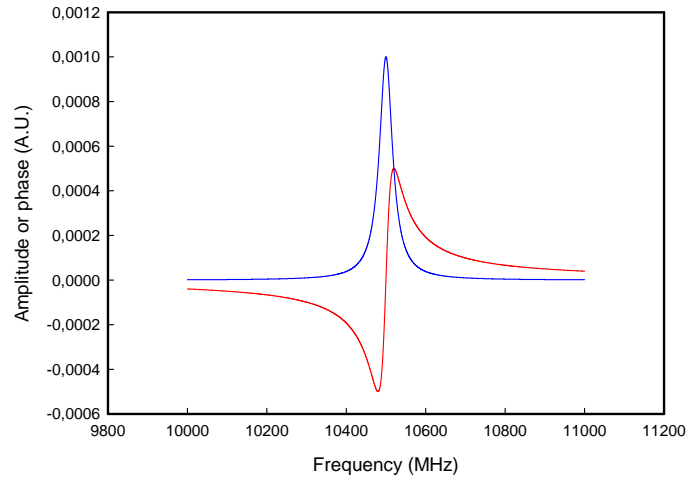

Figure 6.10: Spectra measured for phase (red) or for amplitude (blue).

We performed some simulations adding Gaussian noise to ideal (complex) spectra so as to see the behavior of the system working in phase or in amplitude measurements. The theoretical values used were a BFS of 10.785GHz, a Brillouin bandwidth of 40MHz and a g_1 of 0.0305m/W. When performing regular fits for the same level of noise, we have what depicted in figure 6.11: almost identical behavior for phase or for amplitude fits. So, there is not any advantage between amplitude measurements or phase measurements while using OSSB modulation in regular BOTDA measurements.
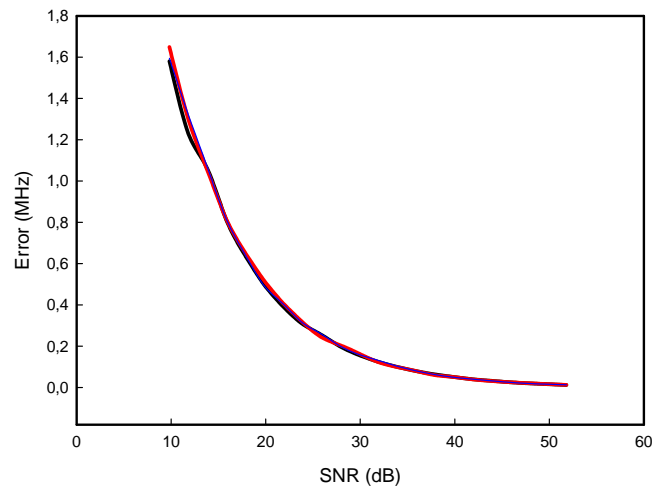
Figure 6.11: Error in the BFS for phase or amplitude fits depending on the SNR measured for phase (red) or for amplitude (blue) OSSB or direct detection (dark line) with OSSB modulation.

6.3.2.1.1 EXPERIMENTAL BRILLOUIN PHASE SHIFT MEASUREMENTS WITH OSSB

We first performed measurements, with the same setup as depicted in figure 6.4, but using an OSSB modulator for the probe power. This way, with simple synchronous demodulation the Brillouin phase shift is measured. The modulating frequency for the probe signal was chosen to operate at 500MHz. This way we generate the desired modulation format for self-heterodyne detection, which is illustrated in figure 6.12. The probe wave power was measured to be -22dBm, and the pump pulses were of 21dBm. We performed measurements in a 25km fiber with 6m resolution. In figure 6.13 we show the results of the measurements, in which we depict the distributed measurements of the gain and phase-shift. Note that as explained in section 6.3, the measured spectra are not symmetric, due to the effect of the Brillouin interaction with the remaining spectral lines of OSSB modulated signal that contains the probe. In the last section of the fiber, where the fiber is heated up to 50ºC, the Brillouin phase and gain are shifted in frequency according to the temperature change.
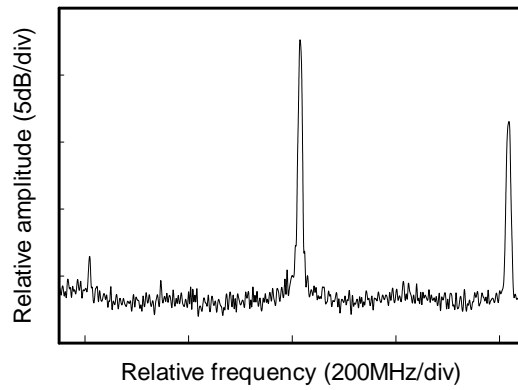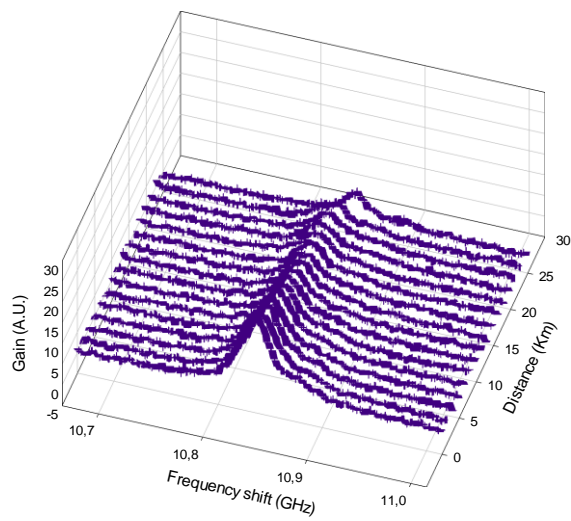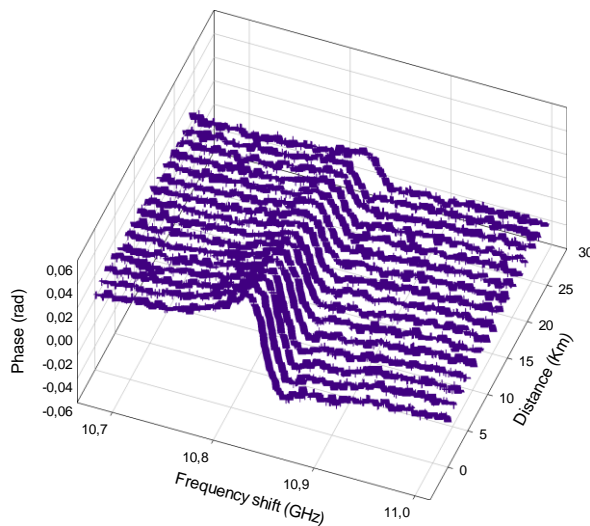
139

Figure 6.12: OSSB modulation measured with heterodyne detection, the upper sideband is the probe wave.

(a)

(b)

Figure 6.13: Distributed measurements of the Brillouin gain spectra (a) and phase-shift spectra (b) performed with OSSB modulation and self-heterodyne detection.
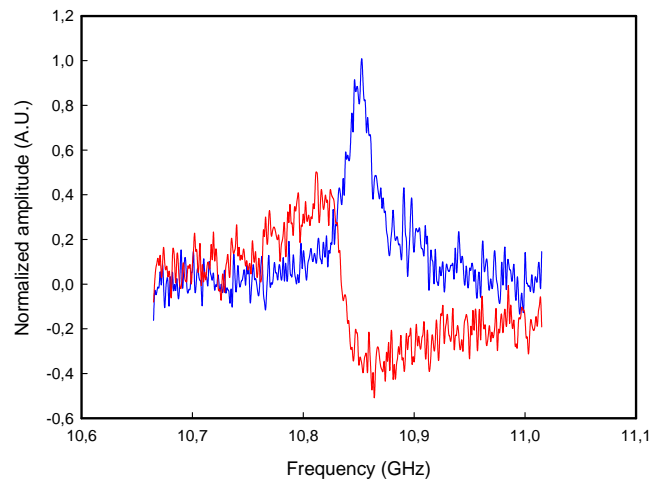
140

Figure 6.14: Experimental measurements of phase and amplitude signals with OSSB modulation.

In figure 6.14 a detailed view of the spectral profiles of the amplitude and phase signals is depicted. As predicted in the previous analysis, they exhibit the same level of noise compared with their excursion from the maximum to the minimum.

6.3.2.2 PM MODULATION FORMAT

When using phase modulation instead of OSSB is when phase measurements become more interesting. The measured phase, in expression (6.16), can be approximated to the following expression when small g_B values are present:

$$\phi_{PM}(t,f) \cong -\arctan\left(2\frac{\Delta \nu(t,f)}{\Delta \nu_B}\right)$$

(6.30)

Note that in this approximation, the phase is independent from the power or the Brillouin gain. Some simulations where performed varying the Brillouin gain, as shown in figure 6.15 to be sure of this approximation. We can see that while the amplitude varies considerably in figure 6.15(a), the phase remains the same in all cases in figure 6.15(b). Moreover there is no difference between the simulated phase spectra. This has an important implication for field measurements, because while the amplitude of the generated signal is vulnerable to loss by mechanical stress, the phase-shift is immune to this loss. That is, the phase shift measured will be the same independently from the amplitude of the signal.
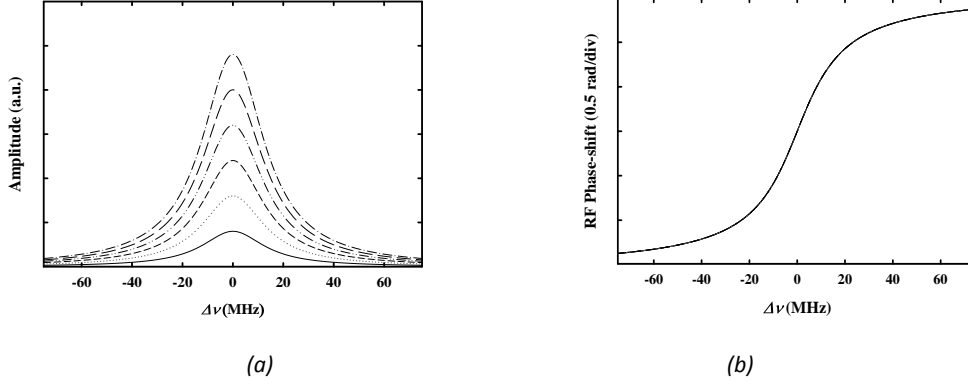
141

(a)   *(b)*

Figure 6.15: Calculated (a) amplitude at conventional BOTDA and (b) RF phase-shift of the proposed technique for different values of g_B.

The overall phase taking into account the noise, again taking into account the phasorial decomposition of figure 6.3, can be then written as follows:

$$\theta_{PM} = \phi_{PM}(t,f) + \beta(t) = -\arctan\left(2\frac{\Delta v(t,f)}{\Delta v_B}\right) + \arctan\left(\frac{n'_Q(t)}{|A(t,f)| + n'_I(t)}\right) = -\arctan\left(2\frac{\Delta v(t,f)}{\Delta v_B}\right)$$

$$+ \arctan\left(\frac{|n(t)|\sin(\varphi-\phi)}{|A(t,f)| + |n(t)|\cos(\varphi-\phi)}\right) \approx -\arctan\left(2\frac{\Delta v(t,f)}{\Delta v_B}\right) + \arctan\left(\frac{n_I(t)}{|A(t,f)| + n_Q(t)}\right) =$$

$$= -\arctan\left(2\frac{\Delta v(t,f)}{\Delta v_B}\right) + \arctan\left(\frac{n_I(t)}{\dfrac{2g_B R_D \sqrt{P_0 P_{SB}}}{\sqrt{1 + \left(2\dfrac{\Delta v(t,f)}{\Delta v_B}\right)^2}} + n_Q(t)}\right)$$

(6.31)

In this case we cannot approximate the SNR the same as in the OSSB case for a general case, since depending on the value of $\Delta v(t,f)$, $n_Q(t)$ is negligible or not. For very low SNR values or cases in which we are far away from the BFS, where $n_Q(t)$ and $n_I(t)$ are greater than the amplitude of the signal we have:

$$\theta_{PM} \cong \pm\pi + \arctan\left(\frac{n_I(t)}{n_Q(t)}\right)$$

(6.32)

Where $n_I(t)/n_Q(t)$ follows a Cauchy distribution. However, in the case in which we are near the BFS, with $\Delta v(t,f)\sim 0$, we have:

142

$$\theta_{PM} \cong -\left(2\frac{\Delta v(t,f)}{\Delta v_B}\right) + \frac{n_I(t)}{2g_B R_D\sqrt{P_0 P_{SB}}\sqrt{1+\left(2\frac{\Delta v(t,f)}{\Delta v_B}\right)^2}} = -\left(2\frac{\Delta v(t,f)}{\Delta v_B}\right) + \frac{n_I(t)}{2R_D\sqrt{P_0 P_{SB}}}\frac{\sqrt{1+\left(2\frac{\Delta v(t,f)}{\Delta v_B}\right)^2}}{g_B} \quad (6.33)$$

Therefore in phase measurements we must perform fitting with weighted non-linear regression, assuming the amplitude spectrum as the weighting factor, as it is clear in expression 6.31, where $n_I(t)$, the noise, is divided by the amplitude. However, the greater the measurement span or the lower SNR, will make the previous assumption a wrong approximation.

6.4 DYNAMIC MEASUREMENTS USING COHERENT SELF-HETERODYNE DETECTION TO MEASURE THE BRILLOUIN PHASE SHIFT

6.4.1 INTRODUCTION

In figure 6.10 and 6.15(b), we can observe that the measured phase shift spectra exhibit an almost linear behavior near the Brillouin frequency shift, the region of maximum gain. This can be very interesting to be exploited in dynamic measurements, which as we have seen in chapter 1, one open research line in BOTDA. When using the slope technique, the value of the frequency shift between pump and probe are fixed so as monitor the output signal for temporal changes [BERNINI 2009. In these measurements the noise of the spectrum in a given frequency span is very important: if all the points show a standard deviation of less than an equivalent value of frequency, we have that we can measure BFS changes of a value equal to the given frequency span. We have two possibilities to perform phase shift measurements: OSSB modulation and PM modulation. In this introduction we will study theoretically both cases and the possibilities they offer by theoretical simulations.
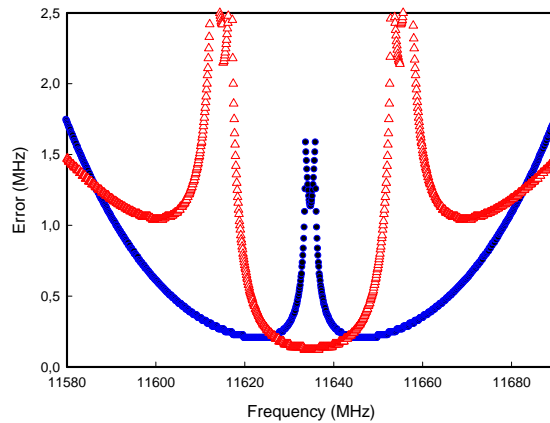
Figure 6.16: error at each point for a fixed value of SNR of 50dB, for amplitude (blue circles) and phase (red triangles) with OSSB modulation.
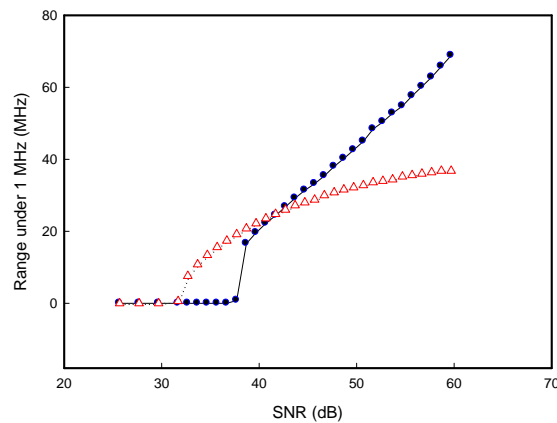

Figure 6.17: measurable span with an accuracy of 1MHz for amplitude measurements (blue circles) and phase (red triangles) with OSSB modulation.

We performed a simulation for a measurement of a fixed SNR value of 50dB, a BFS of 10.785GHz, a Brillouin bandwidth of 40MHz, a g_B of 0.0305 and depicted the accuracy we can obtain at each point depending on the frequency difference it exhibits in figure 6.16. These modulations were performed calculating the error in phase and in amplitude produced by a given Gaussian noise at each point of the spectral profile, and converting this noise to the error it would cause in the frequency domain. We can see that the maximum accuracy is better when using phase measurements, and it is because we can center the measurement in the maximum value of SNR, unlike in amplitude measurements.

We can perform the same as the previous simulation but varying the SNR, so we can study in detail the behavior of the system depending on the SNR and the measurable span for a given accuracy. We varied the SNR value from 26dB to 60dB. The measurable frequency span that exhibited a 1MHz accuracy or better is depicted in

figure 6.17. We can see that for low SNR values up to 42dB, phase measurements are clearly better, because we benefit from having the maximum gain inside the measuring span. However, for high values of SNR we reach the limit of the range, equal to the bandwidth of the Brillouin spectrum (40MHz in this case), which cannot be further increased because the linear region of the profile is limited to this region, while the amplitude measurements have a greater range. Therefore dynamic OSSB phase measurements are better than the amplitude measurements only until certain SNR value, 42dB for a 1MHz precision for example. For better values of SNR, amplitude measurements should be used.

When using PM phase shift measurements we must take into account that for $\Delta v(t,f) \sim 0$, we can assume $n_I(t) < g_B$ from equation (6.32). This means that we have an important reduction of noise compared to all the other cases: amplitude measurements for both modulation formats, or phase measurements using OSSB. Therefore, taking into account that the measured phase profile is linear in a wide range, as depicted in figure 6.15(b), plus the reduction of noise, PM phase measurements a very promising technique to perform dynamic measurements. In figure 6.18 the error at each point is calculated, the same as in the OSSB case, for a fixed SNR value of 50dB, a BFS of 10.785GHz, a Brillouin bandwidth of 40MHz and a g_B of 0.0305. We can see that the range under a 1MHz error increases from 47.5MHz in amplitude-PM or 42.6MHz in amplitude-OSSB and 32.2MHz in phase-OSSB to 68.5MHz when using PM phase measurements. Furthermore, if we study the measurable range with an accuracy of 1MHz varying the SNR from 25.69dB to 57.69dB, we have that the range measured in PM is always the best case, as depicted in figure 6.19. This shows us that for dynamic measurements, PM phase measurements are the best choice. Furthermore, among other advantages compared with other techniques we have the immunity to loss in the fiber, the SNR improvement obtained with self-heterodyne detection, or a greater measuring range for a given accuracy of the measurement. We will concentrate in a detailed study of dynamic measurements using PM phase measurements from now on.
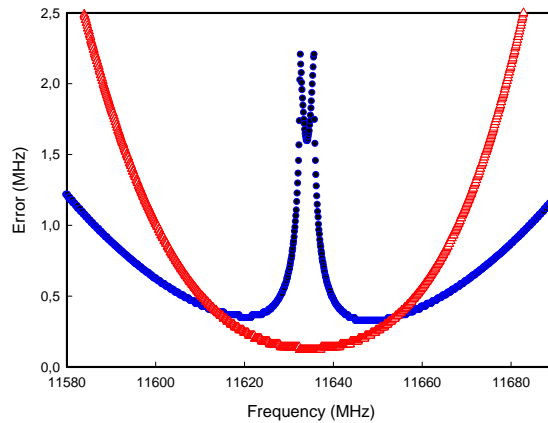
145

Figure 6.18: error at each point for a fixed value of SNR of 50dB for phase (red triangles) or amplitude (blue circles) measurements using PM modulation.
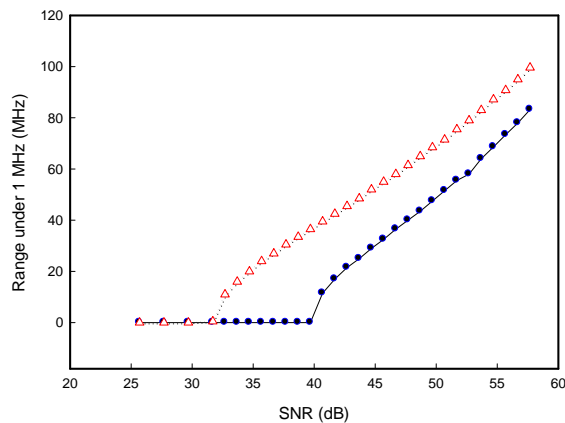

Figure 6.19: measurable frequency range for a 1MHz accuracy for phase (red triangles) or amplitude (blue circles) measurements using PM modulation.

6.4.2   OPERATING PRINCIPLE

We have seen that phase-PM measurements are very promising for dynamic distributed measurements using BOTDA. Therefore, in this section we propose how to perform such measurements using PM phase BOTDA.

The operating principle of the system that we propose is the same as the one presented in [CUI 2011], with the difference that the measurement is obtained taking into account the phase of the signal instead of the amplitude. So, we have a phase modulated continuous probe wave counter-propagating a pulsed pump wave in the fiber under test, as depicted in figure 6.20. The frequency difference between both signals is centered in the BFS of the fiber. Note that ideally we are supposing that there is not any variation of the BFS along the fiber. This is not likely to be found in field measurements, since there are always differences due to different concentration of

dopants, any pre-strain applied while embedding or gluing the fiber in the structure, or also temperature differences in different sections. However, in the applications of dynamic measurements, these variations are low, and do not affect the overall measuring range. After the interaction, the phase modulated signal is detected and demodulated so as to obtain the phase shift information of the signal. The detected signal is measured continuously, and transformed from the temporal to the spatial domain. The width of the pump pulses will give the spatial resolution of the measurements, as in regular BOTDAs. The variation of the BFS in any of the section generates an equal variation of the measured phase in the corresponding section of the measured signal. The variation is given by expression (6.29).
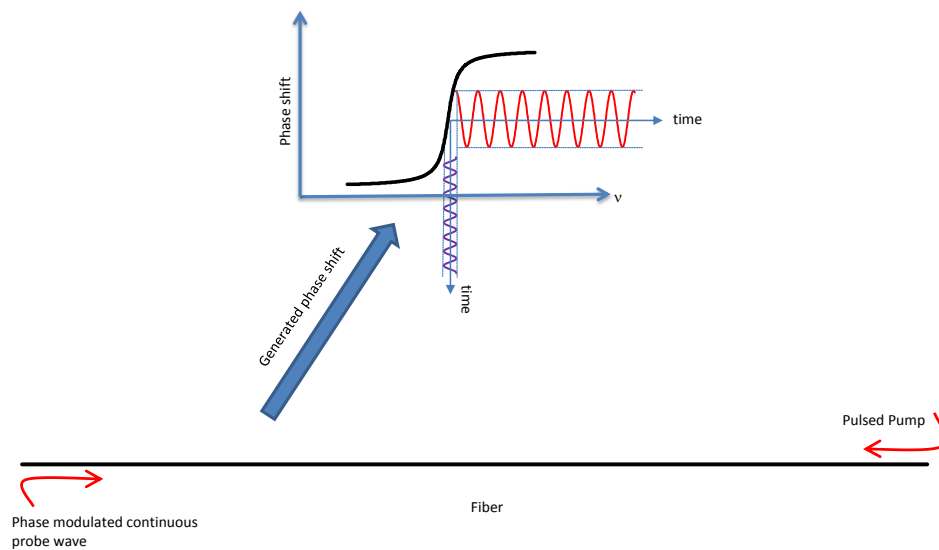

Figure 6.20: Operation principle of the dynamic BOTDA system based on phase measurements.

As it has been explained before, in phase PM measurements the amplitude dependence is negligible. So if the loss in the fiber varies, we will not notice it in the measurand. This is very interesting, since any loss because of mechanical stress, which is likely to happen in field measurements, do not cause an error in the measurements. However, care must be taken, since even if the level is always the same, the noise will not: the SNR decreases with amplitude, as it can be read from (6.29). With systems such as [BERNINI 2009] or [CUI 2011], the loss would be misread as a strain variation, causing an error in the measurements, but not in our case with phase measurements.

6.4.3   EXPERIMENTAL SETUP

As an evolution of the previous setup performing self-heterodyne detection, in figure 6.4, a novel and enhanced functionality and simplicity setup is presented in figure 6.21. This sensor, apart from benefiting from self-heterodyne detection, enhances the SNR and performance of the sensor while minimizing non-local effects.
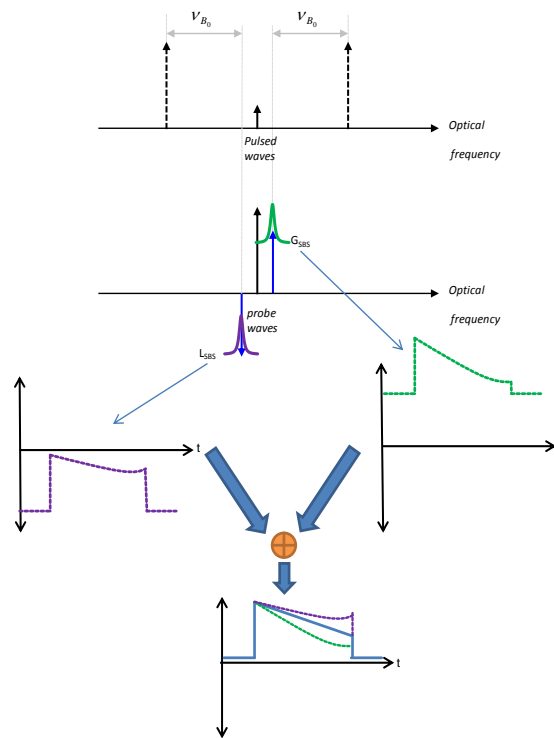
147

Figure 6.21: Schematic diagram of the double gain-loss interaction and detection principle of the high performance self-heterodyne BOTDA setup.

The principle behind this particular setup consists in taking advantage from having two different interactions simultaneously in the fiber, one in gain and another in loss. Similar schemes, using two spectral lines with a single probe beam, have been proved to mitigate errors coming from non-local effects [BERNINI 2011]. Non-local effects occur when the Brillouin interaction affects the amplitude of the pulses as explained in chapter 1. In gain configuration, the pulse is depleted while in loss configuration, the pulse is amplified. If both systems work at the same time, the pulse depletion that occurs in gain is compensated by the amplification of the pulse that occurs in loss. Taking two probe waves, which are the sidebands of a phase modulation, the field of such signal could be written as:

$$E(t) = \left[-E_{SB} \exp\left(-j2\pi f_{IF} t\right) + E_0 + E_{SB} \exp\left(j2\pi f_{IF} t\right) \right] \exp\left(j2\pi v_0 t\right) \tag{6.34}$$

Note that the pulses are the sidebands of a DSB-SC modulation, at a frequency equal to the BFS of the fiber plus f_{IF}. With such scheme, the upper pulsed sideband will generate gain in the upper sideband of the phase modulation, while the lower pulsed sideband will generate loss in the lower sideband of the phase modulation, as depicted in figure 6.21. If the frequency difference of the pulses with the carrier is the BFS of the fiber minus f_{IF}, the upper pulsed sideband will generate gain in the lower sideband of the phase modulation, while the lower pulsed sideband will generate loss in the upper

sideband of the phase modulation, but the system behavior would be the same. So, the field of the probe waves after the BOTDA interaction in the fiber could be written as follows:

$$E(t) = -E_{SB}H_{SBS\_loss}(\nu_0 - f_{IF}, z)\exp(j2\pi(\nu_0 - f_{IF})t) + E_0\exp(j2\pi\nu_0 t)$$
$$+ E_{SB}H_{SBS\_gain}(\nu_0 + f_{IF}, z)\exp(j2\pi(\nu_0 + f_{IF})t)$$

(6.35)

What can be simplified for small Brillouin gain, taking the approximations $H_{SBS\_gain} \cong (1+g_{SBS})exp(j\phi_{SBS})$ and $H_{SBS\_loss} \cong (1-g_{SBS})exp(-j\phi_{SBS})$:

$$E(t) = E_{SB}(g_{SBS} - 1)\exp(j2\pi(\nu_0 - f_{IF})t - \phi_{SBS}) + E_0\exp(j2\pi\nu_0 t)$$
$$+ E_{SB}(1 + g_{SBS})\exp(j2\pi(\nu_0 + f_{IF})t + \phi_{SBS})$$

(6.36)

Since the phase modulation sidebands are equal in amplitude but with a π delay between them, after self-heterodyne detection, the obtained electrical current is:

$$I_C(t) = 4R_D g_{SBS}\sqrt{P_{S0}P_{LO}} \ \cos(2\pi f_{IF}t - \phi_{SBS})$$

(6.37)

So, we can see that the gain and loss traces are added instead of subtracted, as depicted in figure 6.25. This has several connotations. The first one is that the SNR is doubled compared with the setup from section 6.2, because the amplitude of the measured BOTDA is doubled (note the 2 factor multiplying in (6.36)). The second is that, as in setups like in [BERNINI 2011], the distortion happening in gain and loss due to non-local effects is mitigated. However there is a slight difference with [BERNINI 2011]: the gain and loss processes happen independently, in different peaks, and it is the detection itself the one responsible for their combination.

In figure 6.22 we depict the high performance setup presented. It is based in the self-heterodyne detection BOTDA setup discussed in section 6.2, but with some simplifications: there is no need for any FBG or unwanted side-band filtering and the microwave synthesizer is substituted with a microwave local oscillator (LO) following the changes in [BERNINI 2009] and [CUI 2011]. The output of the laser is divided in two branches by a power splitter. In the upper branch a pulsed DSB-SC modulation at a frequency near the Brillouin frequency shift of the fiber plus f_{IF} is generated via RF-pulse shaping technique. After that these pulses are amplified in an EDFA and a polarization device is used to minimize the polarization dependence of Brillouin interaction on the fiber. In the lower branch, a phase modulator is driven by a RF signal at a frequency f_{IF}, and its output is directed to the fiber were it interacts with the counter-propagating pulses.
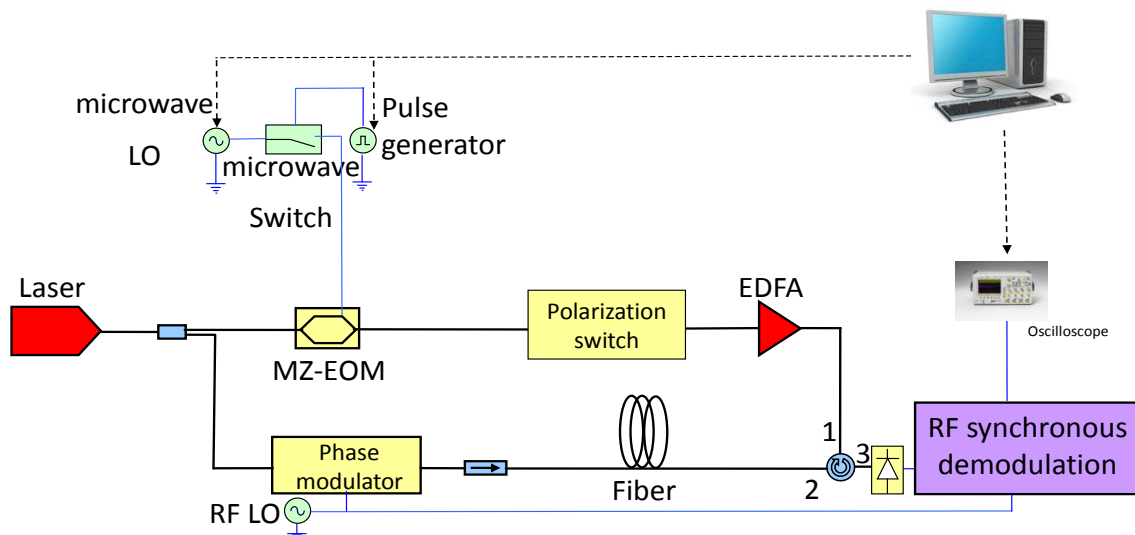
Figure 6.22: Experimental setup diagram of the proposed dynamic BOTDA system based on phase measurements.

The upper pulsed side-band is the pump pulse for the upper side-band of the phase modulation, and the lower pulsed side-band is the probe for the lower side-band of the pump modulation. After the interaction, the probe signals are converted to the electrical domain through self-heterodyne detection. In order to measure the BOTDA gain and phase, RF synchronous demodulation is performed. Then, we have a simpler BOTDA setup, which moreover, has a better performance.

It is advisable to use a low f_{IF}, between 200MHz and 2GHz for example, so the cost of the setup does not increase. For lower f_{IF} expression (6.37) is a little bit more complex, since the interaction of each pulse with each probe wave (carrier and two sidebands) must be taken into account. The frequency shift between pump and probe is fixed to the mean Brillouin frequency shift of the fiber after a calibration. So the frequencies f_{IF} and microwave LO, $f_{\mu w}$, are fixed to a value $f_{\mu w}$-f_{IF}= v_B.

6.4.4 MEASUREMENTS AND DISCUSSION

We assembled the experimental setup of figure 6.22 to perform an experimental demonstration of dynamic distributed measurements based in PM self-heterodyne BOTDA. The probe, pump and optical LO powers were 21dBm, -14dBm and 0dBm respectively. The spatial resolution of the system was set to 1m, using 10ns long pump pulses. The modulation frequencies were set to 850MHz for the probe powers and 11.625GHz for the pump pulses. A 160-m long SMF fiber was used as sensing fiber.

In order to prove experimentally that the detected phase shift is independent from the amplitude variations of the BOTDA signal, several spectra were measured for different attenuation values of the pulse and probe signals. For this purpose, we placed a

variable optical attenuator before detection and performed a whole scan of the Brillouin amplitude and phase profiles shown in figure 6.23. We can see that that the detected phase-shift remains unaltered in figure 6.23 (a) while the amplitude suffers severe attenuation in figure 6.23(b).
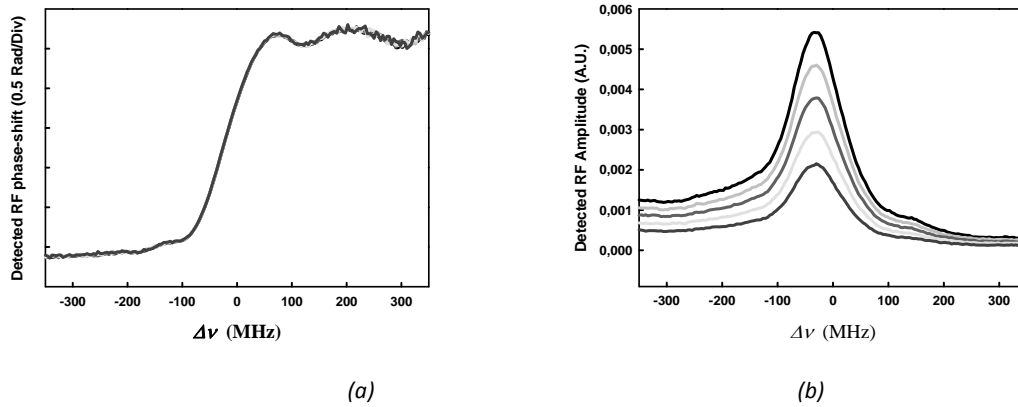

Figure 6.23. (a) Scanned phase-shift and amplitude spectra for different attenuation values of the pulse and probe signals, and (b) fast-acquisition measurement of the induced strain at the cantilever beam.

We glued a 1-m long section of the 160-m fiber to a metallic cantilever beam using epoxy resin. This section, as depicted in figure 6.24, was subject to vibrations, so we could perform distributed dynamic strain measurements based on PM self-heterodyne BOTDA. In figure 6.25 we show the detail of the correspondent measurement we performed in the section glued to the cantilever beam subject to vibration.

The precision of these measurements was measured to be 20 µε with an averaging of 64 acquisitions. In dynamic distributed strain measurements, the sampling rate only depends on the length of the sensing fiber [BERNINI 2009]. Furthermore we can describe the relationship with:

$$f < \frac{1}{4\tau N}$$ (6.39)

where τ and N, as defined in chapter 4, are the propagation time needed to travel through the fiber and the number of averages respectively. Therefore, a potential sampling rate of 625 kHz could be achieved for a 160m long fiber at 64 acquisitions averaging. However, this was limited by the available instrumentation achieving a measurement rate of 1.66 kHz.
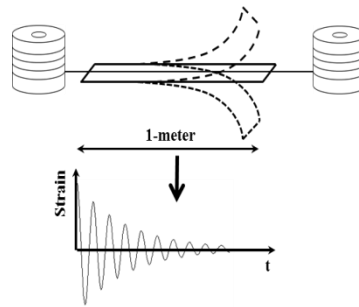
151

Figure 6.24: Detail of the section of the fiber glued to the cantilever to perform dynamic strain measurements based on PM self-heterodyne BOTDA.
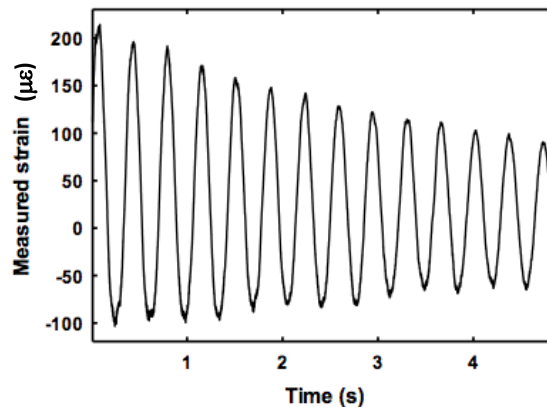

Figure 6.25: Measured variation of strain vs time in the section glued to the cantilever beam subject to vibration.

6.5 CONCLUSION

In this chapter we have discussed and demonstrated the benefit of using self-heterodyne detection in BOTDA setups so as to enhance the sensor performance and perform dynamic strain measurements.

While in a conventional system the SNR is limited by the maximum pump pulse and probe power, using coherent self-heterodyne detection the SNR of the measurements is increased using a strong local oscillator. Since pump and probe powers cannot be incremented above a threshold value because of non-local effects, MI or spontaneous Raman scattering, self-heterodyne detection is proven to be a valid solution, and we have experimentally demonstrated an increase of 7.89dB in the SNR in long range measurements.

Furthermore we have shown that PM self-heterodyne BOTDA measurements can be exploited to perform dynamic distributed measurements. They show important advantages when compared with other technologies based on BOTDA. The first one is the immunity to amplitude variations, which could be given by mechanical stress induced loss. While other sensing schemes would misread the amplitude variation as a

152

variation of the strain causing an error in the measurements, in PM self-heterodyne BOTDA the measurement does not suffer such alteration. Another advantage is that since the SNR is greater, the measuring range is increased compared with amplitude measurements. This SNR increase is not only given by the advantage of using self-heterodyne detection. It is also because of the profile of the measured phase shift with PM self-heterodyne BOTDA, linear in the maximum Brillouin gain region, and with a lower level of noise.

It should also be noted that PM self-heterodyne BOTDA measurements open a new degree of freedom in BOTDA setup designs, since some of its advantages could be exploited in different ways. For example, the immunity to Brillouin gain could be exploited to avoid non-local effect induced errors in long range measurements.

6.6   REFERENCES

[AGRAWAL 1997] Agrawal, G. P., *Fiber optic communication systems*, 3rd ed., New York: John Wiley and sons. 1997.

[ALASIA 2005] Alasia, D., Herráez, M.G., Abrardi, L., López, S.M. & Thévenaz, L. 2005, "Detrimental effect of modulation instability on distributed optical fibre sensors using stimulated Brillouin scattering", pp. 587.

[BERNINI 2009] Bernini, R., Minardo, A. & Zeni, L. 2009, "Dynamic strain measurement in optical fibers by stimulated brillouin scattering", *Optics Letters,* vol. 34, no. 17, pp. 2613-2615.

[BERNINI 2011] Bernini, R., Minardo, A. & Zeni, L. 2011, "Long-range distributed Brillouin fiber sensors by use of an unbalanced double sideband probe", *Optics Express,* vol. 19, no. 24, pp. 23845-23856.

[CUI 2011] Cui, Q., Pamukcu, S., Xiao, W. & Pervizpour, M. 2011, "Truly distributed fiber vibration sensor using pulse base BOTDA with wide dynamic range", *IEEE Photonics Technology Letters,* vol. 23, no. 24, pp. 1887-1889.

[DONG 2011] Dong, Y., Chen, L. & Bao, X. 2011, "Time-division multiplexing-based BOTDA over 100 km sensing length", *Optics Letters,* vol. 36, no. 2, pp. 277-279.

[HORIGUCHI 1995] Horiguchi, T., Shimizu, K., Kurashima, T., Tateda, M. & Koyamada, Y. 1995, "Development of a distributed sensing technique using Brillouin scattering", *Journal of Lightwave Technology,* vol. 13, no. 7, pp. 1296-1302.

[MINARDO 2005] Minardo, A., Bernini, R., Zeni, L., Thevenaz, L. & Briffod, F. 2005, "A reconstruction technique for long-range stimulated Brillouin scattering distributed

fibre-optic sensors: Experimental results", *Measurement Science and Technology,* vol. 16, no. 4, pp. 900-908.

[OKOSHI 1980] Okoshi, T., Kikuchi, K. & Nakayama, A. 1980, "NOVEL METHOD FOR HIGH RESOLUTION MEASUREMENT OF LASER OUTPUT SPECTRUM.", *Electronics Letters,* vol. 16, no. 16, pp. 630-631.

[SOTO 2010] Soto, M.A., Bolognini, G. & Pasquale, F.D. 2010, "Analysis of pulse modulation format in coded BOTDA sensors", *Optics Express,* vol. 18, no. 14, pp. 14395-14400.

[SOTO 2013] Soto, M.A., Thévenaz, L. 2013, "Modeling and evaluating the performance of Brillouin distributed optical fiber sensors", Optics Express, vol. 21, no. 25, pp. 31347-31366.

[THEVENAZ 2011] Thévenaz, L., Foaleng Mafang, S. & Lin, J. 2011, "Impact of pump depletion on the determination of the Brillouin gain frequency in distributed fiber sensors", *Proceedings of SPIE - The International Society for Optical Engineering*, 775322.

[THOMAS 2006] Thomas, T.G., Chandra S., *Communication Theory*, New Delhi, India, 2006, Tata McGraw-Hill Education.

[URRICELQUI 2012a] Urricelqui, J., Zornoza, A., Sagues, M., and Loayssa, A., 2012, "Dynamic BOTDA measurements based on Brillouin phase-shift and RF demodulation". *Optics Express,* vol. 20, no. 24, pp 26942-26949.

[URRICELQUI 2012b] Urricelqui, J., Zornoza, A., Sagues, M., Loayssa, A., "Dynamic BOTDA measurements using Brillouin phase-shift", *Proceedings of SPIE - The International Society for Optical Engineering*. Accepted for publication.

[ZORNOZA 2010] Zornoza, A., Pérez-Herrera, R.A., Elosúa, C., Diaz, S., Bariain, C., Loayssa, A. & Lopez-Amo, M. 2010, "Long-range hybrid network with point and distributed Brillouin sensors using Raman amplification", *Optics Express,* vol. 18, no. 9, pp. 9531-9541.

[ZORNOZA 2011] Zornoza, A., Minardo, A., Bernini, R., Loayssa, A. & Zeni, L. 2011, "Pulsing the probe wave to reduce nonlocal effects in brillouin optical time-domain analysis (BOTDA) sensors", *IEEE Sensors Journal,* vol. 11, no. 4, pp. 1067-1068.

[ZORNOZA 2011] Zornoza, A., Olier, D. & Loayssa, A. 2011, "Self-heterodyne synchronous detection for SNR improvement and distributed Brillouin phase shift measurements in BOTDA sensors", *Proceedings of SPIE - The International Society for Optical Engineering*.

[ZORNOZA 2012] Zornoza, A., Sagues, M. & Loayssa, A. 2012, "Self-heterodyne detection for SNR improvement and distributed phase-shift measurements in BOTDA", *Journal of Lightwave Technology,* vol. 30, no. 8, pp. 1066-1072.

CHAPTER 7

CONCLUSIONS AND FUTURE WORK

7.1   CONCLUSIONS

In this thesis new techniques to contribute to the improvement of distributed fiber optic sensor based on SBS, mainly applied to BOTDA, have been presented. An extensive introduction to distributed optical fiber sensors, their limiting factors and the state of the art of BOTDA have been key to identify the research trends in these sensors. The performance of sensors by theoretical models has been studied. Especially we have centered in models for a detailed study of the SNR and non-local effects, which are two of the main limitations of the performance of the sensor. We have seen that SNR is usually low in BOTDA measurements, since the signals deployed are very weak, and consequently so is the interaction. This makes the temperature and strain measurements noisy. Non-local effects limit the performance of the sensor in long range measurements. When they are present, the main problem is an error in the Brillouin frequency shift estimation, and consequently an error in the temperature or strain measurement. The other factors that limit BOTDA sensors, that is, MI, self-phase modulation, spontaneous Raman scattering, the measuring time and the discrimination between temperature and strain are all related to SNR too. MI, self-phase modulation and spontaneous Raman scattering limit the pump pulse power. Since the SNR is proportional to the gain caused in the interaction, and this is dependent in the pump pulse power, there is a maximum value which cannot be

exceeded. In the case of the measuring time, averaging, sweep span and resolutions are the limiting factors. However, averaging is performed so as to increase SNR, and the more detail in the sweep the better the obtained fit. Therefore, the measuring time is also related to SNR. Finally, the discrimination between temperature and strain can be easily achieved by using two fibers, one of them loose so it only measures temperature. However this means doubling the measuring range, so doubling the fiber loss, and consequently reducing SNR. In high resolution measurements, that is, using short pump pulses, the measured Brillouin profile is given by the convolution between the pulse spectrum and Brillouin spectrum. Therefore, since the first spreads over a great span combined with the reduction of Brillouin gain due to a shorter interaction, gives a noisier measurement. Another limitation of Brillouin distributed sensors is that setups are complex, so any effort in reducing their cost is welcome by the clients. In order to contribute to the development of these sensors the different solutions presented in this thesis are listed below.

A theoretical model was developed in order to study the behavior of pulses with leakage in long range BOTDA measurements. From that study is concluded that the leakage of pump pulses contributes to the enhancement of non-local effects: the leakage increases the level of the probe wave, so a greater depletion of the pulse occurs. As a solution to reduce the leakage of the pulses a BOTDA sensing setup based on the RF-shaping of pump pulses has been presented. With this setup the leakage of pump pulses is reduced two orders of magnitude compared to other state of the art setups. Also, since the pulsing and the frequency shift are made in a single electrical-to-optical step, just one electric-to optic device is needed, instead of the two that other state-of-the-art setups deploy. So, this contributes to simplify the setup as well as enlarging the measuring range. Experimental measurements with 21dB, 28dB and 60dB ER show errors of 3MHz, 1.5MHz and less than 1MHz respectively, being the last one the case of the RF-shaping of pump pulses.

An alternative Brillouin spectrum scan technique has also been presented: the wavelength sweep BOTDA. This technique, which takes advantage of the linear dependence of the Brillouin frequency shift with wavelength, does not require a synthesized microwave generator. It consists in changing simultaneously the probe and pump wavelength while keeping their frequency difference constant. The relationship between wavelength at which the Brillouin gain is maximum and temperature and strain has been studied and an expression of this relationship has been discussed. A solution to mitigate the effect of chromatic dispersion is also given. In order to experimentally demonstrate the capability of method we have presented measurements in a 10km fiber at 24m spatial resolution with a BOTDA experimental

setup tailored to the wavelength sweep method. This technique introduces a new degree of freedom to be exploited in Brillouin distributed sensors.

The TDM-BOTDA technique gives the possibility to control non-local effects while enhancing SNR in detection in long range measurements. The main drawback of this technique is the increase of measuring time. However, depending on the application, SNR, measuring time or non-local effects can be traded off, in order to obtain the desired performance of the sensor. Measurements in 50km long fibers have been presented in order to show the possibilities of the technique, in which the non-local effects were significantly reduced.

Two solutions to design a fiber optic point and distributed sensing hybrid network have also been presented, a very interesting solution in structures that require different kinds of monitoring. The main problem we have while including point sensors in a distributed network is the loss introduced by the devices responsible for multiplexing. This, combined with the loss of the fiber, can be very destructive for the measurements quality. Therefore, we use Raman distributed amplification so as to enhance the SNR of the system, what has supposed a big breakthrough in BOTDA sensors. In the first network, the point sensors performance is limited by ASS. So, a second network is designed, in which ASS is minimized is also presented. Measurements in a 46km fiber at 3m spatial resolutions have been obtained simultaneously with four point sensors distributed along the sensing network.

Finally, by taking advantage of coherent detection techniques, we show the application of self-heterodyne detection to BOTDA. It gives the possibility to enhance the SNR in detection considerably, making it very interesting for long range measurements. Actually an increase of 7.89dB in SNR has been experimentally proved compared to conventional BOTDA. Furthermore, the phase shift information generated by the Brillouin interaction in the fiber is not lost in detection. This is of special interest to perform dynamic BOTDA measurements, since the phase can be independent from Brillouin gain, avoiding errors in the measurements caused by mechanical stress induced loss. A theoretical model has shown that dynamic phase measurements have a better behavior than dynamic gain measurements in terms of SNR: they can perform within the same error as the gain measurements in a greater range. Experimental measurements in a 160m fiber at 1m spatial resolutions at a rate of 1.66KHz have been demonstrated.

159

Figure 7.1: BOTDA prototype

Furthermore, one of the consequences of this thesis is the development of a BOTDA prototype based on the research we have been carrying out. The first version of the prototype is shown in figure 7.1. We have already applied this prototype to measuring strain in field applications. In figure 7.2 a field measurement is shown, where the fiber was glued to a concrete cantilever beam where different loads where applied. We can see that the sections of fiber affected by the load show a variation of the measured Brillouin frequency shift, which was used to calibrate the response of the fibers. Note that the dynamic measurements of chapter 6 were also performed with this prototype.
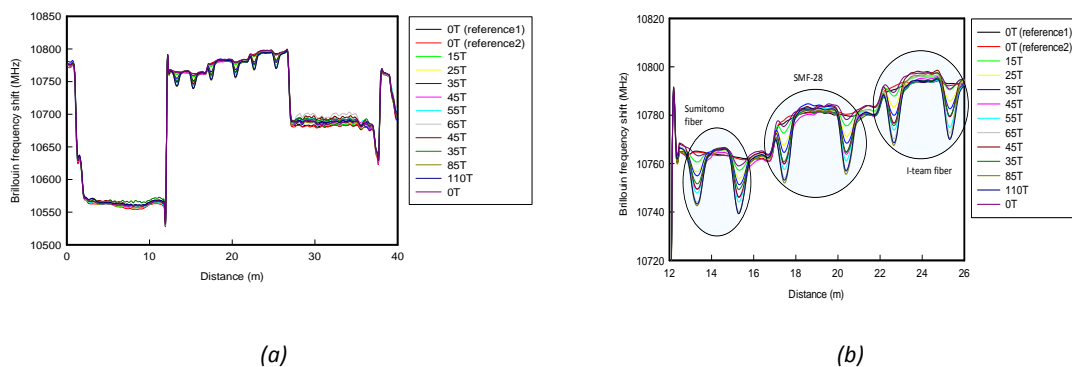

(a)

(b)

Figure 7.2: Preliminary measurements performed with the prototype with different loads in a cantilever beam. In (a) the whole fiber under test is shown, while in (b) a zoom to the sections where load was applied is shown.

7.2   FUTURE WORK

The work carried out in this thesis has supposed the start of a new research line in the optical communications group in the UPNA. Therefore, in order to continue with the research of these thesis, some future trends can be defined.

The wavelength sweep based Brillouin scan has been applied in other fields of microwave photonics [LI 2011, YANG 2012]. And furthermore, it can be applied to further overcome some of the limitations of SF-BOTDA: in SF-BOTDA the

measurements are limited to a 100MHz range, which could be improved by using more spectral lines at different wavelengths.

By combining RF-shaping of pump pulses technique and the two spectral lines technique, a high performance sensor can be designed, avoiding non-local effects and with low leakage levels. However there is a compatibility problem between them: by generating a pulsed DSB-SC signal as pump wave, by applying it to a probe wave, one of the bands generates loss while the other generates gain, so the overall interaction is null. However a solution has been presented in chapter 6, which requires further research.

The Independence of phase shift measurements using PM is very promising too. Apart from avoiding errors due to mechanically induced loss, it can be used for other applications. For instance, since there is no dependence with pump pulse power, the distortion generated by non-local effects is not present. This can be very interesting to exploit in long range measurements. The research started in this thesis was followed and recently published [URRICELQUI 2013].

On the other hand, by combining the different techniques presented in this thesis with other such as the ones tailored for high spatial measurements or simplex coding is a possibility to perform high performance measurements, because there is still room for improvement in BOTDA sensors.

In distributed sensing, it is hard to design a smart network, that can overcome a failure such as a collapse in the fiber. A preliminary work where a new optical sensors network based on BOTDA technology have been presented and experimentally validated in [ULLAN 2012]. A fast remotely powered and controlled optical switch has been used to select the structure to be sensed, so as to perform temperature distributed measurements along 2 different sections of fiber. Therefore, if failure occurs in one of the fibers, the other one can be remotely chosen so as to continue measuring.

Finally, the aim of developing our own BOTDA prototype, contributes to build our own experience in field measurements. This is of particular importance, since new research trends come from the new particular applications of the sensors and the challenges found when applying sensors to field measurements, an experience that is hard to achieve while working exclusively in a lab.

7.1   REFERENCES

[LI 2011] Li, W., Zhu, N.H. & Wang, L.X. 2011, "Photonic phase shifter based on wavelength dependence of Brillouin frequency shift", *IEEE Photonics Technology Letters,* vol. 23, no. 14, pp. 1013-1015.

[ULLAN 2012] Ullán, A., Bravo, Zornoza, A., Loayssa, A., Lopez-Amo,. M, Lopez-Higuera, J.M., "BOTDA sensor network with power-by-light remote switching". *Accepted for publication in the 22nd conference of Optical Fiber Sensors.*

[URRICELQUI 2013] Javier Urricelqui, Mikel Sagues, and Alayn Loayssa. BOTDA measurements tolerant to non-local effects by using a phase-modulated probe wave and RF demodulation. *Optics Express,* Volume: 21 (14), July 2013.

[YANG 2012] Yang, B., Jin, X., Chi, H., Zhang, X., Zheng, S., Zou, S., Chen, H., Tangdiongga, E. & Koonen, T. 2012, "Optically tunable frequency-doubling brillouin optoelectronic oscillator with carrier phase-shifted double sideband modulation", *IEEE Photonics Technology Letters,* vol. 24, no. 12, pp. 1051-1053.

APPENDIX I

LIST OF PUBLICATIONS

I.1   INTERNATIONAL PAPERS

1. Zornoza, A., Pérez-Herrera, R.A., Elosúa, C., Diaz, S., Bariain, C., Loayssa, A. & Lopez-Amo, M. 2010, "Long-range hybrid network with point and distributed Brillouin sensors using Raman amplification", *Optics Express,* vol. 18, no. 9, pp. 9531-9541.

2. Zornoza, A., Olier, D., Sagues, M. & Loayssa, A. 2010, "Brillouin distributed sensor using RF shaping of pump pulses", *Measurement Science and Technology,* vol. 21, no. 9, 094021.

3. Zornoza, A., Olier, D., Sagues, M. & Loayssa, A. 2011, "Brillouin spectral scanning using the wavelength dependence of the frequency shift", *IEEE Sensors Journal,* vol. 11, no. 2, pp. 382-383.

4. Fernandez-Vallejo, M., Olier, D., Zornoza, A., Perez-Herrera, R.A., Diaz, S., Elosua, C., Bariain, C., Loayssa, A. & Lopez-Amo, M. 2012, "46-km-long raman amplified hybrid double-bus network with point and distributed brillouin sensors", *IEEE Sensors Journal,* vol. 12, no. 1, pp. 184-188.

163

5. Zornoza, A., Sagues, M. & Loayssa, A. 2012, "Self-heterodyne detection for SNR improvement and distributed phase-shift measurements in BOTDA", *Journal of Lightwave Technology,* vol. 30, no. 8, pp. 1066-1072.

6. Zornoza, A., Minardo, A., Bernini, R., Loayssa, A. & Zeni, L. 2011, "Pulsing the probe wave to reduce nonlocal effects in brillouin optical time-domain analysis (BOTDA) sensors", *IEEE Sensors Journal,* vol. 11, no. 4, pp. 1067-1068.

7. Urricelqui, J., Zornoza, A., Sagues, M., and Loayssa, A., 2012, "Dynamic BOTDA measurements based on Brillouin phase-shift and RF demodulation". *Optics Express,* vol. 20, no. 24, pp 26942-26949.

8. Bravo, M., Ullan, A., Zornoza, A., Loayssa, A., Lopez-Amo, M., Lopez-Higuera, J. M., 2013, Application of Remote Power-by-Light Switching in a Simplified BOTDA Sensor, vol. 13, no. 12 , pp. 17434-17444.

I.2   INTERNATIONAL CONFERENCES

1. Zornoza, A., Olier, D., Sagues, M. & Loayssa, A. 2009, "Distortion-free Brillouin distributed sensor using RF shaping of pump pulses", *Proceedings of SPIE - The International Society for Optical Engineering*.

2. Zornoza, A., Olier, D., Díaz, S. & Loayssa, A. 2009, "Simplified Brillouin distributed sensing scheme using ultra-high extinction ratio RF Pulses", *Proceedings of IEEE Sensors*, pp. 433.

3. Fernandez-Vallejo, M., Olier, D., Zornoza, A., Perez-Herrera, R.A., Díaza, S., Elosúa, C., Bariain, C., Loayssa, A. & Lopez-Amo, M. 2010, "Long-range hybrid double-bus network with point and distributed Brillouin sensors using Raman amplification", *Proceedings of SPIE - The International Society for Optical Engineering*, 76533R.

4. Zornoza, A., Olier, D. & Loayssa, A. 2011, "Self-heterodyne synchronous detection for SNR improvement and distributed Brillouin phase shift measurements in BOTDA sensors", *Proceedings of SPIE - The International Society for Optical Engineering*, 77532F.

5. Urricelqui, J., Zornoza, A., Sagues, M., Loayssa, A., "Dynamic BOTDA measurements using Brillouin phase-shift", *Proceedings of SPIE - The International Society for Optical Engineering*. *Accepted for publication in the 22nd conference of Optical Fiber Sensors.*

6. Ullán, A., Bravo, Zornoza, A., Loayssa, A., Lopez-Amo,. M, Lopez-Higuera, J.M., "BOTDA sensor network with power-by-light remote switching". Optical fiber sensors 22. Proceedings of SPIE - The International Society for Optical Engineering 8421, art. no. 84218E. Beijing (China). October 14th 2012.

I.3 PATENTS

1. Ander Zornoza, Alayn Loayssa and Mikel Sagues, "Dispositvo y procedimiento para la medida de la distribución de magnitudes fisicas en una fibra óptica", P201130773, Spain, 13th of May 2011. Universidad pública de Navarra.

2. Ander Zornoza, Alayn Loayssa and Mikel Sagues. *Dispositivo y procedimiento para la medida de la distribución de magnitudes físicas en una fibra óp*tica. Number of application: P201130773. Priority country: Spain. Priority date: 13th of May 2011. Institution: Universidad Publica de Navarra. Extended worldwide.

I.4 BOOK CHAPTERS

1. "Smart sensor technologies" Ed. Kris Iniewsky, chapter "Recent advances in distributed fiber-optic sensors based on the Brillouin scattering effect", by Alayn Loayssa, Mikel Sagues and Ander Zornoza.